(A) Constructing a Three-Dimensional DNA Nanomachine to Achieve Rapid Isothermal Signal Amplification for Nucleic Acid Detection

(B) Regulation of DNA Strand Displacement Using an Allosteric DNA Toehold

Xiaolong Yang

A Thesis Submitted to the Department of Chemistry

In Partial Fulfillment of the Requirements for the

Degree of Master of Science

Brock University

St. Catharines, Ontario

Abstract

(A) We developed a new strategy to achieve rapid isothermal signal amplification through the construction of DNA nanomachine. DNA nanomachine built from a DNA functionalized gold nanoparticle (DNA−AuNP), which moves a DNA walker along a three-dimensional (3-D) DNA−AuNP track and executes the task of releasing signal reporters (SRs) to generate fluorescence. The movement of the DNA walker is powered by a nicking endonuclease that cleaves specific DNA substrates on the track. During the movement, each DNA walker cleaves multiple substrates, resulting in the rapid release of SRs to achieve signal amplification at a constant temperature. The 3-D DNA nanomachine is highly efficient due to the high local effective concentrations of all DNA components that have been co-conjugated on the same AuNP. Moreover, the activity of the 3-D DNA nanomachine can be controlled by introducing a protecting DNA probe that can hybridize to or dehybridize from the DNA walker in a target-specific manner. This property allows us to tailor the DNA nanomachine into a DNA nanosensor that is able to achieve rapid, isothermal, and homogeneous signal amplification for detection of nucleic acids in both buffer and a complicated biomatrix.

(B) Toehold-mediated DNA strand displacement has proven extremely powerful in the construction and operation of DNA devices, including reconfigurable structures, DNA circuits, and amplifications. To achieve the construction of such DNA devices, toeholds are required for controllable activation and regulation. Usually, the complicated strand displacement behaviors and functions are achieved by combining conventional toehold-mediated strand displacement, associative toehold-mediated strand displacement, and remote toehold strand displacement toehold activation mechanisms. We still need to enrich the toolbox of strand displacement techniques with alternative approaches for toehold activation to construct devices of higher complexity. Here we introduce an allosteric DNA toehold (A-toehold) design that allows flexible activation or regulation of DNA strand displacement.

Acknowledgement

I would first like to thank my thesis advisor Professor Feng Li, for his advice, direction and support throughout my research. The door to Professor Feng Li office was always open whenever I ran into a trouble spot or had a question about my research or writing. He is an excellent scientific supervisor supporting his students in every possible way for their future.

I would like to thank my supervisory committee members, Professor Heather Gordon and Professor Art van der Est for their valuable advice and insightful comments throughout all my Master studies.

I thank Dr. Jeffrey Atkinson, Dr. Hongbin (Tony) Yan, and Dr. David W. Dealer, Xing Shi for their valuable advice to my seminer.

I would like to acknowledge the important contributions to this work made by Sean Mason, who helped me with the synthesis of the 3-D DNA nanomachines. I thank Sarah Traynor for her contributions in allosteric toehold project. My sincere thanks also to my fellow labmates: Zechen Yu, Trevior Ealaschuk, Ryan Alt, Dr. Hayam Mansour, Guan Wang, Tianyu Dong, Romano Brujic, Nicole Dewey, Dr. Xiaoyu Xie and Dr. Fangfang Chen.

I thank the encouragement from my best friends Zhipeng Lian, Yunpeng Bai, Yue Pan, Naming Dai, Kai Bai, Jie Gao, Ting Wang, Wenqing Li, Zongyuan Wu, Ning Lou, Jiangbin Li, Shan Liu and Ling Shao.

I would like to thank all my family members for their supportings and encouragements.

Finally, I want to acknowledge the Brock University for their financial support.

Table of Contents

List of Tables

List of Figures

List of Schemes

List of Abbreviations

DNA	deoxyribonucleic acid
RNA	ribonucleic acid
C	cytosine
G	guanine
A	adenine
T	thymine
PCR	polymerase chain reaction
RT	reverse transcription
LCR	ligase chain reaction
RCA	rolling circle amplification
EXPAR	exponential amplification reaction
dNTPs	deoxynucleotide triphosphates
TH	toehold
BM	branch migration
A-toehold	allosteric DNA toehold
DW	DNA walker
SR	signal reporter
FAM	fluorescein amidite
TAMRA	5-Carboxytetramethylrhodamine
AuNP	gold nanoparticle
DNA-AuNPs	DNA functionalized AuNPs
DTT	dithiothreitol

P	protecting DNA probe
PAGE	polyacrylamide gel electrophoresis
P.C.	positive control
N.C.	negative control
TON	turnover number
APS	ammonium persulfate
TEMED	N,N,N',N'-tetramethylethylene-diamine
HPLC	high performance liquid chromatography
EDTA	ethylenediaminetetraacetic acid
dT	deoxy-thymidine nucleotides

Chapter 1

Constructing a Three-Dimensional DNA Nanomachine to Achieve Rapid Isothermal Signal Amplification for Nucleic Acid Detection

1.1 Introduction

Genes, which are made up of double helical deoxyribonucleic acid (DNA), act as the basic physical and functional units of heredity in living organisms. DNA provides the cells with instruction codes to make molecules called proteins through an intermediate process involving another type of nucleic acid, ribonucleic acid (RNA). RNA is a polymeric molecule which plays important biological roles in regulation, expression, coding, and decoding of genes [1]. The unique base pairing function of DNA, as well as its function in programming essential components in cells, make the sequence of DNA applicable to the area of disease diagnosis. [2]

This chapter will discuss the principles of classic signal amplification techniques, including non-isothermal amplification and isothermal amplification in DNA detection. Furthermore, this chapter will introduce the concept of our three-dimensional DNA nanomachine, as well as the objectives of this research.

1.2 Nucleic Acid Detection

DNA has a double stranded structure composed of simpler monomer units called nucleotides.[1] Each strand is a chain of deoxyribonucleotide units termed polynucleotides composed of covalently bonded three parts- a nitrogenous base, a deoxyribose sugar and a phosphoric acid residue (Figure 1-1). The four different nitrogen bases in DNA are cytosine (C), guanine (G), adenine (A), and thymine (T). Commonly, DNA bases follow the Watson-Crick rules, forming pairs between the two strands: A with T and C with G (Figure 1.2). Among DNA bases, cytosine selectively hydrogen bonds with guanine, and thymine selectively hydrogen bonds with adenine. The specificity of base pairing in DNA can be used in developing techniques applyed to nucleic acid detection.

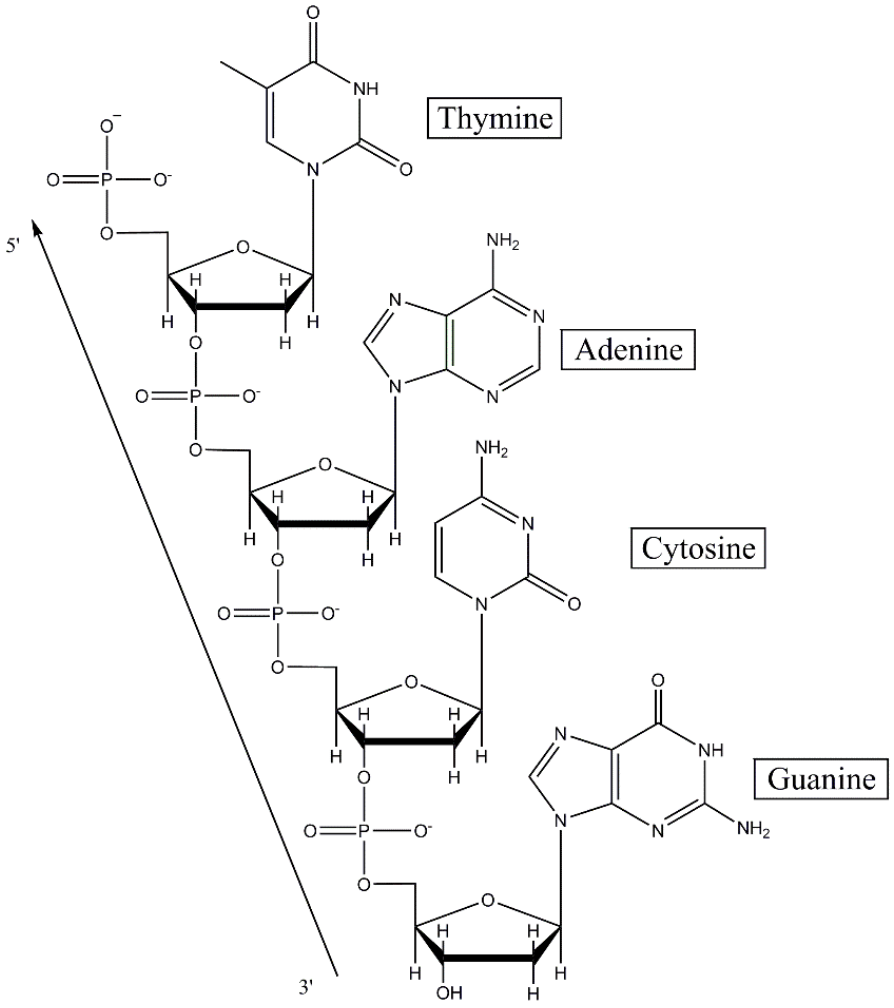

Figure 1-1. Structure of a stranded DNA chain.

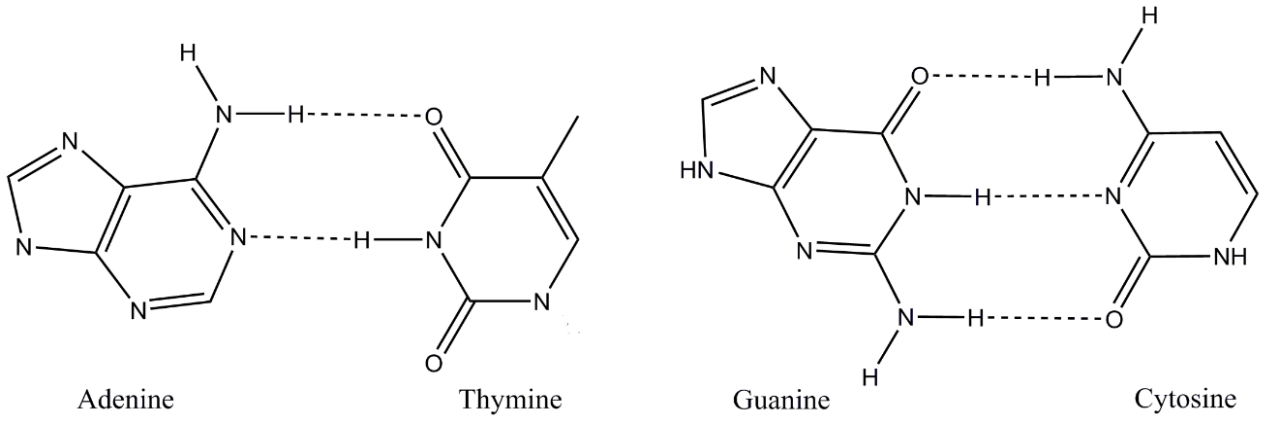

Figure 1-2. DNA bases. a) Adenine (A) and thymine (T) hydrogen bonds, b) Guanine (G) and Cytosine (C) hydrogen bonds.

DNA plays a significant role in the synthesis of functional proteins and regulating cell functions [1]. The presence, absence, mutation or expression level of certain genes is closely related to certain infectious diseases, cancers [2] and auto-immune diseases [3]. The detection of nucleic acids is fundamental for the development of disease diagnostics. Therefore, determining the nucleic acids in a complex system requires highly sensitive and specific analytical techniques.

Detection of nucleic acids is based on DNA strand complementarity and the ability of the single stranded DNA to form double stranded molecules in vitro or in vivo. Thus, specific nucleic acids can be detected in a prepared sample in solution. Much effort has been devoted to biosensors in the detection of nucleic acids incorporating signal amplification including non-isothermal signal amplification and isothermal signal amplification. [6, 7, 9, 10]

1.3 Non-isothermal Signal Amplification for Nucleic Acid Detection

Commonly, nucleic acid amplification is a molecular technique used to detect and amplify the DNA. Non-isothermal signal amplification strategies, such as polymerase chain reaction (PCR) [4] and ligase chain reaction (LCR) [7], often require operating conditions with a wide range of temperature to achieve signal amplification.

1.3.1 Polymerase Chain Reaction (PCR)

Polymerase chain reaction (PCR), invented by Mullis [4] was the first nucleic acid non-isothermal signal amplification method. PCR enables the production of multiple copies of defined fragments of DNA in vitro to achieve the amplification of specific regions of DNA. The technique is very specific and extremely sensitive and is currently widely used by researchers and clinicians to diagnose diseases. The following aims to explain how PCR works [4, 7].

Each PCR assay requires four primary components: template DNA to be amplified, gene-specific primers, the DNA polymerase, and nucleotides. The source of template DNA can be either synthesized DNA, genomic DNA isolated from cells, or DNA produced from RNA samples through reverse transcription (RT). Primers are short sequence-specific DNA fragments that are

chemically synthesized to have sequence complementary to a designated DNA sequence of the template DNA. The DNA polymerase is a thermostable enzyme that can withstand the heating and cooling cycles needed for PCR. DNA polymerase enables the linking of individual nucleotides together to generate the PCR product. The nucleotides which serve as building blocks for the creation of the resultant DNA include the four bases, adenine, thymine, cytosine, and guanine (A, T, C, G) that are found in DNA. These building blocks are used by the DNA polymerase to generate the PCR product.

PCR is composed of three consecutive repeating cycles, including denaturation, annealing, and elongation, that require distinct temperature conditions. The DNA amplification is accomplished through a thermal cycler containing an apparatus that holds the samples in a thermal block. The thermal cycler raises and decreases the temperature of the block to attain the suitable temperature in the different phases of the amplification process. As shown in Figure 1-3, the first PCR step, denaturation, separates the double-stranded original DNA by heating the sample mixture to approximately 90 ºC. The double-stranded DNA template is denatured by breaking the hydrogen bonds between complementary bases in the first step, generating two single-stranded DNA molecules. In the next step, the sample is cooled down to 50-65 ºC, which allows the annealing of the primers to each of the single-stranded DNA templates. Two different primers are involved in the reaction process that enables base pairing to each of the two denatured single-stranded DNA molecules obtained in step one. The length of the primers is much shorter than the length of target DNA regions. Each primer hybridizes to the 3’ end of its complementary target. In the third step, the temperature of the mixture is increased to 72 ºC. 72 ºC is the optimal temperature for the activity of Taq polymerase, a commonly used enzyme. [5] Taq polymerase is a thermostable DNA polymerase that is able to withstand high temperature conditions required during PCR [5]. In this step, the polymerase catalyzes the synthesis of a new DNA strand that is complementary to the single-stranded DNA template in the 5’-to-3’ direction by adding free nucleotide triphosphates. The copy

number in each cycle can be doubled by the repetition of these three steps. The copy number is equal to 2^n, where n is the cycle number. Thus, the generated products through PCR assay are exponentially amplified.

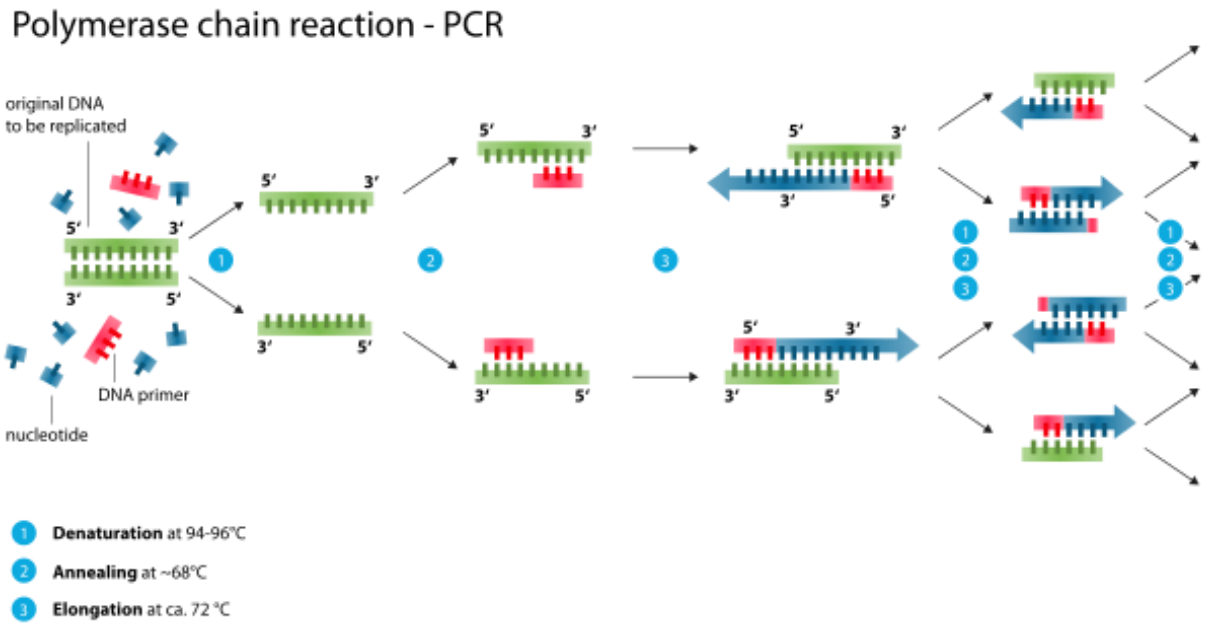

Figure 1-3. Steps in the polymerase chain reaction (PCR). First step, double strands of original DNA to be replicated are denatured at 94-96 ºC; second step, specific DNA primers are annealed by putting the mixture into an optimal temperature range; third step, raising temperature to the optimal activity of the polymerase initiates the elongation process through the addition of nucleotides from the DNA primers to generate new strands of DNA. Original DNA can be amplified by repeating these three steps for 30 to 40 times. Reproduced from wiki Enzoklop own work. https://commons.wikimedia.org/wiki/File:Polymerase_chain_reaction.svg

1.3.2 Ligase Chain Reaction (LCR)

LCR [6] is another method of DNA non-isothermal amplification to detect or amplify a target sequence. Unlike PCR, instead of using DNA polymerase and shorter primers, the ligase reaction uses a thermostable enzyme, DNA ligase [7], and four probe oligo oligonucleotides. The function of DNA ligase [7] is to link two oligonucleotides that are immediately adjacent to each other (Figure 1-

4). Like PCR, this amplification reaction involves three cyclic steps, denaturation, annealing, and ligation, with different working temperatures. After the target double-stranded DNA is denatured through a denaturation cycle, two probes hybridize adjacent to each other on a single-stranded target DNA in the annealing step. In the third step, two adjacent probes are ligated with DNA ligase into a longer sequence. The ligated probes function as a target template DNA for further hybridization, denaturation, annealing, and ligation steps to amplify the original target DNA (Figure 1-4).

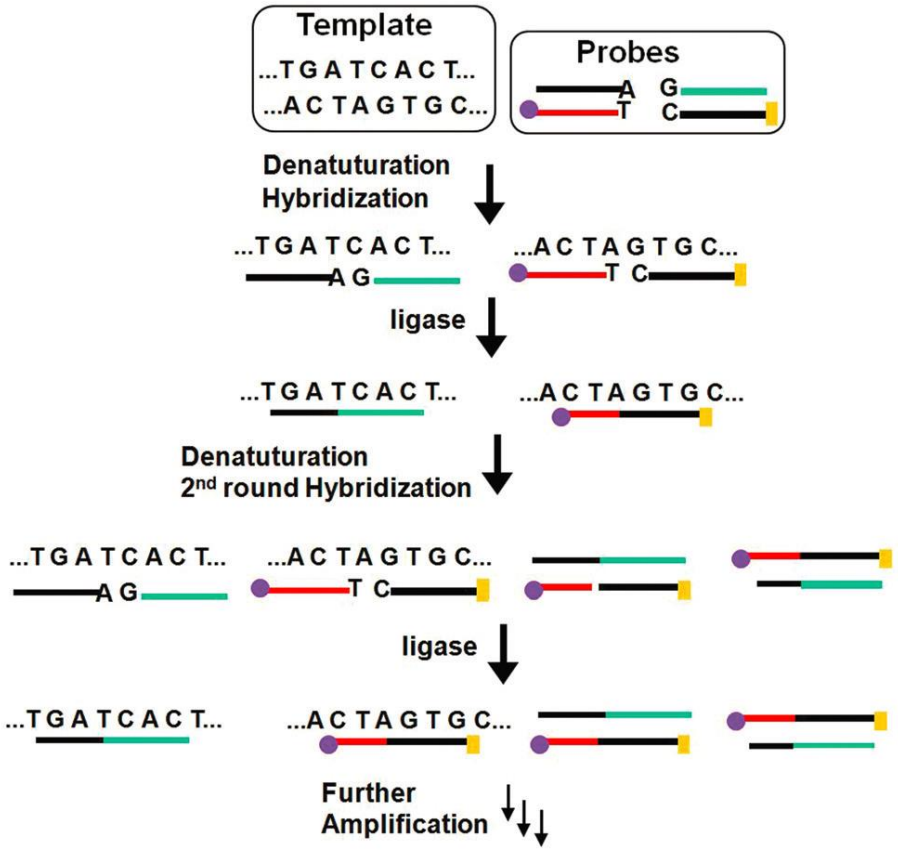

Figure 1-4. Schematic diagram of the ligase chain reaction. First, target DNA are separated by raising temperature to its melting temperature. Second, each strand is then hybridized to two probes which are adjacent to each other. Third, these two probes are ligated by T4 DNA ligase into a longer sequence to form new double-stranded DNA. The target DNA can be amplified through repeating these three steps. Reproduced with permission from ref. 54.

1.4 Isothermal Signal Amplification for Nucleic Acid Detection

Isothermal nucleic acid amplification assays usually work at a constant temperature, alleviating the need for a thermal cycler. The following are two isothermal amplification methods: rolling circle amplification (RCA) [10], and the exponential amplification reaction (EXPAR) [16].

1.4.1 Rolling circle amplification (RCA)

Unlike PCR, which requires thermostable DNA polymerases and a thermal cycler, the Rolling circle amplification (RCA) is a simple and efficient isothermal DNA amplification strategy.[10] Typically, four components are involved in an RCA reaction, including (1) DNA polymerase; (2) a short DNA or RNA primer; (3) a circular DNA template; and (4) deoxynucleotide triphosphates (dNTPs) (building blocks of the RCA product). The rolling circle amplification (RCA) strategy uses a circular DNA 25-100 nucleotides in length that acts as a template for a DNA or an RNA polymerase. Polymerase has exceptional processivity and strand displacement ability. After a short DNA or RNA primer is hybridized to template circular DNA or RNA, RCA can use a unique DNA or RNA polymerase, such as Phi29, Bst, Vent exo-DNA polymerase, or T7 RNA polymerase, to continuously add nucleotides to the primer to develop long single-stranded DNA and RNA at a constant temperature (room temperature to 37 ºC) to achieve isothermal DNA amplification within a few hours. [8-13] (Figure 1-5)

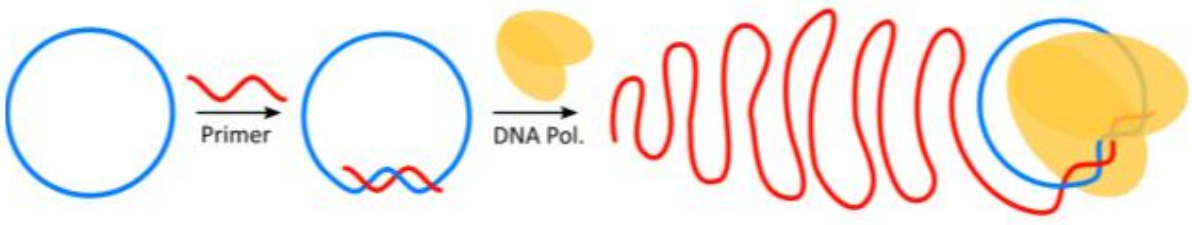

Figure 1-5. Rolling circle DNA synthesis process. *Reproduced with permission from ref. 54.* Copyright © 2016, American Chemical SocietyThe "padlock" probes [14] incorporated with a polymerase in RCA amplification was first introduced in 1998.[15] The padlock probe (labelled with

blue and green ends) is used to detect specific DNAs by using two ends of a padlock to hybridize to target DNAs (Figure 1-6). The target DNA also serves as a ligation template for a padlock to generate the circle by using DNA ligase (Figure 1-6).[15] When a single base in the target strand is mismatched to the probe strand , the mismatch between the probe and target strand can prevent the circularization of the padlock. In the presence of specific target DNA sequences, the target is complementary to the padlock to trigger the generation of circularization of the padlock. RCA is then performed to detect the circular strand to achieve the isothermal DNA amplification.[15]

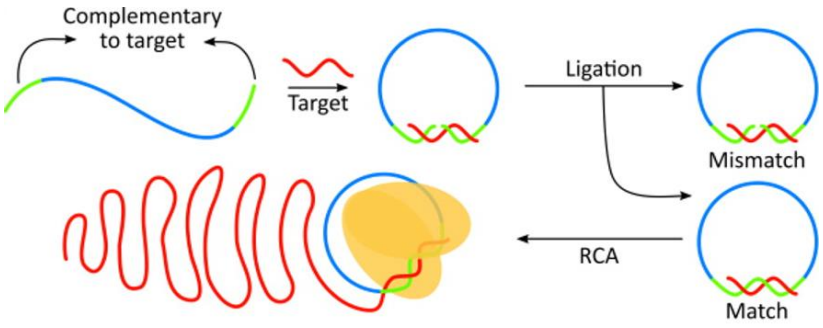

Figure 1-6. Padlock probes. Reproduced with permission from ref. *54*. Copyright © 2016,American Chemical Society.

1.4.2 Exponential amplification reaction (EXPAR)

The exponential amplification reaction (EXPAR) is a highly efficient isothermal DNA amplification method and was developed by Van Ness et al. in 2003.[16] This isothermal molecular chain reaction uses the products of one reaction to catalyze further reactions generating the same products.[16] Two enzymatic processes, polymerase strand extension and single-strand nicking, are involved in EXPAR. EXPAR occurs at 55 ºC, which permits the activity and stability of the DNA polymerase and nicking endonuclease for amplification.[17] A short oligonucleotide, trigger X acting as the analyte, is amplified by this reaction. EXPAR is initiated when trigger X primers (target strand) hybridized with the amplification template X' which contains two complementary sequences X and X', separated by nine bases that are recognized and cleaved by the nicking enzyme (Figure 1-7). After the trigger strands extended by the DNA polymerase have generated a double-

stranded template, the nicking enzyme nicks the extended strand regenerating another trigger oligonucleotide that is displaced from the amplification template. The top strand of trigger producing template is then elongated by DNA polymerase generating another trigger in the same manner. All the generated triggers then act as primers to other amplification templates, achieving the chain reaction.

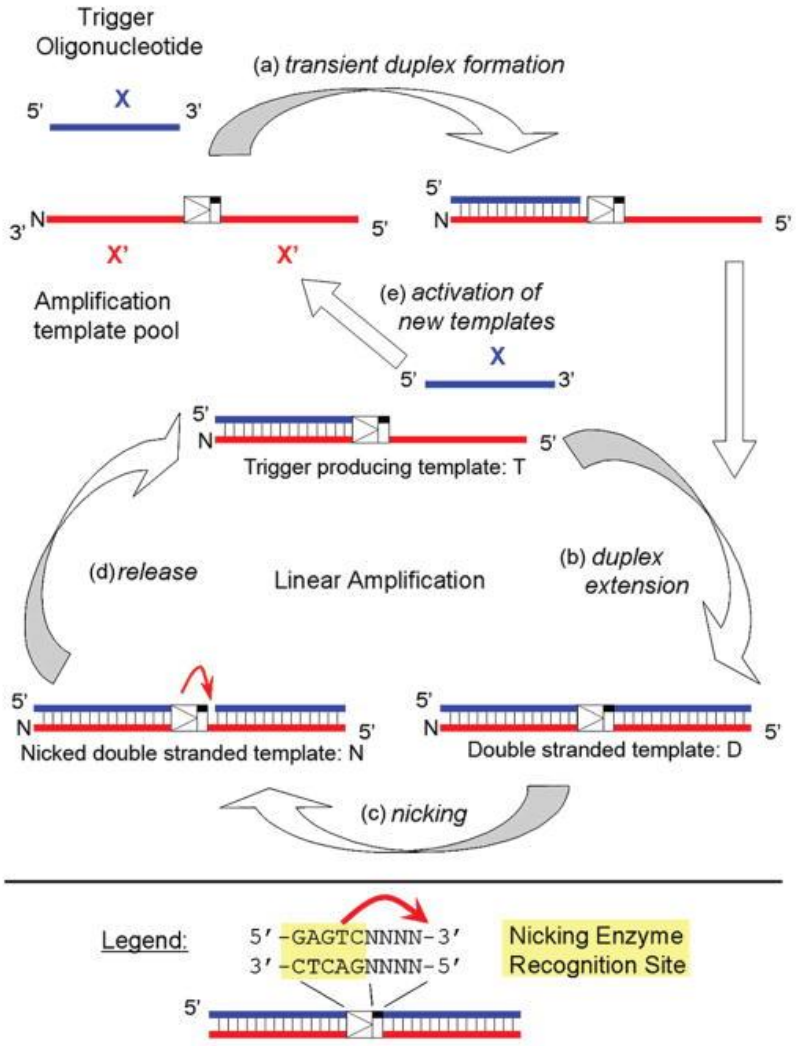

Figure 1-7. Schematic of the exponential amplification reaction (EXPAR). (a) Trigger X hybridizes to the complementary recognition sequence at the 3'-end of the amplification template X'. (b) The trigger X is extended by the DNA polymerase, forming the double-strand containing a nicking enzyme recognition site (5' -GAGTCNNNN- 3') on the top strand. (c) The top strand can

be cleaved using the nicking endonuclease (Nt.BstNBI). (d) By heating the temperature to 55 °C, the newly formed trigger can be released from the amplification template. The trigger producing templates will re-join the linear amplification cycle, and new trigger oligonucleotides are produced through the process of extension, nicking, and release. (e) The newly formed trigger oligonucleotides then activate additional amplification template to exponential amplify trigger X. Reproduced with permission from ref. 6.

1.5 Limitations of existing signal amplification for nucleic acid detection

Both PCR and LCR contain non-isothermal steps during the amplification process including denaturation, annealing, and elongation requiring the heating and cooling cycles. Thus, PCR and LCR use thermocycler to control the increase and decrease of temperature and require special heat-stable DNA polymerase and ligase.[6, 7, 18] To overcome these constraints of PCR and LCR, researchers are interested in developing simple nucleic acid amplification methods that are isothermal. [19, 20] RCA can be performed at a constant temperature between room temperature and 37 ºC to achieve the DNA amplification. [21] But the assay time of RCA often extends to a few hours. [8-13] EXPAR is a simple and efficient isothermal signal amplification method that requires a constant temperature at 55 ºC.[17] The constraint of the EXPAR is its operating temperature, which is higher than the temperature of a cell surface or cell interior in human biological system when applying this method to achieve signal amplification in the complex biological environment.

1.6 Objective

We aim to develop a new strategy to achieve rapid isothermal (37 ºC) signal amplification for detection of nucleic acids through the construction of a three-dimensional (3-D) DNA nanomachine [49]. The nanomachine is essentially a DNA-functionalized gold nanoparticle (DNA-AuNP) that can be operated in the presence of nicking endonuclease. Two types of DNA motifs are used and co-conjugated onto the same AuNP through a salt aging method [24] . One motif is a fluorescently-labeled signal reporter (SR) DNA which contains a nicking cleavage site. The other motif is a 57

nt long single-stranded DNA referred to as a DNA walker (DW) that contains a complementary nicking recognition site. In the presence of the nicking endonuclease enzyme, DW moves along the 3-D AuNP track by hybridizing and subsequently cleaving SRs. Since initially the fluorescence of SR is quenched by the AuNP, the operation of the DNA naonmachine amplifies fluorescence signals. By introducing a protecting DNA probe, P, which can hybridize to the DW, the 3D-DNA nanomachine can be converted to a 3-D nanosensor for specific nucleic acid detection. In the presence of the target, the DW is released through a toehold exchange reaction [23] and then the 3D-DNA nanosensor is converted back to a 3-D DNA nanomachine to amplify fluorescence signals, which can be used to quantify the input target.[49]

Contributions

Xiaolong Yang and Dr. Feng Li conceived and designed the experiments. Xiaolong Yangperformed the experiments and analysed the data. All authors discussed the results and contributed to the preparation and editing of the manuscript.

Chapter 2

Regulation of DNA Strand Displacement using an Allosteric DNA Toehold

2.1 Introduction

The structure of a nucleic acid molecule can be identified by its sequence of nucleotide. The four bases, adenine (A), cytosine (C), guanine (G), and thymine (T) are present in DNA. Nucleic acids have the specificity and predictability of Watson-Crick base pairing, in that two molecules will only bind to each other to form a double helix if the two sequences are complementary, with A only binding to T, and C only binding to G.[24,25] DNA nanotechnology was first introduced by Nadrian Seeman in the early 1980s.[26] In DNA nanotechnology, the bases are rationally designed and manufactured by researchers to develop artificial nucleic acid structures for technological uses.[25, 26] DNA nanotechnologies can be divided into the two overlapping subfields of structural and dynamic DNA nanotechnology. Structural DNA nanotechnology focuses on the construction of two-dimensional and three-dimensional nucleic acid complexes and materials with varying sizes by self-assembly of DNA.[24, 27, 28] In contrast, dynamic DNA nanotechnology focuses on complexes with non-equilibrium dynamics such as the ability to reconfigure rather than on the equilibrium end-states.[34]

This chapter focuses on dynamic DNA nanotechnology using mechanisms of toehold-mediated strand displacement [29], associative toehold-mediated strand displacement [30], and remote toehold-mediated strand displacement [26] to allow the nucleic acid complexes to reconfigure in response to the addition of new nucleic acid strand input. This chapter will show our objectives, regulation of strand displacement by using an allosteric toehold.[32]

2.2 DNA Strand Displacement

DNA strand displacement is the process whereby two strands with partial or full complementarity hybridize to each other to displace one or more pre-complementary strands. DNA strand

displacement can be initiated through a toehold at complementary single-stranded domains and then progressed by a branch migration process.

2.2.1 Toehold-Mediated Strand Displacement

The concept of toeholds was introduced to dynamic DNA nanotechnology by Yurke et al.[35] and was explored in detail by Zhang and Winfree[36] as well as by Yurke and Mills[37]. The process of toehold-mediated strand displacement involves a single-stranded DNA A (input A) reacting with multi-stranded DNA complex X to release a strand B (output B) and a complex Y (Figure 2-1). The toehold-mediated strand displacement reaction is initiated by the binding of toehold domains 3 and 3* to facilitate the generation of multi-stranded complex AX that triggers the domain 2 to undergo branch migration process to release a complex Y and a output B (Figure 2-1 a). One identical sequence displaced by one domain through a series of reversible single nucleobase dissociation and hybridization steps is called branch migration.[33, 34] After the process of branch migration, complex Y is generated and strand B is released. The length and sequence of the toehold domain can be used to predict the kinetics of strand displacement.[36] The range of the value of the second-order rate constant of strand displacement reaction is from 1 $M^{-1}s^{-1}$ to 6×10^6 $M^{-1}s^{-1}$ varying over six orders of magnitude. In Figure 2-1 b, the green curve shows the rate constant for a strong hydrogen-bonding toehold domain with only G/C nucleobases, the red curve shows the rate constant for a less strong hydrogen-bonding toehold domain composed of only A/T nucleobases, and the black curve shows the rate constant for a toehold domain with roughly equal numbers of each base. The grey region reflects the overall range of rate constant values based on the length of toehold domain.[34]

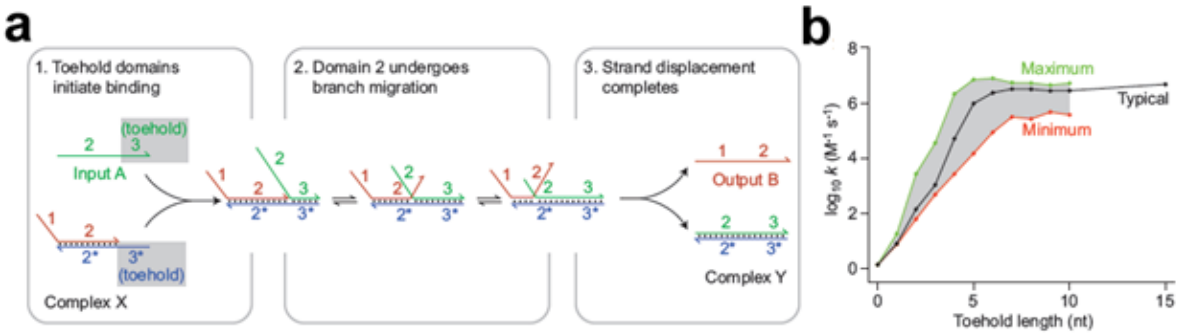

Figure 2-1. Overview of toehold strand displacement. (a) A shows an example of toehold strand displacement reaction. Input A reacts with multi-stranded DNA complex X to release output B and complex Y. (b) Summary of strand displacement rate constant k can be modelled and predicted from the length and sequence of the toehold domain [34] (nt = nucleotide). Reproduced with permission from ref. 34.

2.2.2 Associative Toehold-Mediated Strand Displacement

The associative toehold-mediated strand displacement reaction was first developed by Xi Chen.[30] In contrast to conventional toehold (TH) strand displacement, TH domain was shared same strand with the branch migration (BM) domain, the associative toehold strand is hybridized with the BM strand through hybridized / bulged bases shown as a black region in Figure 2-2. The strand displacement is initiated by the strand of the toehold domain hybridized with the BM strand triggering the generation of the three-way junction[38] complex. Two hybridized/bulged bases at the three-way junction then forward the following strand displacement to release output single-stranded-DNA. The strand displacement reaction can be activated or deactivated by hybridizing the associative toehold to the BM domain. Changing the length of the toehold domain and controlling the three-junction bases (black region in Figure 2-2) allow ~~for the~~ dynamic control of the strand displacement kinetics.

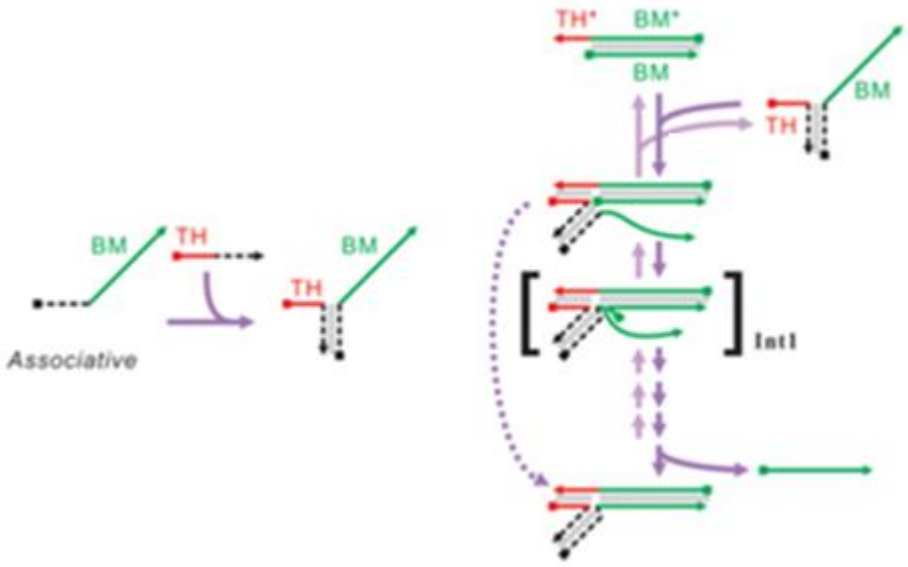

Figure 2-2. Scheme of associative toehold activation and strand displacement. (Left) Hybridization-based associative toehold activation. (Right) Associative toehold-mediated strand displacement across a three-way junction. Reproduced with permission from ref. 30. *Copyright © 2012, American Chemical Society*

2.2.3 Remote Toehold-Mediated Strand Displacement

The remote toehold-mediated strand displacement reaction was first introduced by the Turberfield group in 2011.[31] Compared to conventional toehold-mediated strand displacement, which combines a toehold domain and a BM domain jointly, remote toehold strand displacement uses a spacer to separate the toehold domain and BM domain binding on the same strand, which decouples toehold binding and strand displacement (Figure 2-3). Remote toehold allows additional regulation of strand displacement through tuning of the stiffness of the spacer region. The strand displacement is initiated by the invading strand (I) dockingto the substrate (S) through binding between each remote toehold domain (Figure 2-3). Then, following by an internal diffusion step, the displacement domains align to initiate the BM reaction to displace the target from the substrate. By controlling the hybridization state of the spacer domains, the remote strand displacement rate can be changed by over three orders of magnitude (Figure 2-4). The rate of the displacement

reaction is the highest when both spacers domains are single-stranded. The strand displacement reaction rate can be reduced to two or three orders of magnitude when one or both spacers are rigidly hybridized by extra strands. The strand displacement kinetics can be controlled either by changing the hybridization state or length of the spacer domains or decreasing or increasing the length of the toehold domains.[7, 31]

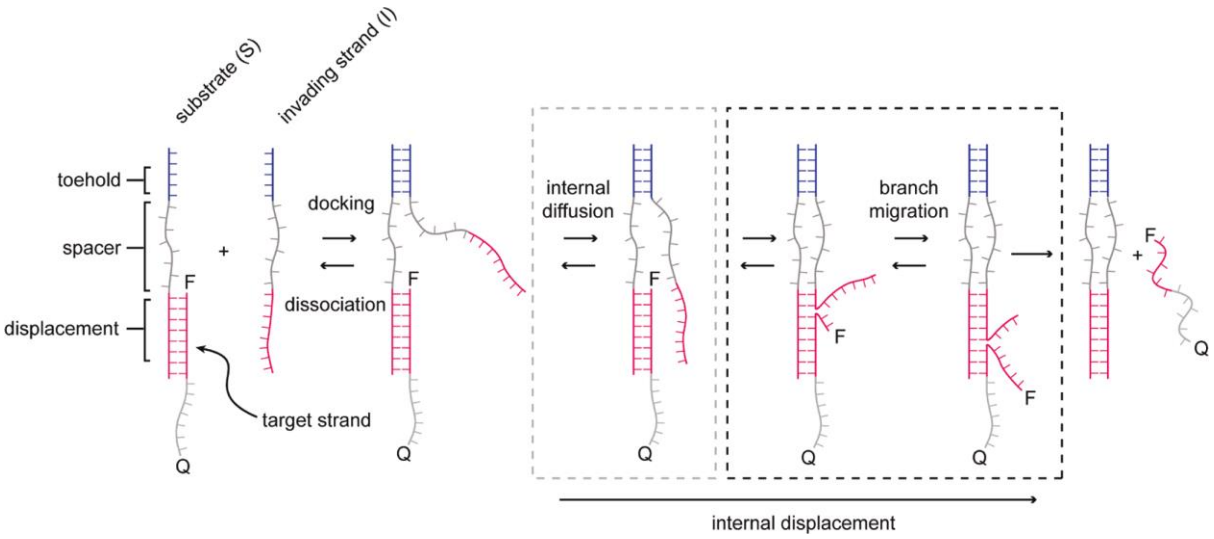

Figure 2-3. Mechanism of the remote toehold-mediated displacement. The target strand was labelled with a fluorophore (F) and a quencher (Q). The target strand is displaced from the substrate (S) by an invading strand (I). The toehold and BM domains on the substrate and invading strands are separated by spacer domains. Docking of the substrate and invading strand through the binding of the toehold domains is followed by an internal diffusion step that enables the alignment of the displacement domains and the BM reaction. The target strand then is displaced from the substrate. The strand displacement is monitored by quenching of fluorescence from the target. Reproduced with permission from ref. 31. *Copyright © 2011, American Chemical Society*

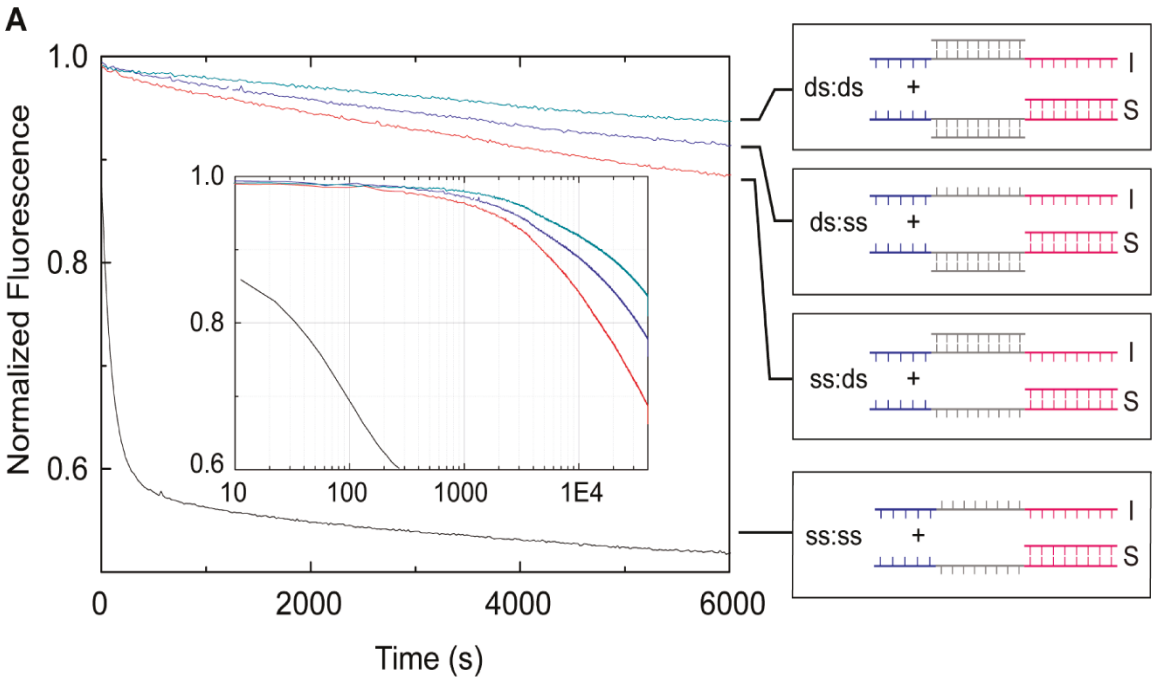

Figure 2-4. Control of strand-displacement rates through control of spacer hybridization. Remote toehold-mediated strand displacement reactions for all combinations of 23 nt single-stranded DNA and double-stranded DNA spacers. Initial concentrations: target strand = 6.6 nM, invading strand = 26 nM, except in the single-stranded (ss)- single-stranded (ss) situation where invading strand = 133 nM. Reproduced with permission from ref. 31. *Copyright © 2011, American Chemical Society*

2.3 DNA Strand Displacement Based Devices

DNA strand displacement reactions can be used to rationally design various devices, including DNA tweezers [39], DNA circuits [34, 40], and catalytic amplifiers [34, 41].

2.3.1 DNA Tweezers

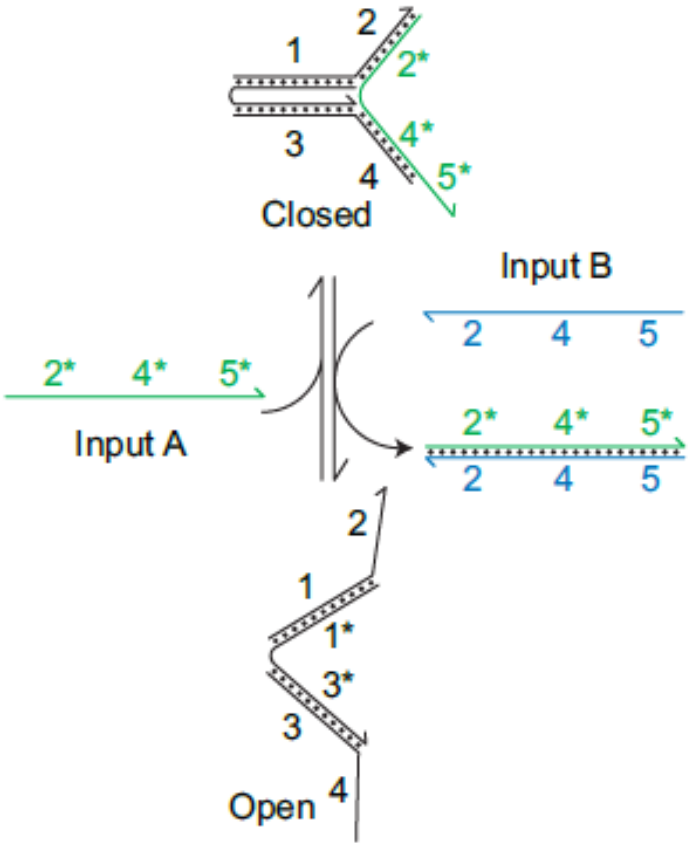

Figure 2-5. DNA tweezers. Domains 2 and 4 of the tweezers are hybridized with input A, changing the configuration of tweezers to a closed state. The binding of toehold domain between 5 on input B and 5* on closed state of tweezer to initiate the strand displacement reaction between the closed- state tweezers (tweezers and input A) and input B, causing the release of open-state DNA tweezers and waste double-stranded by-product (2*-4*-5*/2-4-5). Reproduced with permission from ref. 34.

Yurke et al.[39] were the first to systematically apply toehold-mediated strand displacement in dynamic DNA nanotechnology. Yurke demonstrated a molecular device, DNA tweezers, that uses the same strand of DNA to undergo multiple hybridizations and toehold-mediated strand displacement cycles. In the system, two double-helical arms were connected by a single-stranded flexible hinge that can be repeatedly cycled from an open to a closed state by addition of two

specific single-stranded DNA molecules (Figure 2-5). The domains of 2* and 4* in input A bind to domains 2 and 4 of the open-state tweezers, generating the tweezers in a closed configuration. Input B toehold domain 5 binds to 5* domain of input A, triggering the branch migration process through the binding between two BM domains (2, 4 and 2*, 4*), to displace the tweezers allowing them to relax into an open state. Each full cycle reaction is driven by the formation of additional single-strand DNA (Input A) causing the production of a double strand by-product.

2.3.2 DNA Circuit

In digital logic, the function of an AND logic gate is that output is produced only if two or more of defined inputs are present. An equialent of an AND logic gate can be controlled using toehold-mediated strand displacement reactions. As shown in Figure 2-6, the AND gate was developed by annealing a three single-stranded DNA segment. [34, 40] This three-stranded complex (AND Gate) contains three functional regions, including the toehold recognition region (1), the invading toehold recognition region (2 and 3), and the leaving strand with a bulge loop region (4, 5, and 6). The toehold recognition domain can be binded to the input A toehold domain (1*) through a BM process to generate a double-stranded DNA by-product and activate the secondary toehold recognition domain (3*) on the remaining double-stranded complex. Input B then can hybridize to this double-stranded complex through a same torhold-mediated strand displacement reaction to generate another by-product and output C. Output C can act as another input strand to bind to a downstream complex to carry on the next logic gate. [34, 40]

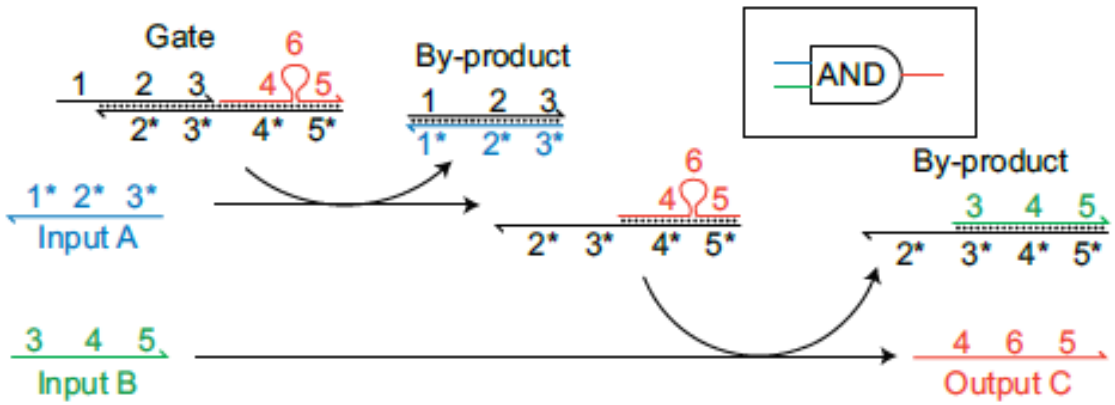

Figure 2-6. AND Logic Gate (Circuit). *Reproduced with permission from ref. 34.*

In a typical AND logic function, an output C is generated if the state of the two inputs A and B are present. No output is generated if only one input or no input is present. Input A hybridizes to the three-stranded complex (gate) to release a waste by-product and active the toehold domain 3* on the remaining two stranded complex. Input B then hybridizes to this complex to release output C and a waste by-product.

2.3.3 DNA Amplification by Non-Covalent Catalysis

One example of DNA amplification by non-covalent catalysis involving cyclic toehold-mediated strand displacement reactions was introduced in 2007 by Yin et al.[41] Input A toehold domain 1 binds to a recognition toehold domain on complex X through a BM reaction to release a single-stranded by-product and generate an intermediate complex containing a secondary recognition toehold domain 5* (Figure 2-7). When addition of input B strand, the second toehold strand displacement reaction can be initiated through the toehold domain binding (5 binds to 5*) to release output A and generate a second by-product. Then output A becomes input A to carry on the next cycle. Input A can catalytically expedite the release of an output A from complex X through two toehold-mediated strand displacement reactions (Figure 2-7).

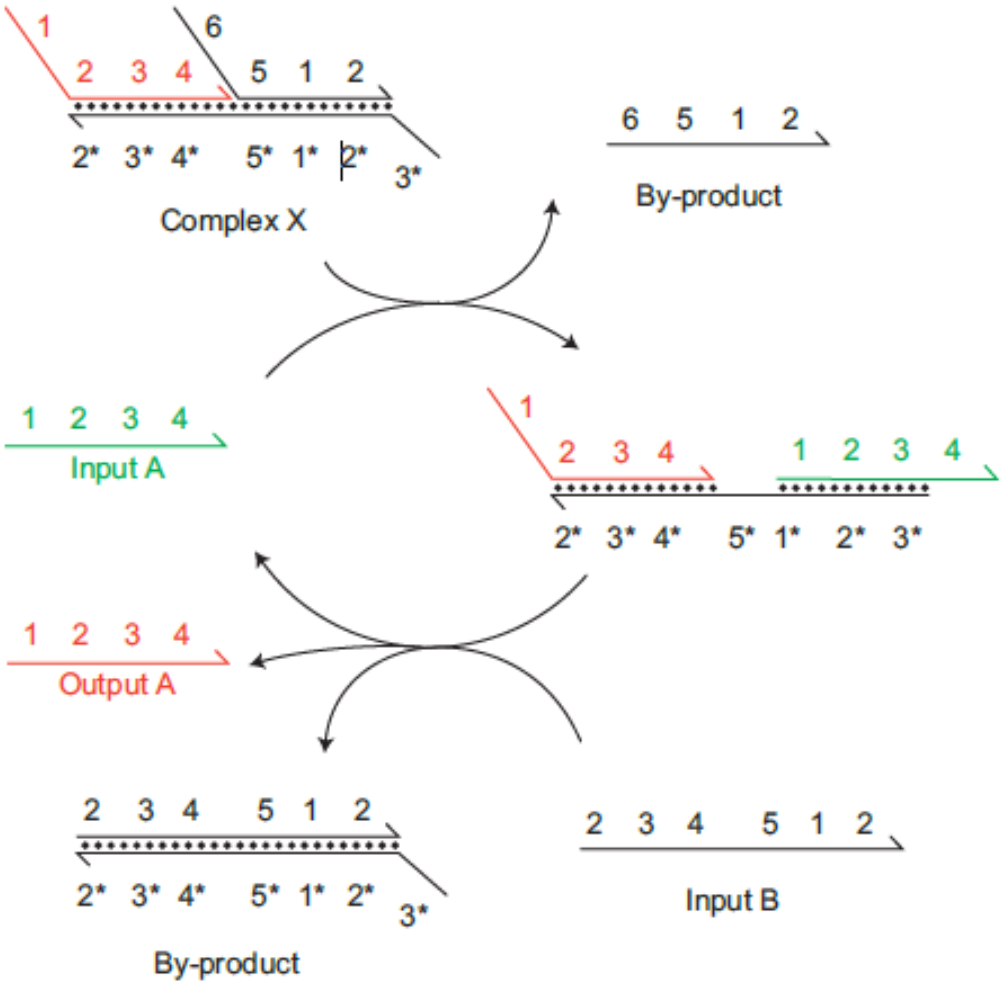

Figure 2-7. DNA Amplification by Non-Covalent Catalysis. Input A catalytically causes the release of an output A (identical to the input) from complex X through the pathway of two toehold-mediated strand displacement reactions. Catalytic cycle was operated by the addition of Strand B and complex X. Output A is released at the end of this reaction and utilized in further catalytic cycles as input A. Reproduced with permission from ref. 34.

2.4 Limitations of Existing Toehold-strand Displacement

Toehold-mediated strand displacement has proven extremely powerful in DNA devices, including reconfigurable structures [39], circuits [34, 40], and amplifications [41]. Construction of devices with multistep, autonomous, as well as complex behaviours requires the controllable activation and regulation of toeholds.

When using the principle of DNA toehold to guide the design and operation of a DNA device, a key mechanism is the controllable activation of a toehold.[34, 39-41] This function is typically achieved by sequestering a toehold into an inter- or intramolecular DNA duplex, which can then be activated by external stimuli and toehold-exchange reactions. [34-39] To construct devices of higher complexity, cascades of toehold-exchange reactions are programmed to recognize complex environmental signals involving multiple input strands. [34-39] Many efforts have been made to enrich the toolbox of strand displacement techniques with alternative approaches for toehold activation. [30-32] For example, Chen described an associative DNA toehold that attached a DNA toehold to a BM domain whenever needed through hybridization, expanding the rule set to control DNA circuits. [30-32]

To simplify the design of complex strand displacement systems with fewer molecular components and to achieve the flexible control over the strand displacement kinetics, it is worthwhile to add new toehold regulation mechanisms to the current strand displacement toolbox.

2.5 Objectives

We aim to design an allosteric DNA toehold (A-toehold) design that allows flexible activation/regulation of DNA strand displacement reactions and continuous control of strand displacement kinetics. The allosteric DNA toehold (A-toehold) design that allows the flexible regulation of DNA strand displacement by splitting an input strand into an A-toehold and branch migration domain. Because of its simplicity, the A-toehold mechanism can be a useful addition to the current toolbox of DNA strand displacement techniques.

2.6 Allosteric Toehold-Mediated Strand Displacement

The allosteric DNA toehold (A-toehold) is designed to flexibly regulate strand displacement by splitting an input strand into an A-toehold and BM domain [32] (Scheme 2-1). As shown in Scheme 2-1, to initiate a strand displacement reaction, A-toehold first reacts with substrate strands (green and blue double-strand) to form a reaction intermediate A-toehold- substrate triplex (green / blue /

red strand), which then reacts with branch migration domain to form branch migration domain complex (purple / green strand) and A-toehold complex (blue / red strand). [32]

Scheme 2-1. Allosteric toehold-mediated strand displacement reaction. Allosteric toehold strand binds to substrate to cause the generation of secondary toehold domain (green strand). BM domain then displaces two double strands through a conventional toehold-mediated strand displacement reaction.

Contributions

Xiaolong Yang and Dr. Feng Li conceived and designed the experiments. Xiaolong Yangperformed the experiments and analysed the data. All authors discussed the results and contributed to the preparation and editing of the manuscript.

Chapter 3

Results and Discussion

Constructing a Three-Dimensional DNA Nanomachine to Achieve Rapid Isothermal Signal Amplification for Nucleic Acid Detection

3.1 3-D DNA Nanomachine for Isothermal Signal Amplification

The key component of our strategy is a 3-D DNA nanomachine. The nanomachine is essentially a DNA-functionalized gold nanoparticle (DNA-AuNP) that can be operated in the presence of nicking endonuclease. Two types of DNA motifs are used and co-conjugated onto the same AuNP through the salt-aging method [22]. One motif is a fluorescently-labelled signal reporter (SR) DNA which contains a nicking cleavage site. The other motif is a long single-stranded DNA termed the DNA walker (DW) that contains a complementary nicking recognition site. In the presence of the nicking endonuclease enzyme at 37 ºC, one DW moves along the 3-D AuNP track by hybridizing and subsequently cleaving the SR one by one, to achieve isothermal signal amplification. Since initially the fluorescence of the SR is quenched by AuNP, the operation of the DNA naonmachine amplifies fluorescence signals (Scheme 3-1).

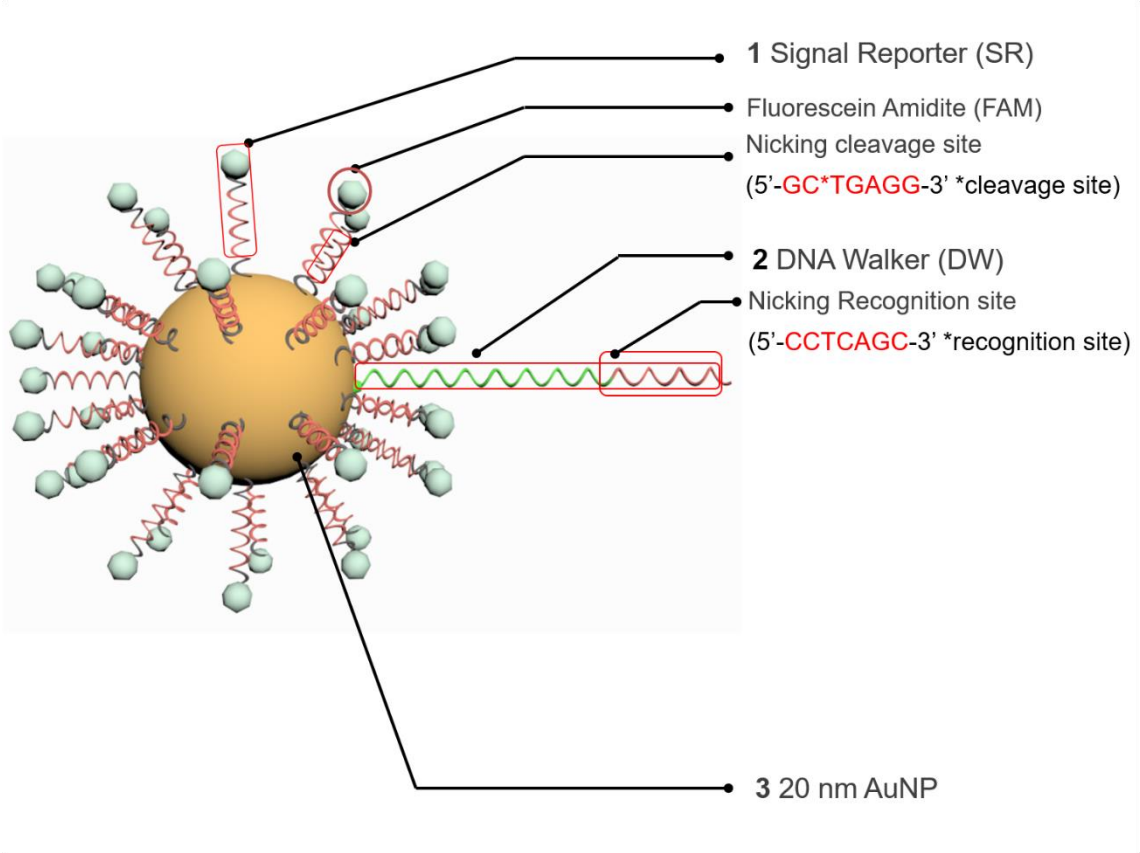

Scheme 3-1. 3-D DNA nanomachine. Signal reporter (SR) contains a nicking cleavage site, 5'-GC*TGAGG-3' on its strand labelled with a fluorescein amidite (FAM). DNA walker contains a nicking recognition site, 5'-CCTCAGC-3'. Signal reporters and DNA walkers are attached on a 20 nm gold nanoparticle (AuNP).

As shown in Scheme 3-2, once SRs are cleaved during DWs movement, SRs can be released from the nanomachine. In principle, our design is particularly advantageous to achieve rapid signal release, because the co-conjugation of all DNA components on the same AuNP can greatly increase their local effective concentrations, thus accelerating the enzymatic cleavage. Moreover, the result of constructing binding-induced molecular translators[23] suggests that the increases in local effective concentrations can also allow for sufficient hybridization between DW and SR before the cleavage (estimated melting temperature T_m = 51.3 °C, ΔG = -4.49 kcal/mol) and rapid dehybridization after the cleavage (T_m < 0 °C, ΔG = 2.77 kcal/mol).

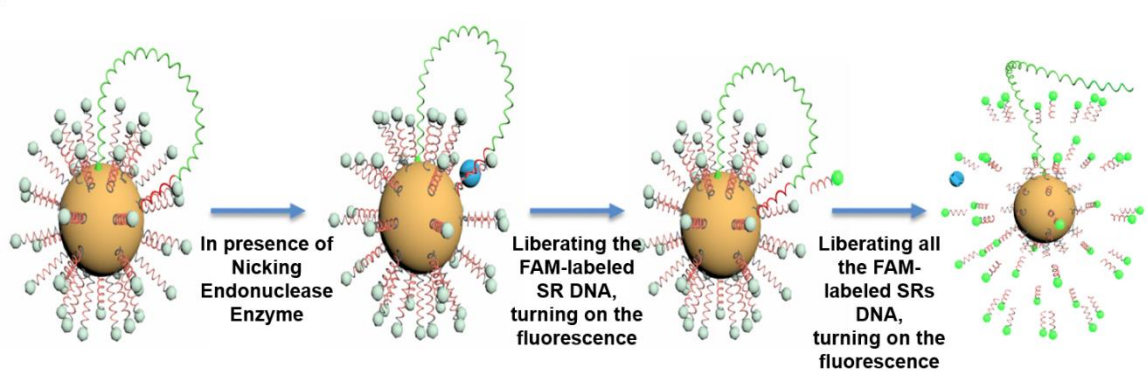

Scheme 3-2. Schematic illustrating the principle of signal amplification achieved by the 3-D DNA nanomachine, which is constructed by co-conjugating DNA walker and SR (substrate) components on a single AuNP. First step, DW binds to SR though the base pairing between nicking recognition site and nicking cleavage site. Second step, nicking enzyme recognizes the formed double-strand recognition-cleavage site. Third step, nicking enzyme cleaves the cleavage site on the SR strand to release SR to generate fluorescent signal. Final step, SRs on DW track are released from the nanomachine to achieve the signal amplification. For actual nanomachine, not only one DW attached on a AuNP.

3.1.1 Construction and Characterization of the 3-D DNA Nanomachine

A 3-D nanomachine is constructed by mixing thioated DWs, thioated fluorescein amidite (FAM) labelled SRs and 20 nm AuNPs through a salt-aging method [24]. The nanomachine attached with DWs and SRs is denoted as DW-SR-AuNP. Initially, The FAM on the SR is in close proximity with AuNP, thus the fluorescence is quenched. Once in the presecne of nicking endonuclease at 37 ºC, each DW moves along the surface of 3-D DNA-AuNP to liberate the FAM-labeled DNAs (SRs), thus turning on the fluorescence to achieve signal amplification (Figure 3-1a). By monitoring the fluorescence increase in real-time, we are able to quantitatively characterize the performance of the 3-D DNA nanomachine.

Figure 3-1 b shows a typical kinetic profile of the DNA nanomachine (DW-SR-AuNP). Immediately after adding 0.2 U/μL (one unit is defined as the amount of enzyme required to convert

1 µg of supercoiled plasmid DNA to open circular form in 1 hour at 37°C in a total reaction volume of 50 µl) nicking endonuclease into a solution containing 100 pM DW-SR-AuNP, a rapid fluorescence increase is observed, which reached saturation within a period of 20 min. The initial rate of the reaction $V_{DW\text{-}SR\text{-}AuNP}$ was measured to be 5.72×10^{-11} Ms^{-1}. This rate was determined by measuring the fluorescence increase every one minute for the first 5 min (Figure 3-1c). To confirm that the rapid fluorescence increase is due to the operation of the DNA nanomachine, we also designed a control DNA-AuNP probe that only contained SR probes (denoted as SR-AuNP). As shown in Figure 3-1 d, little fluorescence increase ($V_{SR\text{-}AuNP} = 3.08 \times 10^{-12}$ Ms^{-1}) was observed due to the spontaneous release of SR by the residual dithiothreitol (DTT) associated with nicking endonuclease (nicking endonuclease orginal stock contained DTT residues from Biolabs). This observation confirms that DW is the key component to driving the quick release of FAM-labeled DNA substrates.

To verify that the DW moves along the 3-D DNA-AuNP surface rather than jumping to cross-react with other nanomachines, we designed a second control by mixing SR-AuNP with an equal amount of a DW-AuNP control that is conjugated with only the DW probe. To ensure the same DW density as for DW-SR-AuNP, DW-AuNP is designed by co-conjugating DW with thiolated poly-dT DNA probes. By comparing the nanomachine with this control (Figure 3-1e), we found that the rate for DW walking on the correct track (5.72×10^{-11} Ms^{-1} for DW-SR-AuNP) was 13.5 times faster than that for DW on the incorrect track (4.24×10^{-12} Ms^{-1} for DW-AuNP control). This means that the large portion of DWs are moving on the correct track over a given time period, suggesting that movement of the DW has been well-defined by the 3-D DNA-AuNP track on each nanomachine.

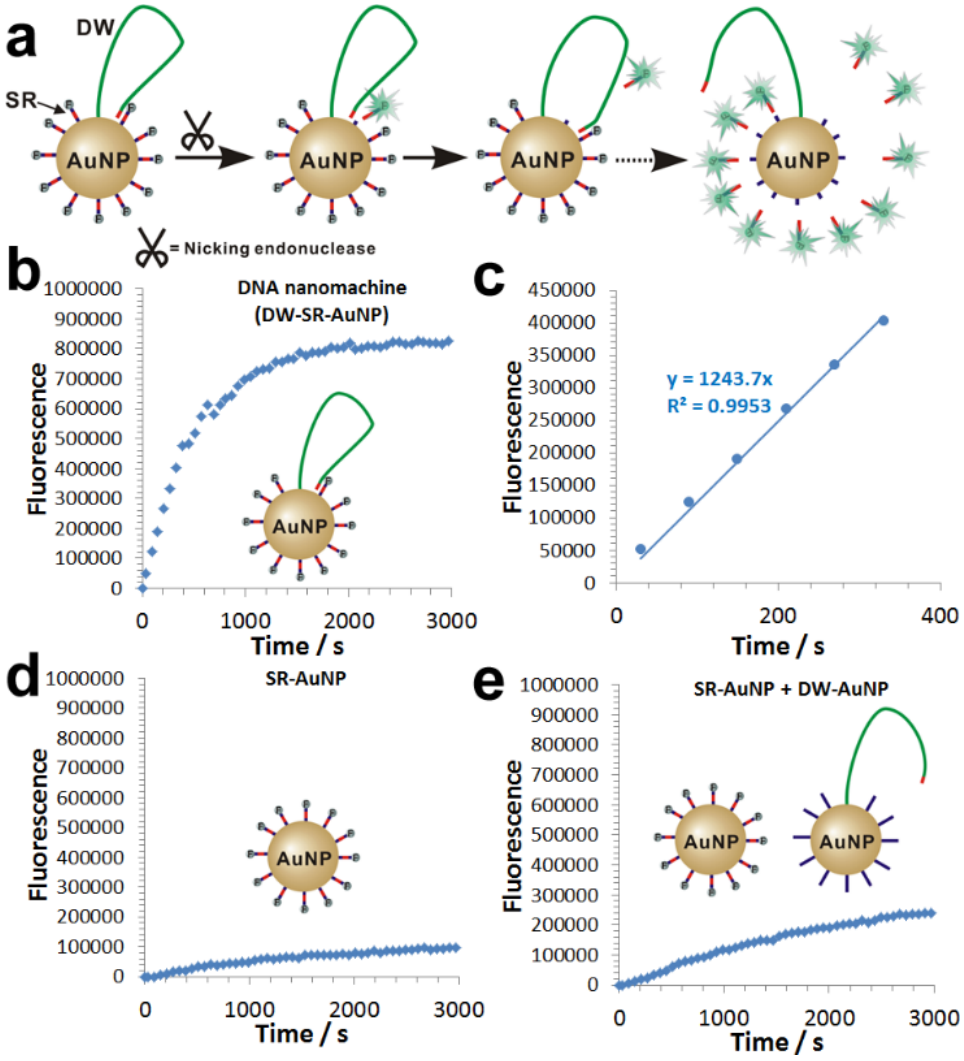

Figure 3-1. Principle of 3-D DNA nanomachine. (a) Schematic illustrating the principle of the fluorogenic 3-D DNA nanomachine, DW-SR-AuNP; (b) Monitoring the fluorescence increase as a function of time from 100 pM DW-SR-AuNP; (c) Determining the initial rate of DW-SR-AuNP by monitoring the fluorescence increase every 1 minute for the first 5 min; (d) Fluorescence increase as a function of time for 100 pM SR-AuNP control; (e) Fluorescence increase for the cross-reaction control that consisted of 100 pM SR-AuNP and 100 pM DW-AuNP.

3.1.2 Kinetic Study of the 3-D DNA Nanomachine towards Efficient SRs Release (Signal Amplification).

Having constructed the 3-D DNA nanomachine, we aim to optimize the design to meet the goal of efficient SR release to achieve rapid isothermal signal amplification. The 3-D DNA nanomachine is a multi-component system and thus each component can potentially have a significant influence on its overall efficiency. To better understand these influences, we quantitatively studied the effect of each component on the kinetics of the nanomachine. Specific parameters include densities of DW (n) and SR (m) on each AuNP, the length of DW (l), and concentrations of nanomachines ($[AuNP]$) and enzyme ($[E]$).

3.1.2.1 Effect of DW Density and Length on each AuNP

We studied the effect of DW design first, including its density on AuNP (n) and length (l). To elucidate the effect of DW density, we maximized the density of SR (~ 400) (method for density of SR measurement described in Chapter 5) on each AuNP and varied the DW density n from 0 to 60 per AuNP. Intuitively, increasing the density of DW should result in a higher reaction rate and release more fluorescence signal. Indeed, this is what we observed when varying n from 0 to 20 per AuNP (Figure 3-2a). When plotting the measured initial rate V versus n in their logarithmic forms, the data points fit a straight line with the slope close to 1, using least square linear regression (Figure 3-2b). The obtained equation, $Log\ (V) = Log\ (n) - 11.5$, can be further converted to $V = 10^{-11.5} \times n$, indicating that, within the limits of experimental error, V is linearly related to n, when $n \leq 20$.

However, when further increasing DW density from 20 to 60 per AuNP, a decrease in reaction rates were observed (Figure 3-2c and Figure 3-3). We suspect that there is interference between DW probes through charge repulsion and steric hindrance when overlapping at the same track region. To test this hypothesis, initial rates of a nanomachine with a shorter DW (l = 42 nt) were measured and plotted against DW density. Because shorter DW will cover a smaller track space, a higher DW density can be used before overlapping one another. In another words, the critical value

of *n*, n_{crit}, *i. e.* the density that enables the maximum initial rate, will shift to a higher value. Indeed, when DW lengths are reduced from 57 nt to 42 nt, n_{crit} shifted from 20 to 40 per AuNP (Figure 3-2d), confirming the critical roles of DW length and density on the performances of the 3-D DNA nanomachine.

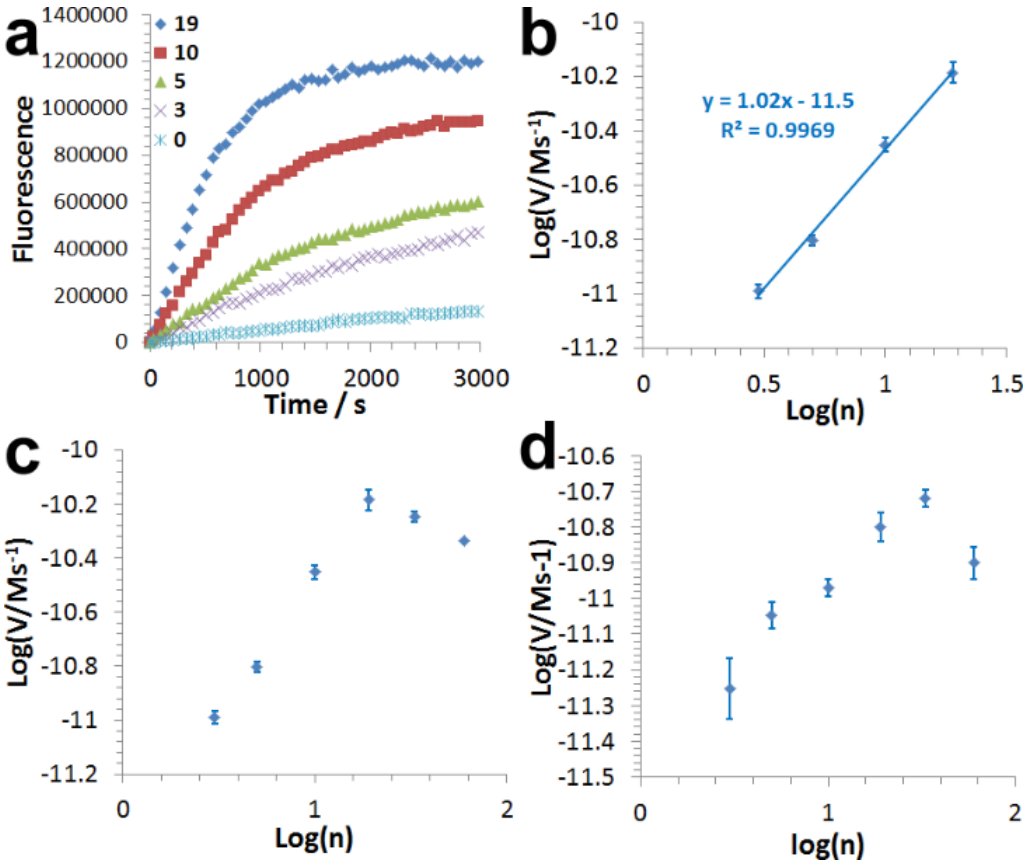

Figure 3-2. Effect of the DW design (density *n* and length *l*) on the kinetics of 3-D DNA nanomachine, DW-SR-AuNP (a) Fluorescence increase as a function of time from DW-SR-AuNP with DW densities *n* varying from 0 to 19 per AuNP; (b) Quantitative relationship between n and corresponding initial rates *V* of DW-SR-AuNP, where n is between 0 and 19, *l* = 57 nt; (c) Quantitative relationship between n and *V*, where n is between 0 and 60, *l* = 57 nt; (d) Quantitative relationship between n and *V*, where n is between 0 and 60, *l* = 42 nt. Error bars represent one standard deviation from triplicate analyses.

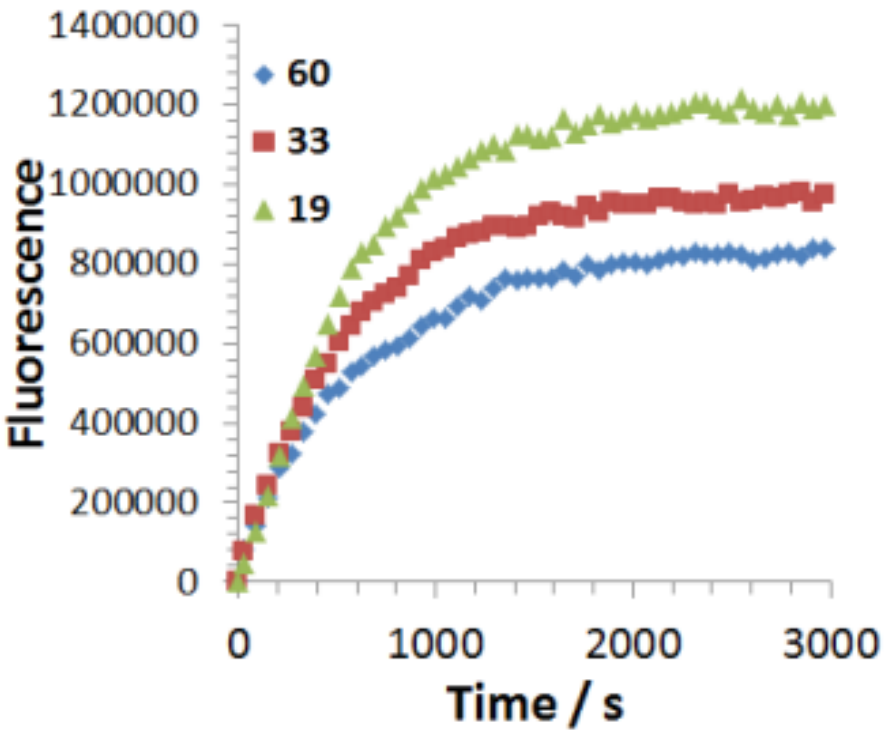

Figure 3-3. Fluorescence increases as a function of time from DW-SR-AuNP with DW densities *n* varying from 19 to 60 per AuNP.

3.1.2.2 Effect of SR Density on each AuNP

SR density is another key factor that can potentially affect the kinetics of the DNA nanomachine. To understand the effect of SR density, we fixed the density of DW to be 20 per AuNP (l = 57 nt) and altered the SR density m from 0 to ~350 per AuNP. As shown in Figure 3-4a, DNA nanomachines of higher SR density release more fluorescent signal. However, increase in SR density does not necessarily lead to a faster initial rate, as shown in Figure 3-4b. When we plotting the measured initial rate V versus SR density m in their logarithmic forms, the data approximately fit a straight line, between m = 10 and m = 163, with a slope of ~0.5 (Figure 3-4c). Increasing m from 163 (about half of the maximum value) to the maximum value does not influence the initial rate (Figure 3-4d), so we could determine a quantitative relationship between V and m as $V \approx 10^{-11.3} m^{1/2}$, ($m \leq 1/2\ m_{max}$).

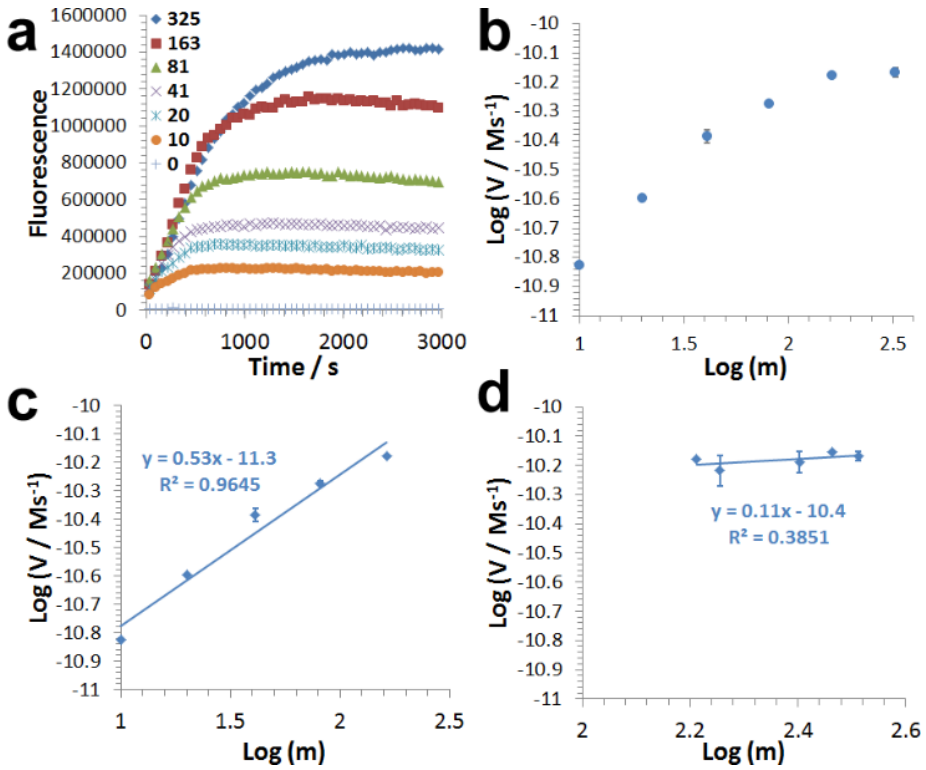

Figure 3-4. Effect of the SR density on the kinetics of the 3-D DNA nanomachine. (a) Fluorescence increase as a function of time for DW-SR-AuNP with SR densities *m* varying from 0 to 325 per AuNP; (b) Quantitative relationship between *m* and corresponding initial rates *V*, where *m* is between 0 and 325; (c) Quantitative relationship between *m* and *V*, where m is between 0 and 163; (d) Quantitative relationship between *m* and *V*, where *m* is between 163 and 325. Error bars represent one standard deviation from triplicate analyses.

3.1.2.3 Effect of the Concentration of Nicking Endonuclease

In addition to DW and SR, we studied the effect of the concentration of nicking endonuclease (Figure 3-5). As shown in Figure 3-5c, the initial rate *V* of the nanomachine is linearly dependent on the concentration of the nicking endonuclease *[E]*, when $[E] \leq 5$ U/100 µl. At $[E] > 5$ U/100 µl, no further increase in the initial rate was observed (Figure 3-5d).

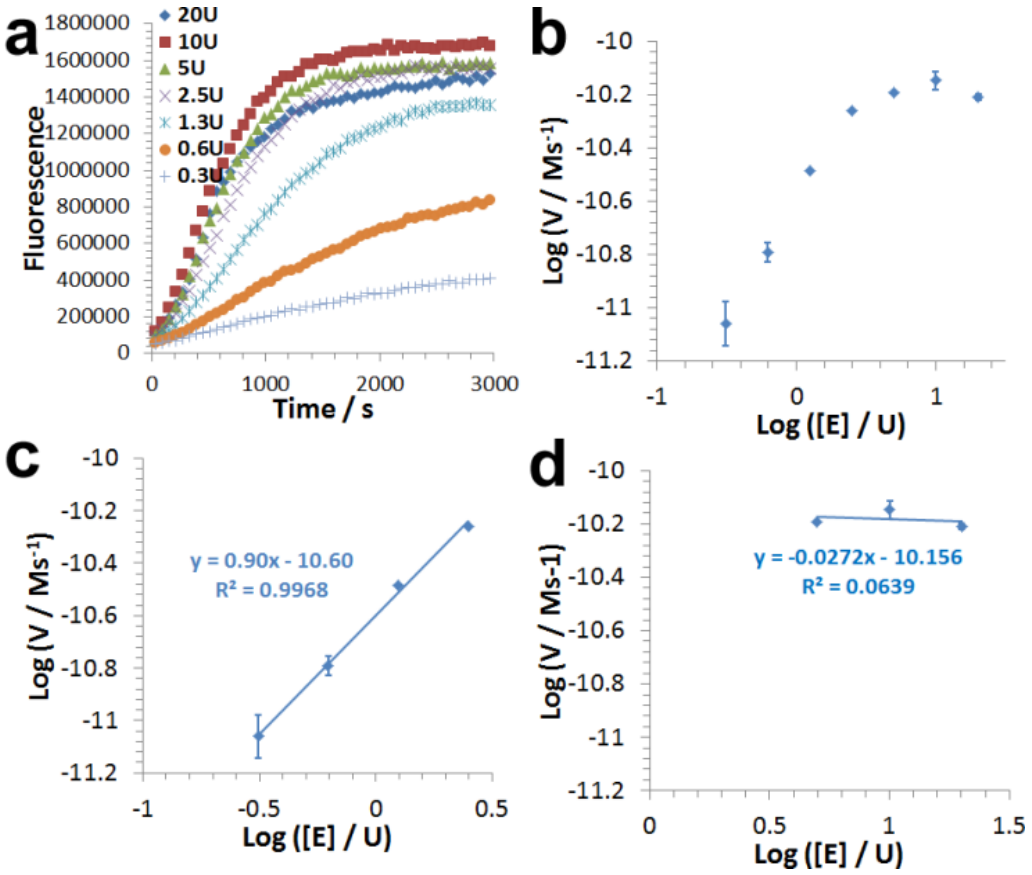

Figure 3-5. Effect of the Concentration of Nicking Endonuclease Concentration effect of nicking endonuclease on the kinetics of 3-D DNA nanomachine, DW-SR-AuNP. (a) Fluorescence increases as a function of time from DW-SR-AuNP with enzyme concentrations *[E]* varying from 0.3 U to 20 U per 100 µL reaction mixture; (b) Quantitative relationship between *[E]* and corresponding initial rates *V* of DW-SR-AuNP, where *[E]* is between 0.3 U and 20 U; (c) Quantitative relationship between *[E]* and *V*, where *[E]* is between 0.3 U and 5 U; (d) Quantitative relationship between *[E]* and *V*, where *[E]* is between 5 U and 20 U. Error bars represent one standard deviation from triplicate analyses.

3.1.2.4 Effect of the Concentration of Individual Nanomachines

As shown in Figure 3-6, *V* is also linearly dependent on the concentration of the nanomachine *[AuNP]* throughout the range tested (6.25 pM to 200 pM). The higher concentration of nanomachines need longer times to achieve the isothermal signal amplification when the amount

of enzyme in the raction is fixed. We aim to develop an isothermal amplification method through the construction of nanomachine to achieve rapid signal amplification. So we did not try the higher concentration of nanomachine in the effect of the concentration of individual nanomachine experiment.

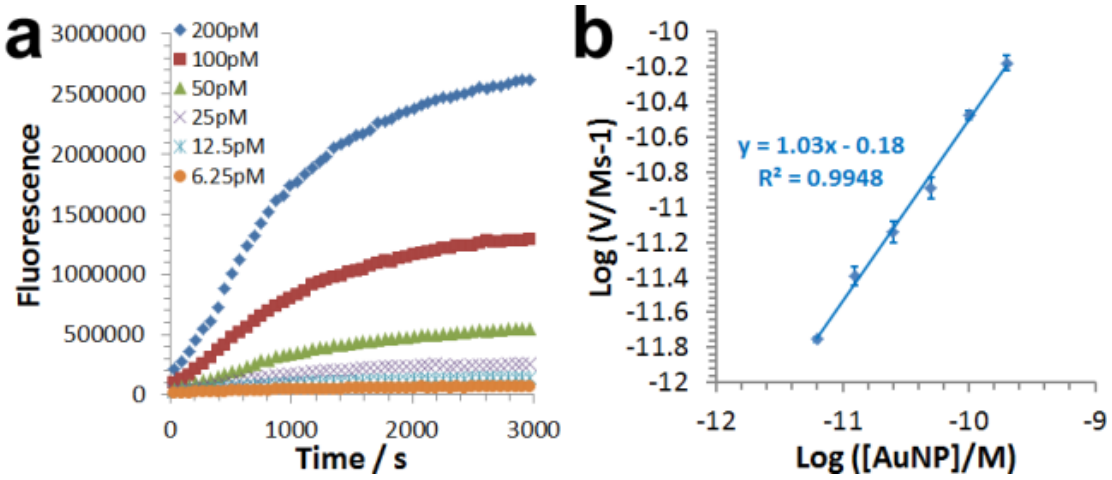

Figure 3-6. Effect of the Concentration of Individual Nanomachines Concentration effect of DNA nanomachine on the kinetics of DW-SR-AuNP. (a) Fluorescence increases as a function of time from DW-SR-AuNP with nanomachine concentrations *[AuNP]* varying from 6.25 pM to 200 pM; (b) Quantitative relationship between *[AuNP]* and corresponding initial rates *V* of DW-SR-AuNP. Error bars represent one standard deviation from triplicate analyses.

3.1.3 Conclusion

We further derived an empirical equation for the overall initial rate to be $V = K \cdot [E] \cdot [AuNP] \cdot m^{1/2} \cdot n$ (*m:* SR density, *n:* DW density), where *K* is a constant, $[E] \leq 5$ U/100 µl, $m \leq 1/2\ m_{max}$, and $n \leq n_{crit}$. This equation suggests that in order to maximize the efficiency for signal release, the density of the substrate on a 3-D DNA nanomachine should be maximized, as well as concentration of enzyme, to their critical values ($m > 1/2\ m_{max}$, $[E] > 5$ U/100 µl). When the values of these two parameters are above their critical values, the initial rate V showed nearly no furter increase (Figure 3-4d and Figure 3-5d). Thus, the empirical equation can be modified to $V = K' \cdot [AuNP] \cdot n$ ($n \leq n_{crit}$),

revealing the critical roles of DW design (both density and length) on the efficiency of signal release.

As the product of *[AuNP]* and *n* is the total fixed concentration of DW, the equation, $V = K' \cdot [AuNP] \cdot n$ ($n \leq n_{crit}$), can be further simplified to $V = K' [DW]$ ($n \leq n_{crit}$). This linear relationship suggests that it is possible to quantify the amount of active DW as a "target" by measuring the initial rate of the nanomachine. On the basis of this principle, we further engineered our 3-D nanomachine into a practically useful nanosensor for amplified detection of target nucleic acids.

3.2 Three-Dimensional DNA Nanosensor

The 3D-DNA nanomachine can be converted to a 3-D nanosensor by introducing a protecting DNA probe, P, which can deactivate the DW, (as shown in the Scheme 3-3) for specific nucleic acid detection. In the presence of the target, the DW can be released, and then the 3D-DNA nanosensor is converted back to 3-D DNA nanomachine to amplify fluorescence signals which can be used to quantify the input target.

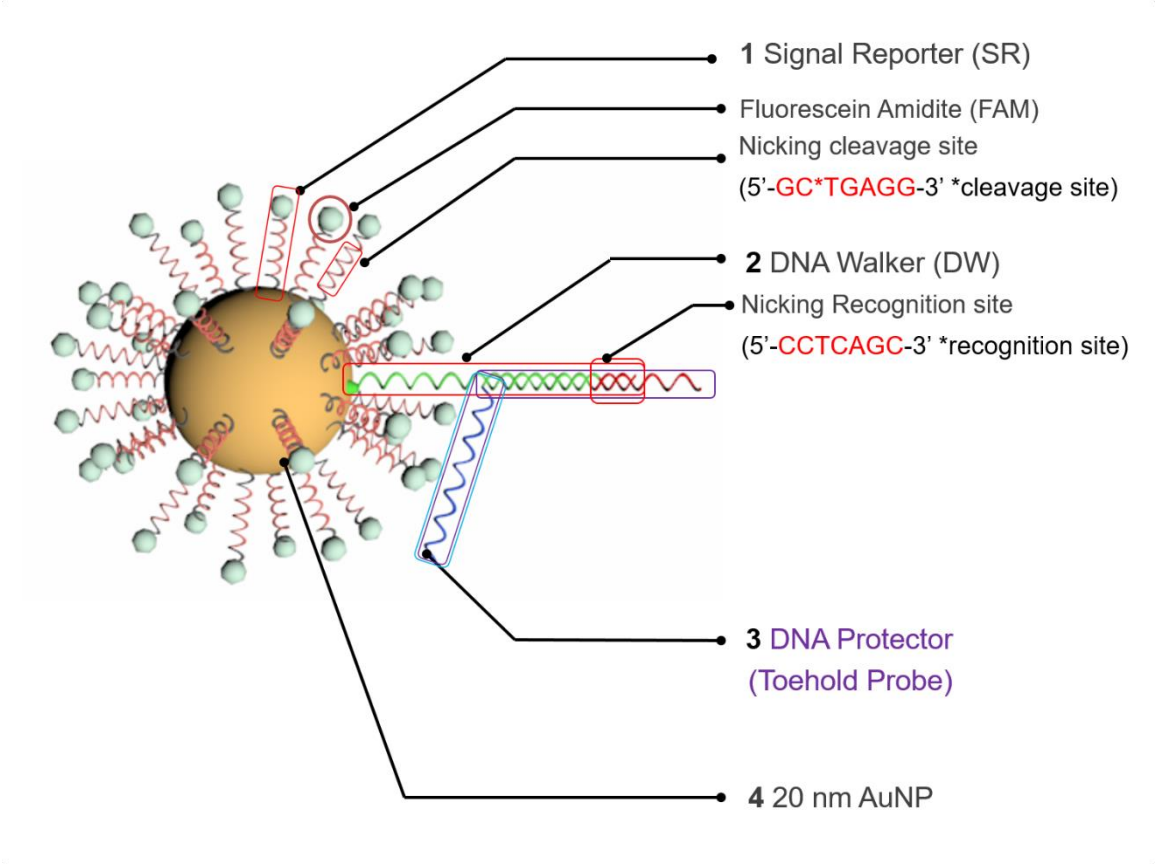

Scheme 3-3. 3-D DNA nanosensor. Signal reporter (SR) contains a nicking cleavage site, 5'-GC*TGAGG-3' on its strand labelled with a fluorescein amidite (FAM). DNA walker contains a nicking recognition site, 5'-CCTCAGC-3' hybridized with a protector DNA. Signal reporters and protected DNA walkers are attached to a 20 nm gold nanoparticle (AuNP).

3.2.1 Engineering the 3-D DNA Nanomachine into a DNA Nanosensor

To convert a 3-D DNA nanomachine into a nanosensor, it is critical to be able to switch on/off the DNA nanomachine in a target specific manner. To achieve this goal, we introduce a protecting DNA probe P that can deactivate the nanomachine by caging the DW through hybridization. As shown in Figure 3-7a, P contains a long complementary region to DW (green and red), including a short DNA sequence (red region) that can partially block the nicking recognition site. P also contains a short DNA overhang (the blue region), which serves as a DNA toehold. In the presence of a target nucleic acid, the target can release P from DW through a toehold exchange mechanism.[23]

Once P is released, the ability of the DNA nanomachine to generate and amplify fluorescent signals is restored. As the active DW in the system corresponds to the amount of target that is used to release P, a quantitative relationship can then be established between initial rates of the nanomachine and concentrations of the input target.

3.2.2 Mechanism of DNA Nanosensor for Amplified detection of Target

To demonstrate proof-of-principle, we chose a sequence from a drug (rifampin)-resistant strain of mycobacterium tuberculosis (MTB) as a target. We then incorporate the target-specific sequence into DW and P. The performance of the MTB specific 3-D DNA nanomachine is shown in Figure 3-7b. The initial rate was measured to be $V = 7.39 \times 10^{-11}$ Ms^{-1} (the method for determination of the initial rate is given in Chapter 5). The introduction of P was found to effectively deactivate the nanomachine to almost background level ($V = 2.46 \times 10^{-12}$ Ms^{-1}, Figure 3-7c). By further investigating the deactivation mechanism, as shown in Figure 3-8, we realized that using P to partially block the nicking recognition site on the DW plays a significant role in obtaining high deactivation efficiency.

3.2.3 Effect of Toehold Length on Probe

The use of the toehold exchange mechanism is key to expanding our sensor to any target sequence of interest because it does not require the target to contain any nicking recognition sequences. To ensure sufficient deactivation of the nanomachine, we fixed the enzyme blocking region to be 5 nt long and varied the toehold length from 5 nt to 10 nt. Previously, Yin and coworkers have demonstrated that a toehold length of 7 nt is sufficient to displace a DNA strand with a 5-nt reverse toehold on the same DNA template for most toehold exchange reactions.[23] We found a similar result when characterizing our toehold exchange probes in a homogenous solution using gel electrophoresis (Figure 3-7d). However, when DW/P duplexes were conjugated onto AuNP, a minimum toehold length of 9 nt was required to trigger a sufficient strand exchange

reaction and restore the activity of the nanomachine (Figure 3-7e), likely due to strong charge repulsion from the dense DNA layer on each AuNP.

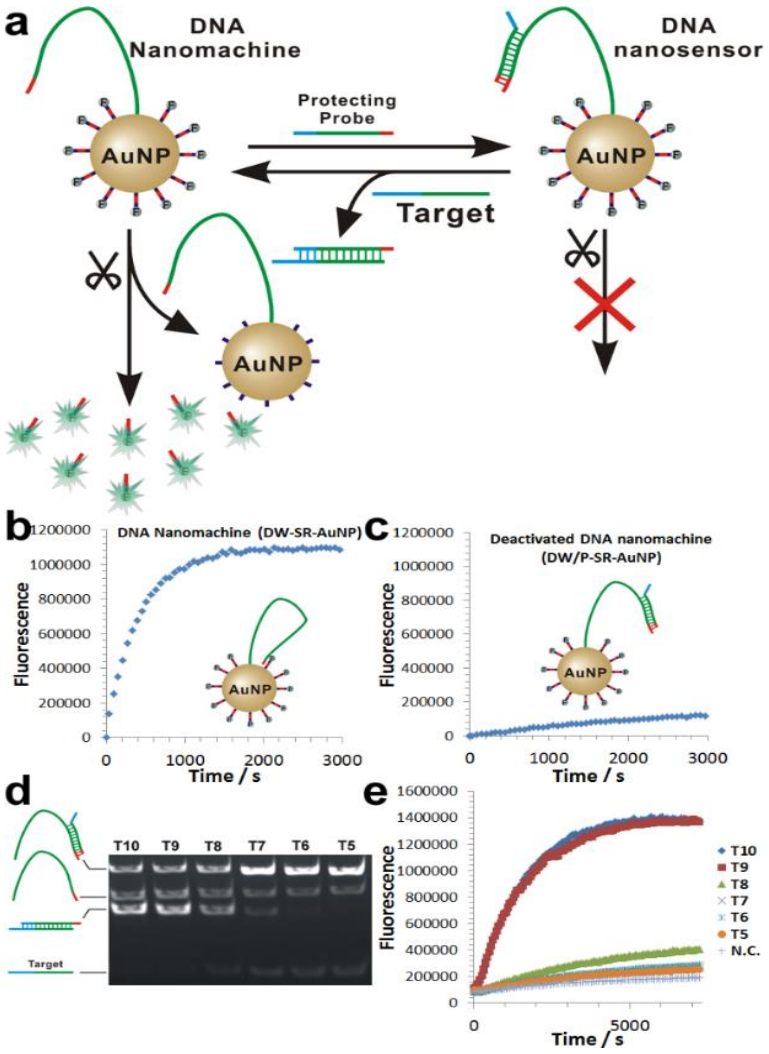

Figure 3-7. Engineering the 3-D DNA Nanomachine into a DNA Nanosensor (a) Schematic illustrating the strategy to convert a 3-D DNA nanomachine into a DNA nanosensor by introducing a protecting DNA design and a toehold-exchange mechanism. (b) Fluorescence increase as a function of time from 100 pM active DNA nanomachine; (c) Fluorescence increase as a function of time when the DNA nanomachine is deactivated by hybridizing DW with the protecting DNA probe (P); (d) Native PAGE characterization of toehold exchange probe designs in solution. Each lane contains 2 µM DW/P duplex and 1 µM target DNA. The toehold length on

P varies from 10 (Lane 1) to 5 (Lane 6); (e) Fluorescence increase as a function of time from a mixture containing 100 pM DNA nanosensors bearing different toehold lengths and 20 nM target DNA.

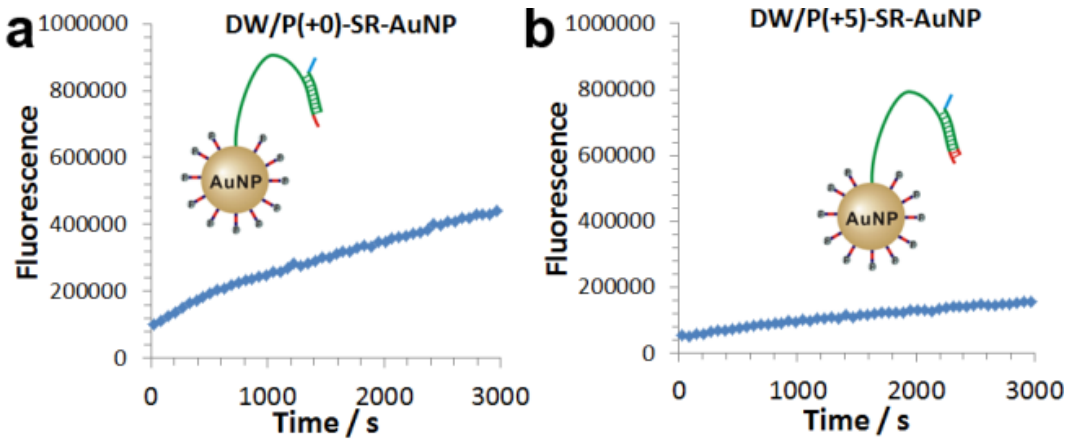

Figure 3-8. Two different protected DNA designs to illustrate the mechanism of protecting DNA on deactivating the 3-D DNA nanomachine. (a) Protecting DNA is designed to hybridize to the DW but does not block any nicking recognition DNA sequence. This protecting DNA is able to slow down the DNA nanomachine by ~ 8 times ($V_{DW/P(+0)-SR-AuNP}$ = 9.43 × 10^{-12} Ms^{-1} versus $V_{DW-SR-AuNP}$ = 7.39 × 10^{-11} Ms^{-1}); (b) Protecting DNA is designed to hybridize to the DW and partially block nicking recognition DNA sequence by 5 nt. This design is able to fully deactivate the DNA nanomachine to a background level ($V_{DW/P(+5)-SR-AuNP}$ = 2.46 × 10^{-12} Ms^{-1}).

3.2.4 Nucleic Acid Analysis using the 3-D DNA Nanosensor

Upon construction of the DNA nanosensor on the basis of the 3-D DNA nanomachine, we then characterized its analytical performance for quantifying the target DNA. In a typical experiment, we first incubated the sensor with the target to regenerate the nanomachine through toehold exchange reactions. As shown in Figure 3-9, this reaction requires only 10 min to restore the activity of the nanomachine.

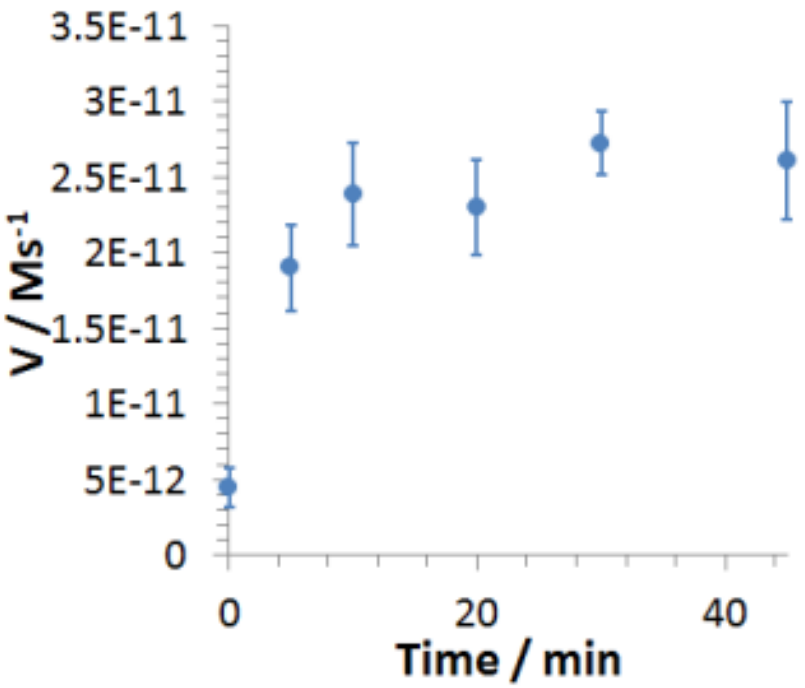

Figure 3-9. Effect of incubation time to restore the activity of the nanomachine. Examine the incubation time that is used to carry out toehold exchange reactions between 20 nM target DNA and 100 pM DNA nanosensor to regenerate the activity of the 3-D DNA nanomachine. Error bars represent one standard deviation from triplicate analyses.

3.2.5 Specificity of Nanosensor

The sensor is also very specific, as shown by the background level of nanomachine activities when incubating with a scrambled DNA control and a control containing 0.1 mg/mL salmon sperm genome DNA fragments (Figure 3-10). Figure 3-10A showed the trend of fluorescence signal of nanosensor mixed with scrambled DNA control (Figure 3-10A) or Salmon sperm DNA control (Figure 3-10B) was almost the same as the blank (only nanosensor) fluorescence signal, revealing the specificity of nanosensor.

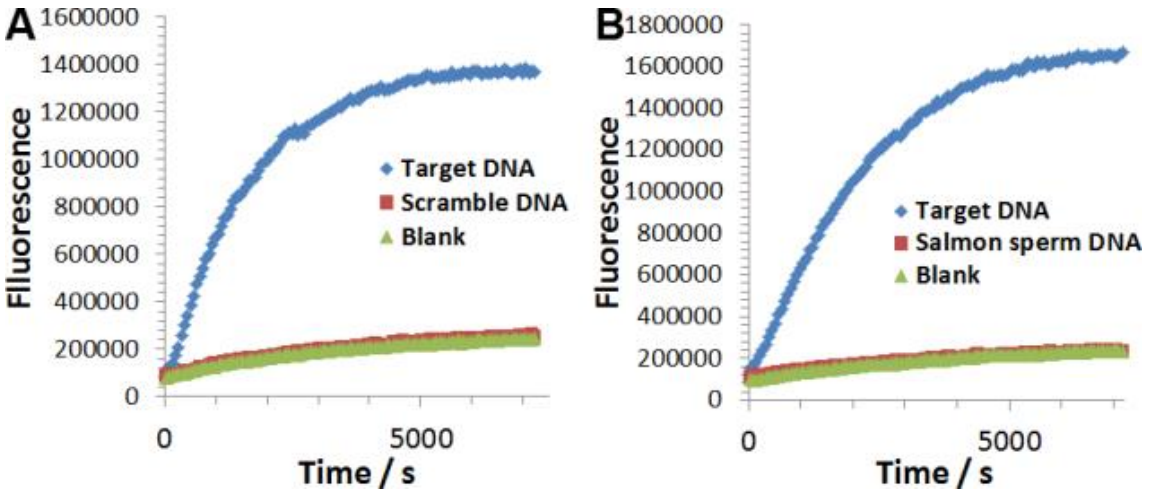

Figure 3-10. Specificity of Nanosensor. Test of specificity of DNA nanosensor by analyzing a scrambled DNA control (A) and a mixture of salmon sperm genome DNA fragments (B). [Target] = 20 nM.

3.2.6 Initial Rate Method for Target DNA Detection

The initial rates of the nanomachines were then measured by monitoring the fluorescence increase every one minute for 5 min after adding nicking endonuclease to power the nanomachine (Figure 3-11a). By plotting the initial rate against target concentration, we were able to detect target DNA across 3 orders of magnitude (5 pM to 5 nM) within 20 min (Figure 3-11b).

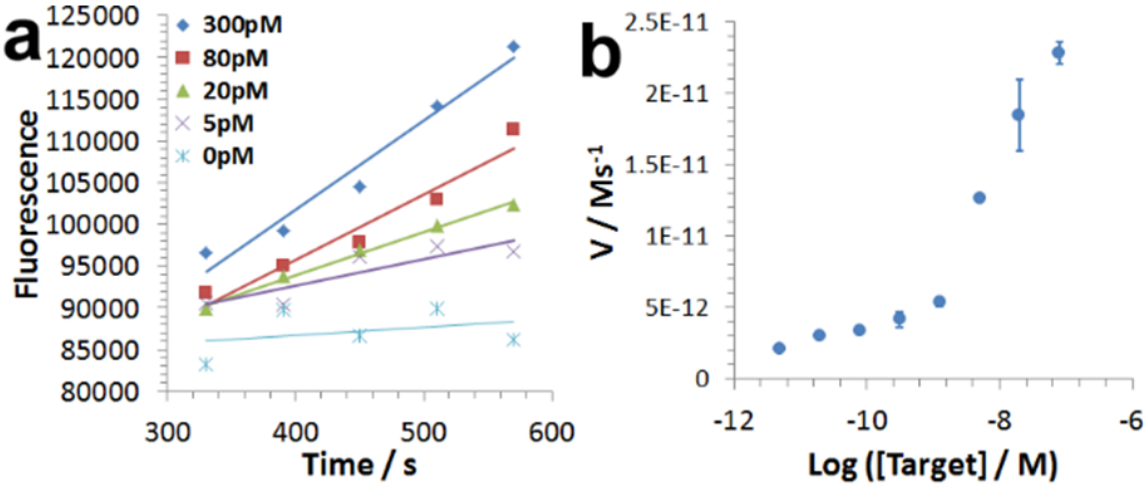

Figure 3-11. Quantification of DNA targets using DNA nanosensors. (a) Determining the initial rate of DNA nanosensors in the presence of target at varying concentrations; (b) Initial rate of DNA nanosensors as a function of target concentration varying from 5 pM to 80 nM;

3.2.7 Endpoint Method for Target DNA Detection

In addition to using the initial rate to detect target DNA, it is also possible to make use of the final fluorescence increase from the sensor to quantify targets (Figure 3-12c). As shown in Figure 3-12d, by running 100 pM nanomachine sensors with the target at varying concentrations at 37 °C for 1 hr, we were able to push the detection limit to 300 fM. This detection limit could be further improved to 75 fM by using sensors of a lower concentration (50 pM) to minimize the background fluorescence (Figure 3-12). A longer reaction time (e.g., 2 hrs) was also required to achieve this better detection limit.

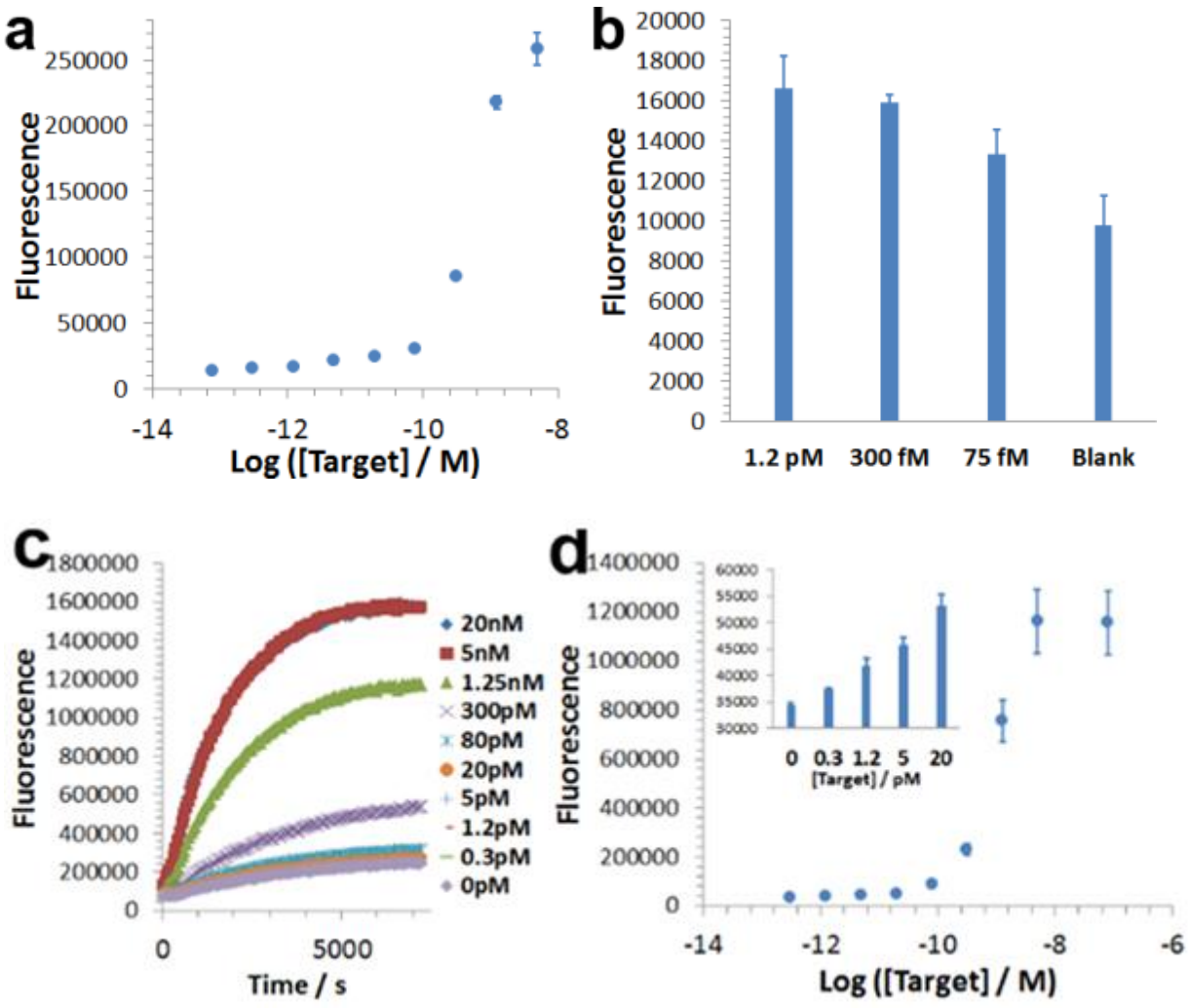

Figure 3-12. (a) and (b) Endpoint Method for Target DNA Detection Quantification of MTB target DNA using 50 pM DNA nanosensor and end-point fluorescence measured at 2 hr. (c) Real-time monitoring of fluorescence increase of DNA nanosensors in the presence of targets over a period of 2 hrs; (d) Quantification of targets using end-point fluorescence measured at 1 hr. Error bars represent one standard deviation from triplicate analyses. Error bars represent one standard deviation from triplicate analyses.

3.2.8 Single Base Mutation Differentiation

By further tuning the lengths of the reverse toehold on the DW/P duplex from 5 nt to 10 nt while fixing the forward toehold length to be 9 nt, we were able to differentiate the target DNA from a

control sequence that is identical to the target except for bearing a single point mutation (Figure 3-13). Figure 3-13A showed the effect of reverse toehold length on the initial rates of DNA nanosensors in the presence of 20 nM target DNA or 20 nM control sequence that is identical to the target except for a single point mutation when forward toehold is fixed at 9 nt. As shown in Figure 3-13B, there are clearly fluorescence signal differences between DNA nanosensors containing 10-nt reverse toehold in the presence of 20 nM target DNA (blue curve) and 20 nM mutation control (red curve), revealing the ability of the DNA nanosensor to detect single point mutation of DNA target.

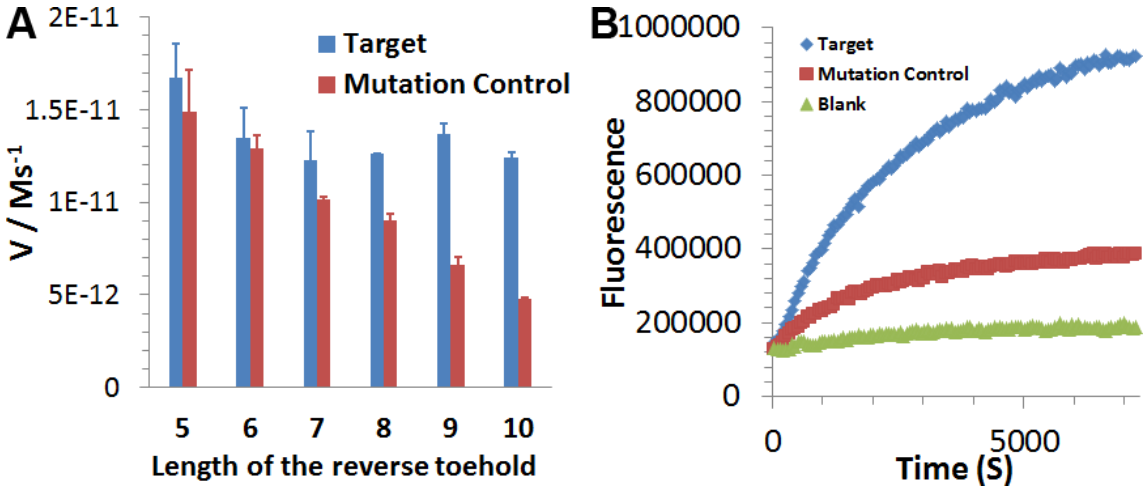

Figure 3-13. Tuning the length of the reverse toehold to achieve the detection of single point mutation of DNA target using DNA nanosensors. (A) Effect of reverse toehold length on the initial rates of DNA nanosensors triggered by 20 nM target DNA or 20 nM control sequence that is identical to the target except for a single point mutation. The length of the forward toehold is fixed at 9 nt. (B) Real-time monitoring the fluorescence increase from 100 pM DNA nanosensors containing 10-nt reverse toehold in the presence of 20 nM target DNA (blue curve), 20 nM mutation control (red curve), or blank (green curve).

3.2.9 Detection of Target DNA in Complicated Mixture

We also tested the ability of our sensor to detect target nucleic acids from a complicated sample matrix by spiking targets of varying concentrations into human serum samples that have been

pretreated with proteinase K. As shown in Figure 3-14, when the signal from the blank is substracted, the sensors are functional in 10-fold diluted human serum samples and a detection limit of 20 pM was achieved. However, it is very challenging to directly quantify target nucleic acids from undiluted serum samples due to the high background signal. To address this challenge, we integrated a 20-min commercially available serum DNA extraction step into our assay. This step eliminated all matrix effects and allowed us to detect target as low as 20 pM directly from undiluted human serum samples (Figure 3-15).

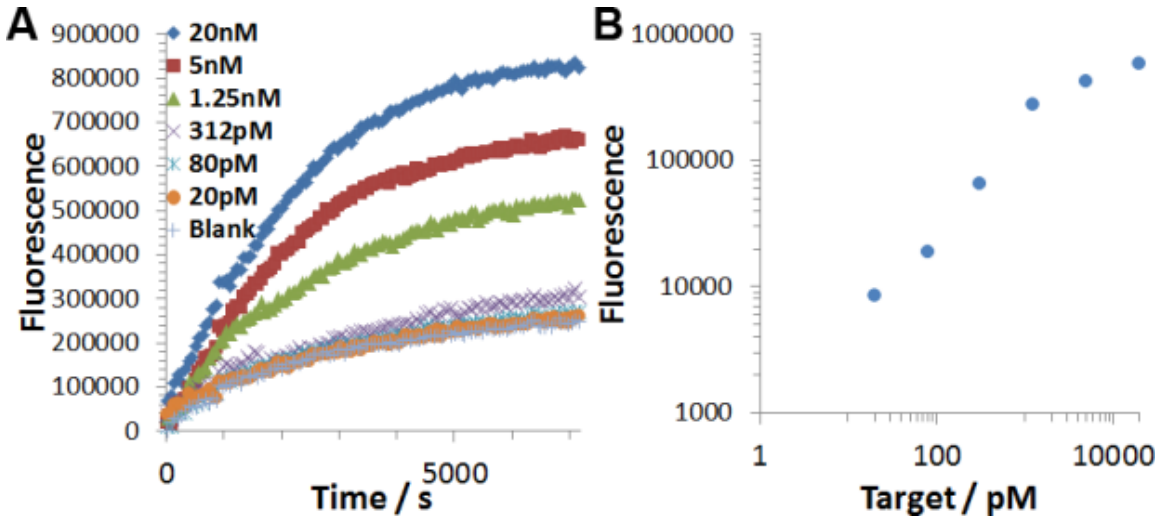

Figure 3-14. Detection of target DNA from 10-fold diluted human serum samples (a) Real-time monitoring of fluorescence increases of DNA nanosensors in the presence of varying concentrations of target DNA spiked in 10-fold diluted human serum samples; (b) Quantification of targets using end-point fluorescence measured at 1 hr (with blank value subtracted).

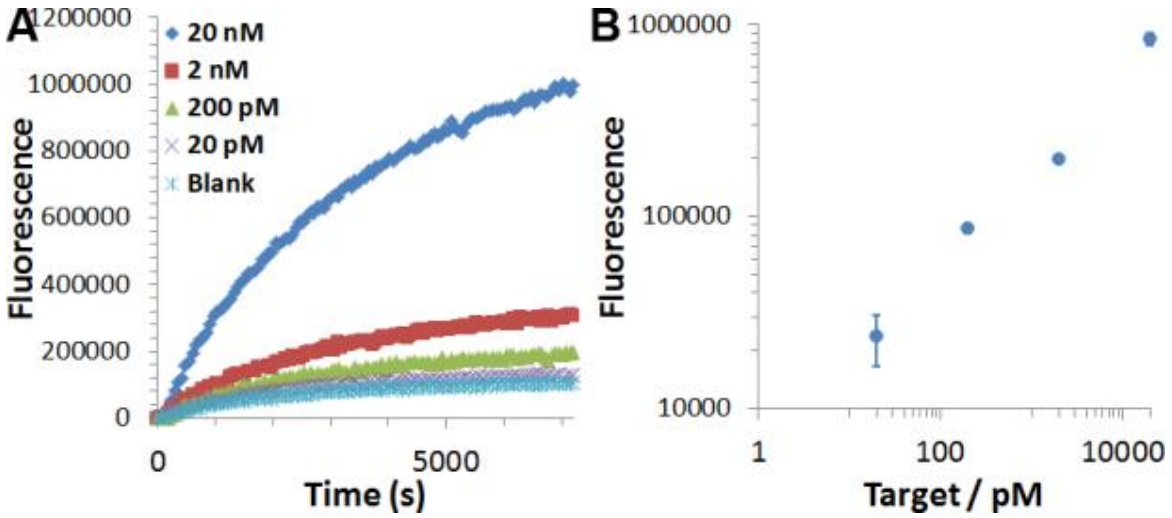

Figure 3-15. Detection of target DNA from undiluted human serum samples. Serum circulating DNA isolation kit was used to isolate and preconcentrate DNA components from human serum samples containing varying concentrations of target DNA. DNA nanosensors were then used to quantify target DNA molecules from preconcentrated samples. (a) Real-time monitoring of fluorescence increase for reaction mixtures as a function of time. (b) Quantification of targets using end-point fluorescence measured at 1 hr (the blank value has been subtracted). Error bars represent one standard deviation from triplicate analyses.

3.3 Conclusions

Polymerase chain reaction (PCR) and ligase chain reaction (LCR) ~~that~~ are powerful signal amplification techniques but require a thermal cycler, RCA is a thermal-cycler-free isothermal signal amplification technique, but requires a long assay time. Exponential amplification reaction (EXPAR) is a rapid and efficient isothermal signal amplification technique but operates not at biological system temperatures. Our enzyme-powered DNA nanomachine is a rapid and highly efficient signal amplification technique that operates at 37 ºC. The co-conjugation of all DNA components on a single AuNP ensures a well-defined space for DNA walking. The corresponding increases in local effective concentrations of DNA probes also accelerated enzymatic cleavage, making the 3-D DNA nanomachine amenable for the task of rapid signal release. The concept of

integrating multiple functional components on a single nanoparticle has also made it easier to expand the functionality of the nanomachine. For example, we have successfully tailored it into a highly sensitive and rapid nanosensor for the specific nucleic acid target by incorporating a toehold-exchange mechanism. Our success in designing the 3-D DNA nanomachine and subsequent nanosensor opens new concepts and strategies in isothermal signal amplification technique, as well as dynamic DNA nanotechnology, which may lead to the development of novel DNA nanodevices and biosensors.

3.4 Future Work

This section provides an overview of the remaining challenges in applying the new isothermal signal amplification method through the construction of DNA nanomachine to detect different targets, like microRNAs.

Constructing a DNA nanosensor for microRNA detection:

Previous probe of DNA nanosensor is designed for detection of MTB DNA target. MicroRNA is a small non-coding RNA molecule with length of about 22 nucleotides found in some viruses, that functions in regulation of gene expression. [52-53] We want to design new microRNA probes to deactivate its corresponding DWs (microRNA DNA Walker)on nanomachine. For this reason, developing new microRNA probes for microRNA is of high importance for future work.

Chapter 4

Results and Discussion

Regulation of DNA Strand Displacement using an Allosteric DNA Toehold

4.1 Allosteric Toehold Principle

Scheme 4-1B shows the principle of an A-toehold. Unlike the conventional DNA toehold that has been combined with the BM domain on the same strand (Scheme 4-1A), the A-toehold sequence is designed into a regulator strand R which is independent of the BM domain (Table 4-1). R contains a toehold motif (domain 1*) and a short (e.g., 7 nt) BM motif (domain 2*), whereas the input DNA X contains only the BM domain (domains 2 and 3). To initiate a strand displacement reaction, R first reacts with CP to form a reaction intermediate CPR triplex, which then reacts with X to form XC and RP (Scheme 4-1B). The overall A-toehold mechanism can be expressed as the following reactions:

$$\text{Reaction 1: } CP + R \leftrightarrow CPR$$

$$\text{Reaction 2: } CPR + X \rightarrow XC + RP$$

The net reaction of the A-toehold system is:

$$X + CP + R \rightarrow XC + RP$$

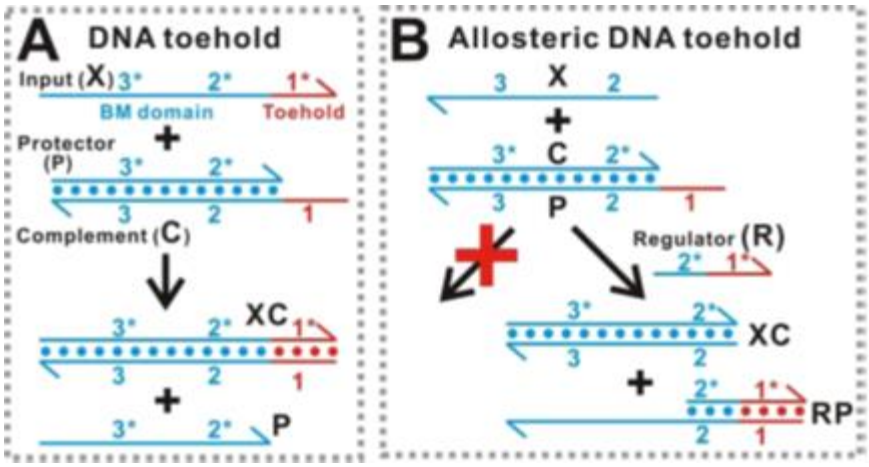

Scheme 4-1. Principles of Toehold-Mediated DNA Strand Displacement (A) and Allosteric Toehold-Mediated DNA Strand Displacement (B)

Table 4-1. Domain Sequences

domain	Sequence (5' to 3')	Length (nt)
1	GTCTCTC	7
2	AAGCGTG	7
3	TATCCCATGTGTCA	14
5	GACAGTC	7
1*	GAGAGAC	7
2*	CACGCTT	7
3*	TGACACATGGGATA	14
3a	TATCCCAT	8
3b	GTGTCA	6
3a*	ATGGGATA	8
3b*	TGACAC	6
5*	GACTGTC	7

Although the free energy of the hybridization between R and CP (reaction 1) is negative, the reaction is reversible and unfavourable when the concentration scale of R is low, as the number of reactants is higher than that of products. However, upon the formation of the CPR triplex, the invading region of R (domain 2*) exposes a short segment of C (domain 2*) that serves as a secondary toehold to drive the strand-exchange between X and CPR (reaction 2), facilitating the net reaction. The A-toehold design separates the toehold domain (R) from the BM domain (X) and thus allows for the independent manipulation of each domain.

4.1.1 Enabling A-Toehold-Mediated Strand Displacement Using Mg^{2+}

Experimental conditions were determined that enable the operation of A-toehold-mediated strand displacement reactions by using a strand displacement beacon. The displacement beacon was made by labelling C and P with a fluorophore and a quencher, respectively (Figure 4-1A). Strand displacement reactions can thus be monitored in real-time by measuring fluorescence signals generated by the beacon. As shown in Figure 4-1B, no obvious strand displacement was observed between CP and X in TE (Tris-EDTA buffer) buffer with 0 mM Mg^{2+}, suggesting that the overall reaction was likely to be limited by reaction 1. We then found that it is possible to overcome this thermodynamic barrier and activate A-toehold-mediated strand displacement by stabilizing CPR triplex using divalent metal cation Mg^{2+}. This result may suggest that the folding of CP and R into the CPR triplex structure brings negatively charged phosphate groups into close proximity, which is destabilizing unless electrostatic repulsion is reduced by Mg^{2+}. [50] Moreover, the effect of Mg^{2+} is concentration dependent and the rate of strand displacement increases when varying [Mg^{2+}] from 5 mM to 100 mM (Figure 4-1B). The kinetic enhancement saturated when [Mg^{2+}] reached 100 mM. TE buffer containing 100 mM Mg^{2+} was then used for all other experiments to ensure that Mg^{2+} was not a rate-limiting reagent.

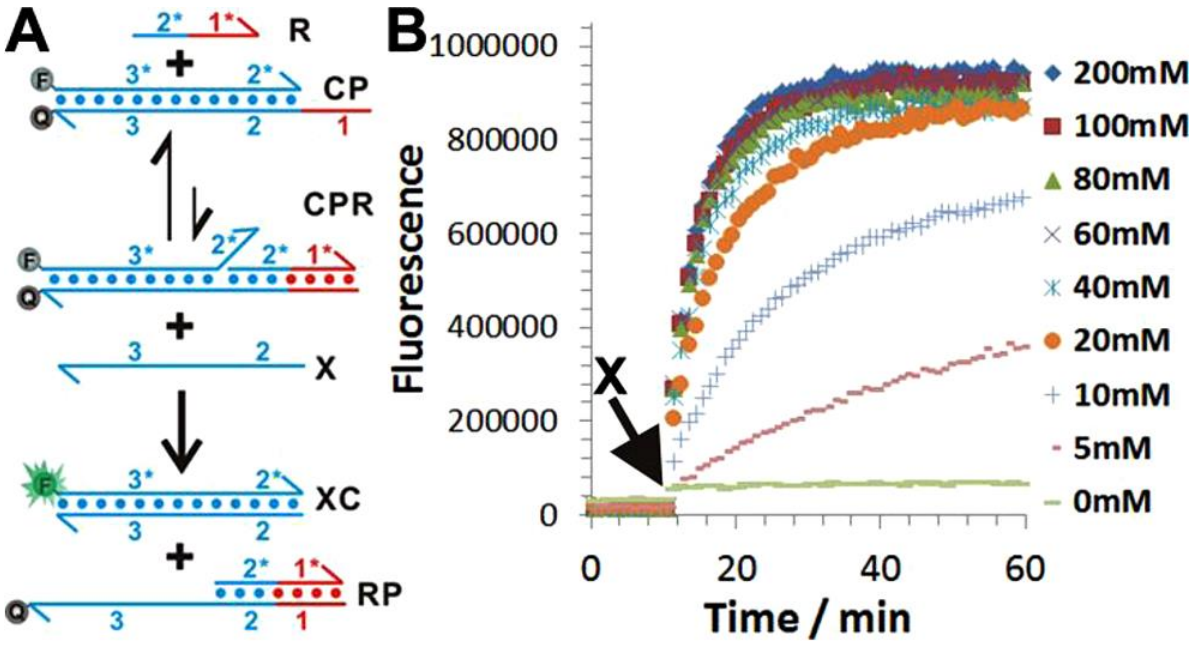

Figure 4-1. Enabling A-Toehold-Mediated Strand Displacement Using Mg^{2+} (A) Schematic illustration of the beacon design for real-time monitoring the A-toehold-mediated DNA strand displacement. (B) Effect of Mg^{2+} on the performance of A-toehold-mediated DNA strand displacement. [X] = 10 nM, [CP] = 20 nM, [R1] = 250 nM.

4.1.2 Characterization of A-Toehold-Mediated DNA Strand Displacement Using NativePolyacrylamide Gel Electrophoresis

A-toehold-mediated strand displacement in the presence of 100 mM Mg^{2+} was confirmed using native polyacrylamide gel electrophoresis (Figure 4-2). To facilitate the gel separation and visualization, X was extended with an additional 30-nt poly-dT domain (domain 4) and C was labelled with a fluorescent dye, 6-FAM (Figure 4-2). To be clear, X containing domain 4 was renamed as Xg. After separation, a gel containing DNA bands was visualized directly without further staining, so that only bands containing C motif can be detected. As shown in Figure 4-2, Lane 2 and 5 show very weak XgC bands, suggesting that minimum levels of strand displacement between Xg and CP occur in the absence of R1 (Lane 2) or in the presence of a nonspecific A-

toehold (R2 in Lane 5). Sufficient strand displacement occurs only when both Xg and corresponding R (R1) are present in the same solution (Lane 4).

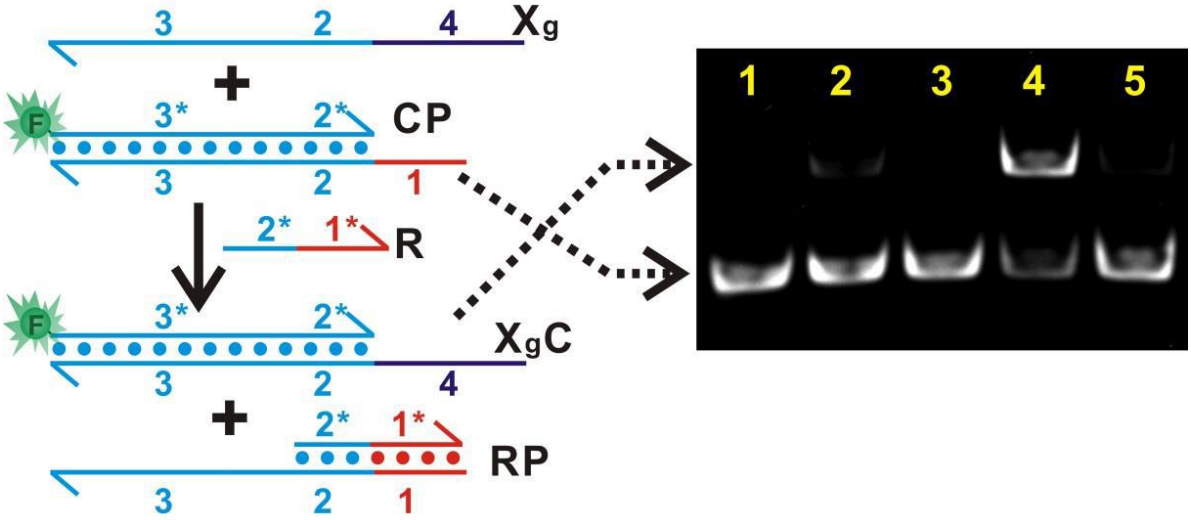

Figure 4-2. Analysis of A-toehold-mediated DNA strand displacement using polyacrylamide gel electrophoresis (PAGE). Lane 1, 1 μM CP; Lane 2, from analysis of a mixture containing 1 μM CP and 1 μM Xg; Lane 3, from analysis of a mixture containing 1 μM CP and 1 μM R; Lane 4, from analysis of a mixture containing 1 μM CP, 1 μM Xg, and 1 μM R1; Lane 5, from analysis of a mixture containing 1 μM CP, 1 μM Xg, and 1 μM nonspecific allosteric toehold R2. The reaction mixtures were incubated at 25 °C for 30 min. The samples were then run on 12% native polyacrylamide gel electrophoresis (PAGE). All the gels were freshly prepared in house. Before loading, DNA samples were mixed with DNA loading buffer at a volume ratio of 5:1. A potential of 12 V/cm was applied for gel electrophoresis. For visualizing the reaction products, C was labelled with a fluorescent dye, 6-FAM. After separation, PAGE gels were imaged directly using Gel Doc XR+ Imager System (BioRad) without staining, therefore only DNA bands containing fluorescently labelled C (either as CP or XgC) can be visualized on the gel.

4.2 Kinetic Study of Strand Displacement Reactions Using an A-Toehold

Method

Fluorescence was monitored in real-time with excitation/emission wavelength at 485 nm/515 nm at a frequency of 1 data point per minute. The measured fluorescence was normalized so that 1 normalized unit (n.u.) of fluorescence corresponded to fluorescence signal generated by 1 nM X. This normalization was achieved by using a positive control (P.C.) containing 10 nM X, 20 nM CP, and 250 nM R1 in TE-Mg (Tris-EDTA 100 mM Mg^{2+}) buffer, and a negative control (N.C.) containing identical reagents in the P.C. except that there was no X added. Fluorescence signals at t = 60 min were used for the P.C. and N.C. for the normalization. When R is in large excess, the effective rate constant k_{eff} can then be estimated using the following second-order rate equation (eq 1):

$$ln\left(\frac{[CP][X]_0}{[X][CP]_0}\right) = ln\left(\frac{([CP]_0-[CP]_t)[X]_0}{([X]_0-[X]_t)[CP]_0}\right) = k_{eff}([CP]_0 - [X]_0)t \qquad \text{eq 1}$$

where $[CP]_0$ and $[X]_0$ are initial concentrations of reactants CP and X, [CP] and [X] are the concentrations of CP and X at time t, $[CP]_t$ and $[X]_t$ are the reacted concentrations of CP and X at time t. [32]

4.3 Tuning the Kinetics of Strand Displacement Reactions Using A-Toehold

Although the A-toehold (domain 1* in Scheme 4-1B) is much less efficient than an equal amount of its toehold counterpart (domain 1* in Scheme 4-1A) (Figure 4-3), it is possible to promote the kinetics of A-toehold-mediated strand displacement to be close to its toehold-mediated strand displacement counterpart by raising the concentration of allosteric regulator R from 10 nM (Figure 4-3) to 250 nM (Figure 4-4). When [R] is in large excess, A toehold-mediated strand displacement is effectively a second order reaction (Figure 4-4). By fitting the kinetic data to the second-order rate equation (eq 1), we determined the effective rate constant k_{eff} to be 2.6×10^5 M^{-1} s^{-1} (Figure 4-

4B), which is in the same order of magnitude as that of a 6-nt long regular toehold ($k_{\{0,6\}} = 5 \times 10^5$ M^{-1} s^{-1} as predicted by Zhang et al.[23]).

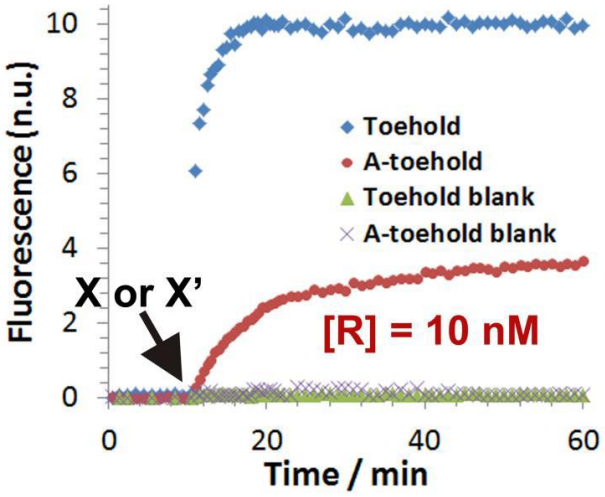

Figure 4-3. Comparing the kinetic performance of A-toehold-mediated DNA strand displacement (red trace) with that of its toehold-mediated strand displacement counterpart (blue trace). [X] = [X'] = 10 nM; [CP] = 20 nM; [R] = 10 nM.

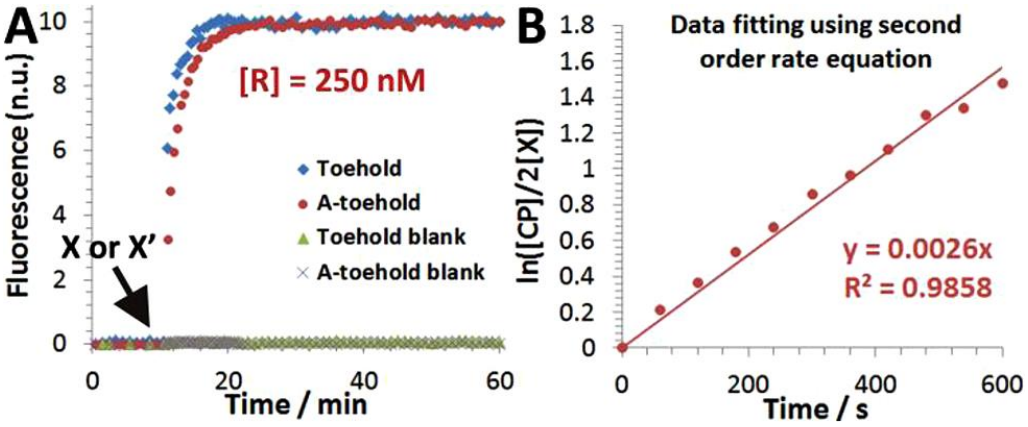

Figure 4-4. Kinetic profile of A-toehold-mediated DNA strand displacement. (A) Comparing A-toehold-mediated DNA strand displacement (red trace) with its toehold-mediated strand displacement counterpart (blue trace). CP was used for both reactions. X′ was used as an input for toehold-mediated strand displacement, whereas X and R were used to trigger A-toehold-mediated strand displacement. $[X]_o = [X']_o$ = 10 nM; $[CP]_o$ = 20 nM; [R1] = 250 nM. (B) Determination of

the effective rate constant k_{eff} by plotting $\ln([CP][X]_0/[X][CP]_0)$ (equal to $\ln([CP]/2[X])$) as a function of time and fitting the data using least-squares linear regression.

Similar to toehold-mediated DNA strand displacement, the rate constant k_{eff} was also found to increase exponentially when varying the A-toehold length m (domain 1*) from 4 nt to 7 nt (Figure 4-5A). The design that the A-toehold is split from the BM domain also allows additional fine-tuning of strand displacement kinetics through two more orthogonal factors: the length of the invading motif n (domain 2*) and the concentration of the regulator R ([R]).

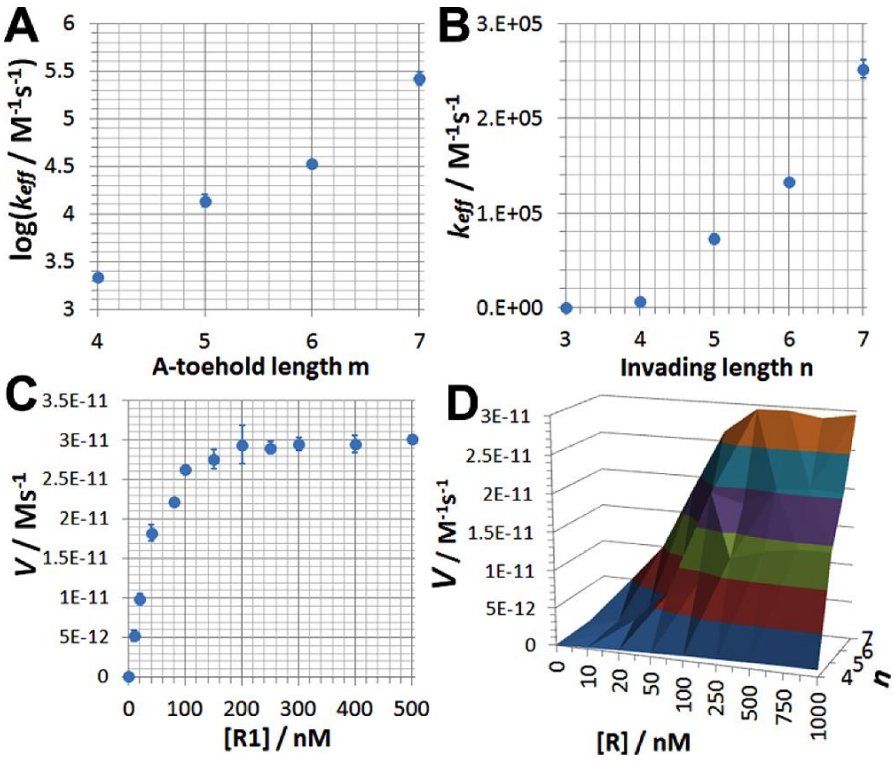

Figure 4-5. Tuning the kinetics of the DNA strand displacement using the allosteric DNA toehold. (A) Coarse-tuning of the effective rate constant k_{eff} by adjusting the A-toehold length m. n = 7; [R] = 250 nM. (B) Fine-tuning of k_{eff} by adjusting the length of the invading motif n. m = 7; [R] = 250 nM. (C) Fine-tuning of displacement rate V using [R]. n = 7; m = 7. (D) Continuous tuning of the displacement rate V by combining the two orthogonal factors: n and [R] (m = 7). For all experiments, [X] = 10 nM, [CP] = 20 nM. Error bars represent one standard deviation from triplicate analyses.

To examine the feasibility of using an A-toehold to fine-tune the rates of strand displacement, we first fixed the A-toehold length m (domain 1*) to be 7 nt and varied invading length n (domain 2*) from 3 to 10 nt. As shown in Figure 4-5B, a linear increase in k_{eff} was observed when varying n from 4 nt to 7 nt. Further increasing n from 7 to 10 nt was found to reduce the displacement rates (Figure 4-6). The decreases in displacement rates can be attributed to the unintended hybridization between X and R (X + R ↔ XR) through domain 2 and 2*, which sequesters X from reacting with CPR (reaction 2).

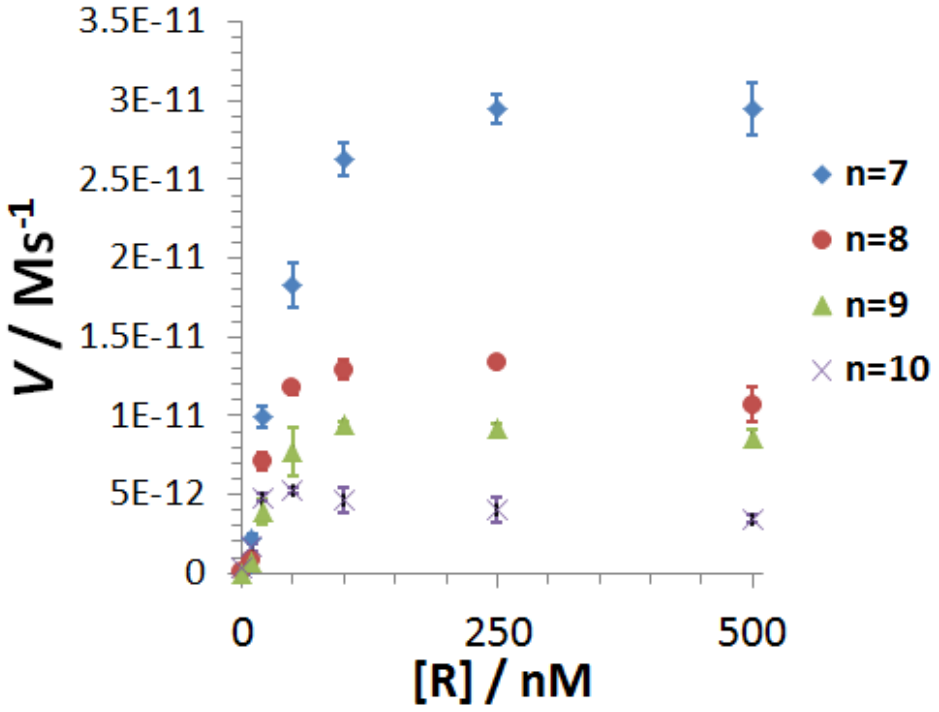

Figure 4-6. Effect of the invading length n (when $n \geq 7$ nt) of allosteric regulator R on the displacement rate *V*. Decrease in strand displacement rates was observed when increasing n from 7 nt to 10 nt. The decrease in displacement rates can be attributed to the unintended hybridization between X and R ($+R \leftrightarrow XR$) through domains 2 and 2*, which sequester X from reacting with CPR (reaction 2). [X] = 10 nM; [CP] = 20 nM. Error bars represent one standard deviation from triplicate analyses.

We then fixed both A-toehold and invading motif to be 7 nt long and tuned the kinetics of strand displacement using [R]. As shown in Figure 4-5C, the initial displacement rate *V* between X and CP increases almost linearly when varying [R] from 10 nM to 100 nM and is saturated when [R] is greater than 200 nM. We then estimated the concentrations of stable CPR using NUPACK (NUPACK is a software for the analysis and design of nucleic acid system including the thermodynamic properties analysis. [51]) by setting the parameters (DNA or RNA, temperature, number of strand species, strand sequences, strand concentrations) to be the same as our experimental conditions. We found that even when the displacement rate was saturated, the conversion from CP to CPR was less than 20% under our experimental conditions ([R] < 250 nM). A nearly complete conversion (90%) requires R to be at least 10 μM and a 50% conversion can be reached when [R] = 1 μM.

It was also found that when [R] was above 40 nM, change in the rate of A-toehold reactions did not significantly alter the equilibrium concentration (fluorescence can indirectly reflect the concentration of XC) of the product XC (Figure 4-7). Moreover, manipulation of [R] is continuous, thus allowing the continuous fine-tuning of the displacement rates. Collectively, the rate of any A-toehold-mediated strand displacement can be regulated independently from the BM domain by a set of three parameters, *m*, *n*, and [R] (Figure 4-5D). This feature can be very useful for simplifying the design and dynamic regulation of various DNA devices and systems.

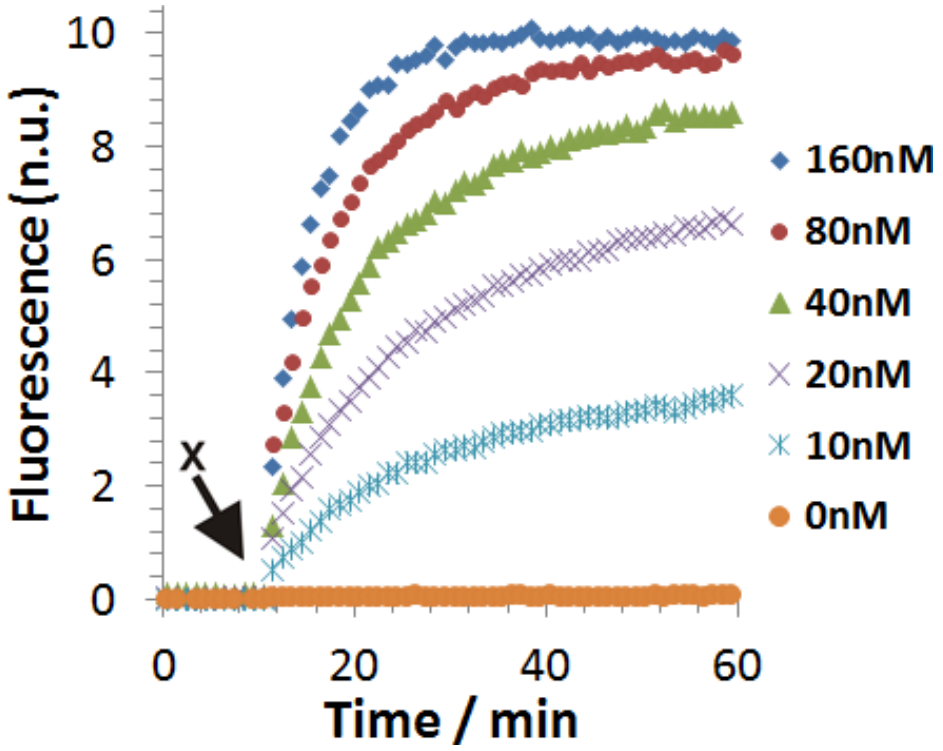

Figure 4-7. Fluorescence increase as a function of time for A-toehold reactions triggered by varying concentrations of R. [X] = 10 nM; [CP] = 20 nM; [R1] varying from 0 to 160 nM.

4.4 Regulation of Strand Displacement Reactions Using A-Toehold

4.4.1 Dynamic Regulation of Strand Displacement Using an A-Toehold.

To demonstrate the dynamic regulation of DNA strand displacement using the A-toehold, we designed an inhibitor I that is fully complementary to the regulator R, so that the effective concentration of R decreases in the presence of I (Figure 4-8A). The progress of strand displacement between X and CP can then be modulated by the addition of R or I. As shown in Figure 4-8B, strand displacement between X and CP was completely turned off when I was in excess and restored when R was in excess. Moreover, the regulation of strand displacement kinetics through the A-toehold is reversible and is shown in the sharp fluorescence changes upon the alternate addition of R or I. Compared to the dynamic allosteric control strategy described by Zhang and Winfree,[42] where dynamic regulation was achieved by controlled activation of an input strand,

the A-toehold strategy allows the direct regulation of "logic gate" molecules. It is more flexible to control a logic gate component rather than an input, as inputs are typically the target molecules with predefined sequences.

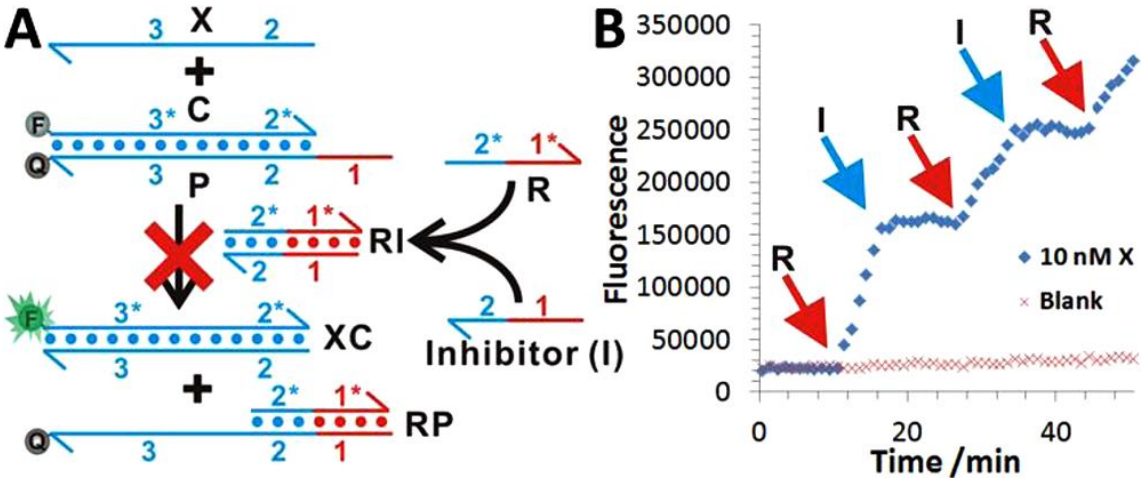

Figure 4-8. Dynamic regulation of DNA strand displacement using the A-toehold strategy. (A) Schematic illustration of the inhibition of A-toehold- mediated DNA strand displacement by quenching the active A-toehold regulator R using an inhibitor strand I. (B) Real-time monitoring of fluorescence signals in response to the addition of R or I. [X] = 10 nM, [CP] = 20 nM, $[R]_{eff}$ = 20 nM, $[I]_{eff}$ = 20 nM ($[R]_{eff}$ and $[I]_{eff}$ are effective concentrations of R and I in the final solution).

4.4.2 Selective Activation of Multiple Strand Displacement Reactions Using A-Toeholds

Another advantage of splitting toehold and BM on the input strand is the possibility of achieving the selective activation of a specific strand displacement reaction from a mixture of multiple substrates using the same BM sequence but with a specific A-toehold. A similar concept, such as combinatorial displacement, has previously been demonstrated by Genot et al. to achieve matrix multiplication and weighted sums.[43] The selective activation of combinatorial displacement was built on the associative toehold design and thus requires a DNA hybridization event to attach a specific toehold to a BM domain.[43] Our A-toehold design has the potential to simplify the selective activation process by eliminating the need for additional hybridization domains to attach toehold and BM motifs. To demonstrate the potential uses of the A-toehold in such applications, as shown

in Figure 4-9A, we designed two displacement beacons by labeling C with two distinct fluorescent dyes, 6-FAM (C1) and 5-Carboxytetramethylrhodamine (TAMRA) (C2), respectively. The complementary protecting sequences P1 and P2 are two different toehold domains (domain 1 for P1 and domain 5 for P2). R1 is designed to contain the specific A-toehold for C1P1 (domain 1*), whereas R2 is designed for C2P2 (containing domain 5*). Equal concentrations of C1P1 and C2P2 (20 nM each) were then mixed together with 10 nM X. By measuring the two fluorescent channels in parallel (Figure 4-9B−D), we observed that the displacement reactions between X and CP were highly specific. When addition of 100 nM of R1 and 0 nM of R2 in the same mixture (C1P1/C2P2/X), fluorescence increases were observed in FAM fluorescent channel. When addition of 0 nM of R1 and 100 nM of R2 in the same mixture (C1P1/C2P2/X), fluorescence increases were observed in TAMRA fluorescent channel. The selectivity was strictly controlled by the A-toehold sequence on R. Moreover, the selective activation can also be achieved in a quantitative manner by simply adjusting the ratio between specific A-toehold regulators (Figure 4-9C and Figure 4-10). When addition of 100 nM of R1 and 100 nM of R2 in a same mixture (C1P1/C2P2/X), by normalizing fluorescence increase in each channel, a same trend of fluorescence increase were observed.

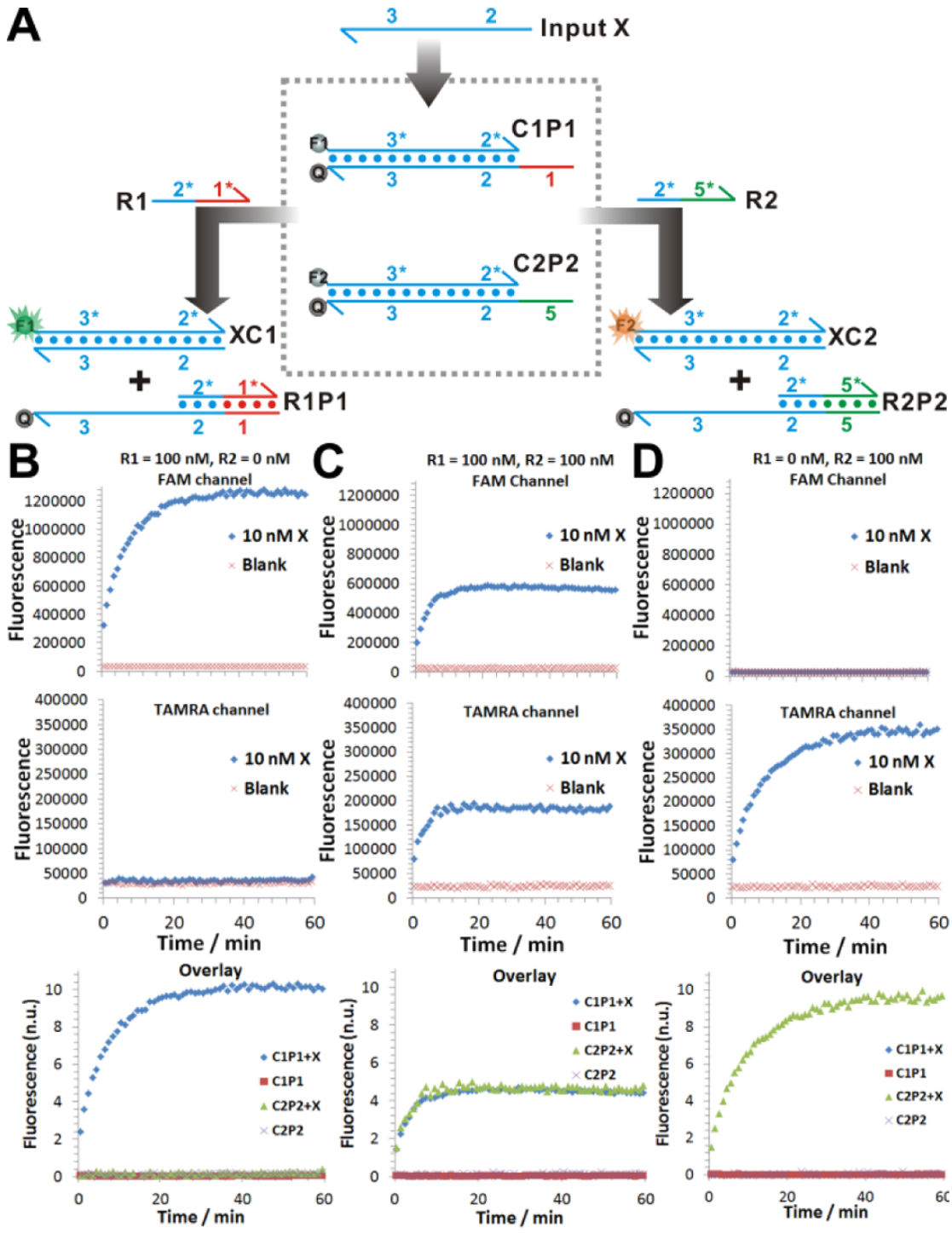

Figure 4-9. Selective Activation of Multiple Strand Displacement Reactions Using A-Toeholds (A) Schematic illustration of the selective activation of multiple displacement reactions using A-toehold regulators. (B−D) Real-time monitoring of fluorescence signals generated by strand displacement reactions activated by R1 (FAM channel) and/or R2 (TAMRA channel). The

overlay plots were obtained by normalizing raw fluorescence signals against fluorescence of 100 nM R1 or R2 and 0 nM R1 or R2 as P.C. and N.C. at t = 60 min. [X] = 10 nM; [C1P1] = [C2P2] = 20 nM.

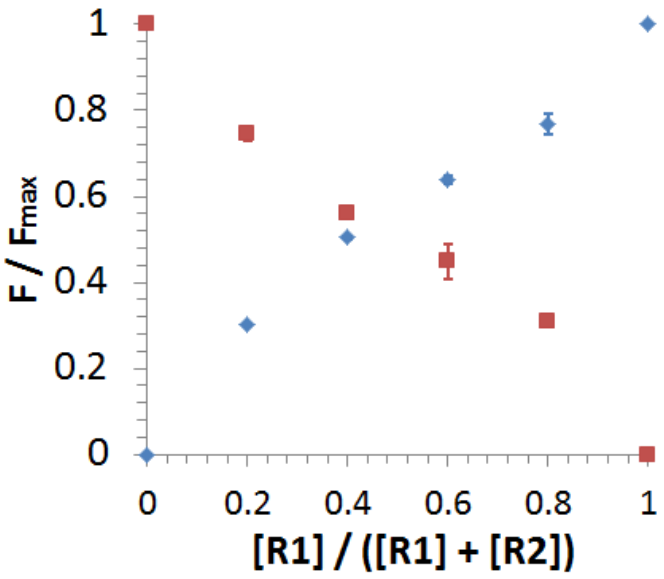

Figure 4-10. Quantitative and selective activation of two strand displacement beacons using the same input X by controlling the ratio between the two specific regulators R1 (blue) and R2 (red). The sum of [R1] and [R2] was kept at 100 nM and the portion of [R1] varies from 0 to 100%. Fluorescence signals (F) were measured after incubating the reaction mixture containing 20 nM displacement beacon CP, 10 nM input X, varying concentrations of R1 and R2 at room temperature for 1 hr. The maximum fluorescent signals were determined by 100% [R1] or [R2]. Error bars represent one standard deviation from triplicate analyses.

4.4.3 Activation of Toehold-Exchange Reactions using an A-Toehold.

Having demonstrated the application of the A-toehold strategy to the dynamic and selective regulation of DNA strand displacement reactions, we aim to further expand this strategy to DNA devices with higher structural complexity. Because toehold-exchange is one of the most widely used mechanisms to construct complexed DNA devices or circuits,[23, 44-48] we first examined the adaptability of our A-toehold design to toehold-exchange reactions. As shown in Figure 4-11, A-

toehold was able to trigger toehold-exchange reactions with the reverse toehold *r* (domain 3b/3b*) ranging from 0 to 7 nt. A clear shift was also observed on the reaction equilibrium toward the reactants when increasing *r* from 0 nt to 7 nt (Figure 5-11B), suggesting that the A-toehold-mediated toehold exchange reaction is reversible and thus is adaptable to the construction of catalytic DNA circuits. Encouraged by this result, we developed an A-toehold-mediated noncovalent DNA catalysis network that resembled an allosteric enzyme.

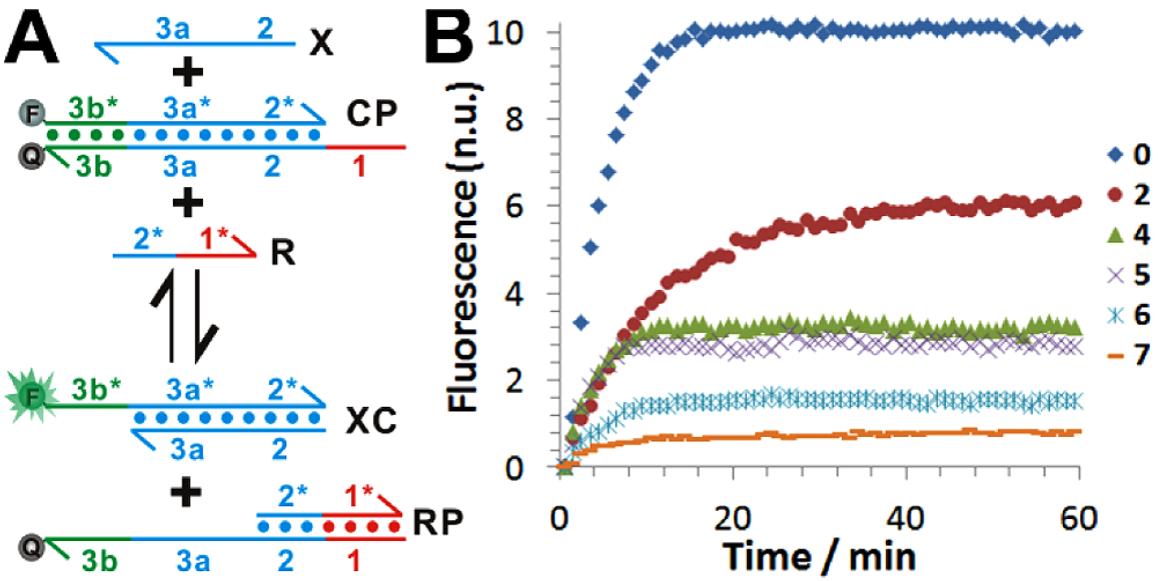

Figure 4-11. Activation of Toehold-Exchange Reactions using A-Toehold. (A) Schematic illustration of A-toehold-mediated toehold-exchange reaction. (B) Fluorescence signals generated by toehold-exchange reactions that are of varying reverse toehold length *r* from 0 to 7 nt. [X-r] = 10 nM; [CP] = 20 nM; [R1] = 250 nM.

4.5 Applications of A-Toehold-Mediated Strand Displacement

4.5.1 A-Toehold-Mediated Noncovalent DNA Catalysis

4.5.1.1 Method

The reaction mixture contained 20 nM CP, 20 nM Y, and 2 nM catalyst X_{cat} in TE-Mg buffer was transferred into a 96-well microplate. The fluorescence was then monitored using the multimode

microplate reader every 1 min for 10 min. The allosteric regulator R1 was then quickly added to the reaction mixture at a final concentration of 150 nM. The fluorescence was then monitored for another 2 h. The measured fluorescence was normalized so that 1 n.u. of fluorescence corresponded to the fluorescence signal generated by 1 nM X (r = 0). This normalization was achieved by using a P.C. containing 2 nM X, 20 nM CP, and 250 nM R1 in TE-Mg buffer, and a N.C. containing identical reagents as in the P.C. except that there was no X added. The turnover number (*TON*) was calculated using the following equation (eq2) [32]:

$$TON = \frac{[CY]+[X_{cat}C]}{[X_{cat}]} = \frac{F_{cat}-B_{cat}}{X_{cat}} \qquad \text{eq2}$$

where F_{cat} is the normalized fluorescence from the reaction mixture containing 2 nM catalyst, X_{cat} (e.g., X-6), 20 nM CP, and 20 nM Y; B_{cat} is the background from the same reaction mixture where no catalyst is added.

4.5.1.2 Principle of A-toehold-mediated DNA catalysis

Figure 4-12A shows the mechanism of A-toehold-mediated DNA catalysis. CP reacts with R, forming reaction intermediate CPR triplex. The catalyst X_{cat} (e.g., X-6) then hybridizes and initiates a branch migration with CPR, leading to the production of $X_{cat}C$. Once $X_{cat}C$ forms, it then reacts with Y through a toehold-exchange mechanism, yielding the product CY. Meanwhile, X_{cat} is released back into the solution and can then be used to catalyze the next cycle of toehold-exchange with CPR. Because R activates the overall reaction but does not involve the catalytic center, mimicking the role of an allosteric effector, A-toehold-mediated DNA catalysis hence resembles an allosteric enzyme. To construct A-toehold-mediated DNA catalysis, we need to characterize a set of design parameters, including allosteric regulator R, substrate Y, and catalyst X_{cat}.

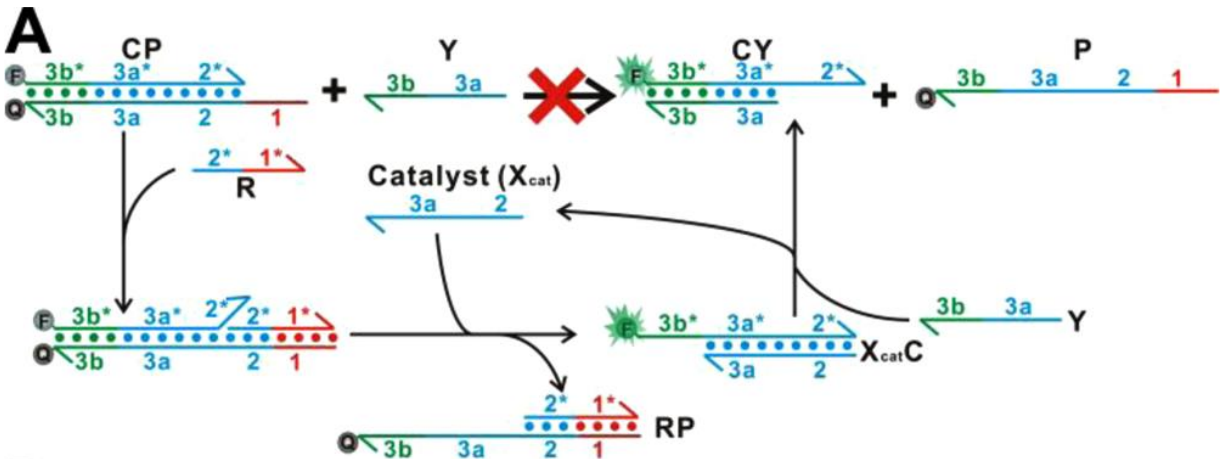

Figure 4-12. Principle of A-toehold-mediated DNA catalysis (A) Schematic illustration of the activation of noncovalent DNA catalysis using the allosteric DNA regulator.

4.5.1.3 Optimization of Designing of Regulator and Substrate for A-toehold-mediated DNA catalysis

We first studied how the design of R affects the performance of the DNA catalysis. We then fixed *m* to be 7 nt and varied the invading length of R (domain 2*) *n* from 3 nt to 9 nt. As shown in Figure 4-13A and Figure 4-13B (fixed *n* then compare fluorescence values between the Blank curve and 2 nM X-6 curve), catalytic reactions with multiple turnovers were observed when *n* was 7 nt or longer (Figure 4-13A). However, a longer invading length also resulted in higher background due to the cross-reaction between CPR and Y (Figure 4-13B). Since Optimal signal-to-noise (S/B) ratio (to each fixed *n*, its signal fluorescence values in Figure 4-13A divide by blank fluorescence values in Figure 4-13B) was achieved to be ~ 10 for regulators with invading length of 7 nt (R1) and 8 nt (R-8-7) (Figure 4-13C). We chose R-8-7 as the optimal allosteric regulator for optimizing other design parameters, because this one leads to a higher turnover number while having the same level of S/B ratio compared to R1. We then optimized the concentration of substrate Y for A-toehold-mediated DNA catalysis. Y was designed to contain the entire domain 3, so that it could release X_{cat} from $X_{cat}C$ through a toehold-exchange reaction. The optimal concentration of Y was determined to be 20 nM, evidenced by the highest S/B ratio (Figure 4-14).

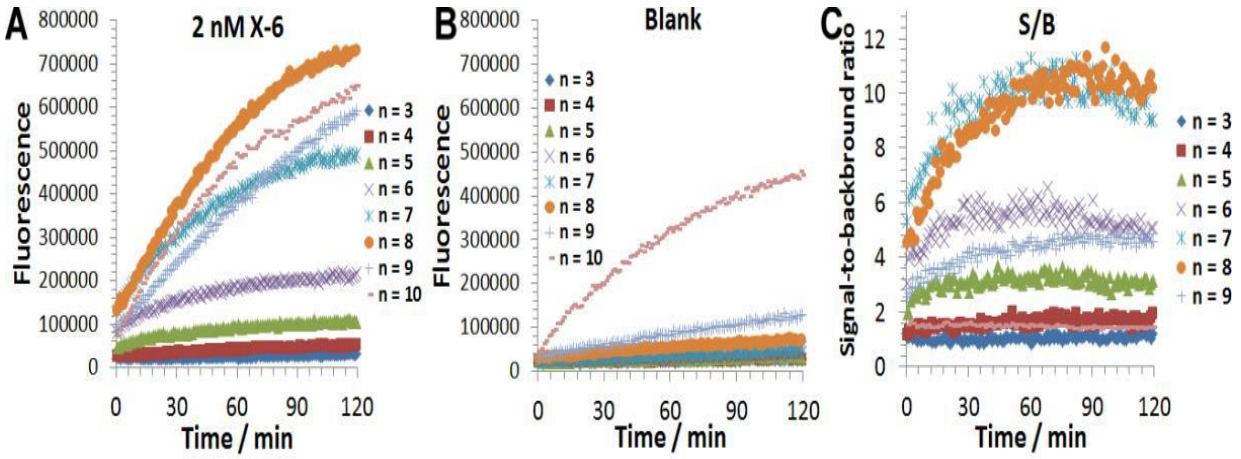

Figure 4-13. Effect of allosteric regulator designs on the performance of the A-toehold-mediated DNA catalysis. Each reaction mixture contained 2 nM catalyst X-6, 20 nM CP, 20 nM Y, and 100 nM R of varying invading length *n* (domain 2*) from 3 to 9. The blank contained identical reagent in the reaction mixture, except that there was no catalyst X-6 added. R-8-7 was chosen as the allosteric regulator for optimizing other design parameters of A-toehold-mediated DNA catalysis, because it has the same level of signal-to-noise ratio as R1 (**C**) but a much higher fluorescence response (**A**).

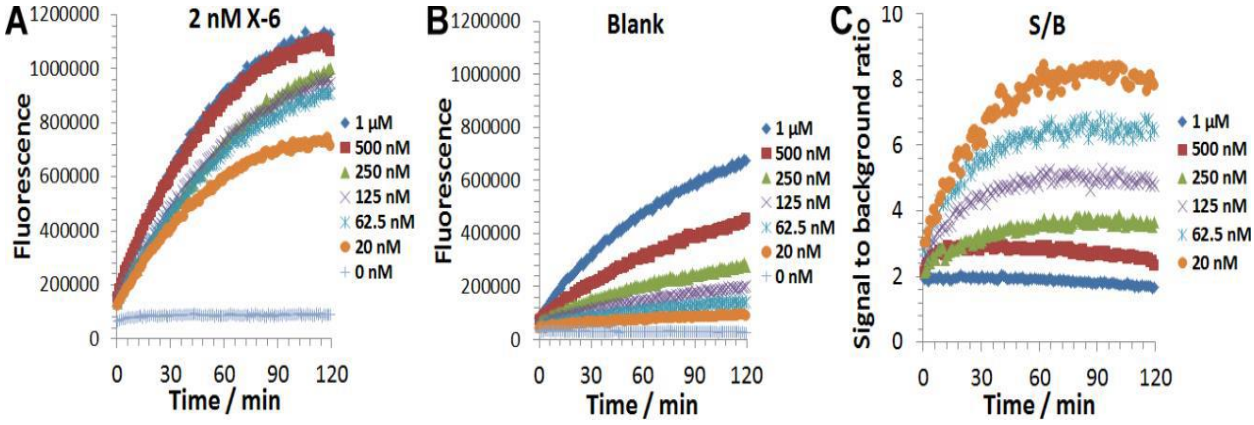

Figure 4-14. Optimization of [Y] for A-toehold-mediated DNA catalysis. Each sample (**A**) contained 2 nM catalyst X-6, 20 nM CP, 100 nM R-8-7, and varying concentrations of Y. Each blank (**B**) contained identical reagent in corresponding sample, except that there was no catalyst

X-6 added. The optimal concentration of Y was determined to be 20 nM, evidenced by the highest signal-to-background ratio (**C**).

4.5.1.4 Optimization of Designing of Catalyst X_{cat} for A-toehold-mediated DNA catalysis

Having optimized the design parameters for A-toehold-mediated DNA catalysis, we compared a set of DNA catalysts X_{cat} designs. Here, various X_{cat} differ from one another by enabling varying reverse toehold lengths *r* (domain 3b*) on C. X_{cat} was then renamed as X-r. For example, X_{cat} with a reverse toehold r = 6 nt on C was named as X-6. We compared X_{cat} designs by varying *r* from 2 nt to 7 nt (Figure 4-15A), and calculated the turnover number (*TON*) at 120 min (Figure 4-15B). It was found that multiple turnovers (*TON* > 1) were achieved when *r* was 4 nt or longer. Catalytic efficiency was found to be enhanced when increasing *r* from 2 nt to 6 nt. Under these conditions, the length effect of the reverse toehold was dominated by promoting the toehold-exchange between Y and $X_{cat}C$. However, keeping increase *r* from 6 nt to 7 nt, a reduced catalytic efficiency (a decreased of fluorescence values from 6 nt to 7 nt) was observed in Figure 4-15A and 4-15B, suggesting that toehold-exchange between $X_{cat}C$ and RP began to play significant roles to the overall reaction. Therefore, we used X-6 to characterize allosteric regulator and DNA catalysis in the main content, because this is the best DNA catalyst under our experimental conditions.

The optimal design was achieved when R-8-7 and X-6 were used as the regulator and the catalyst, and Y had an optimal concentration of 20 nM. The optimal result is shown in Figure 4-15C. DNA catalysis was activated by 150 nM R- 8-7 and mediated by 2 nM catalyst X-6. A *TON* of ~4.5 was achieved over a period of 120 min (Figure 4-15D). The determined *TON* can be overestimated by up to 1, as intermediate $X_{cat}C$ also contributed to the fluorescence signal.

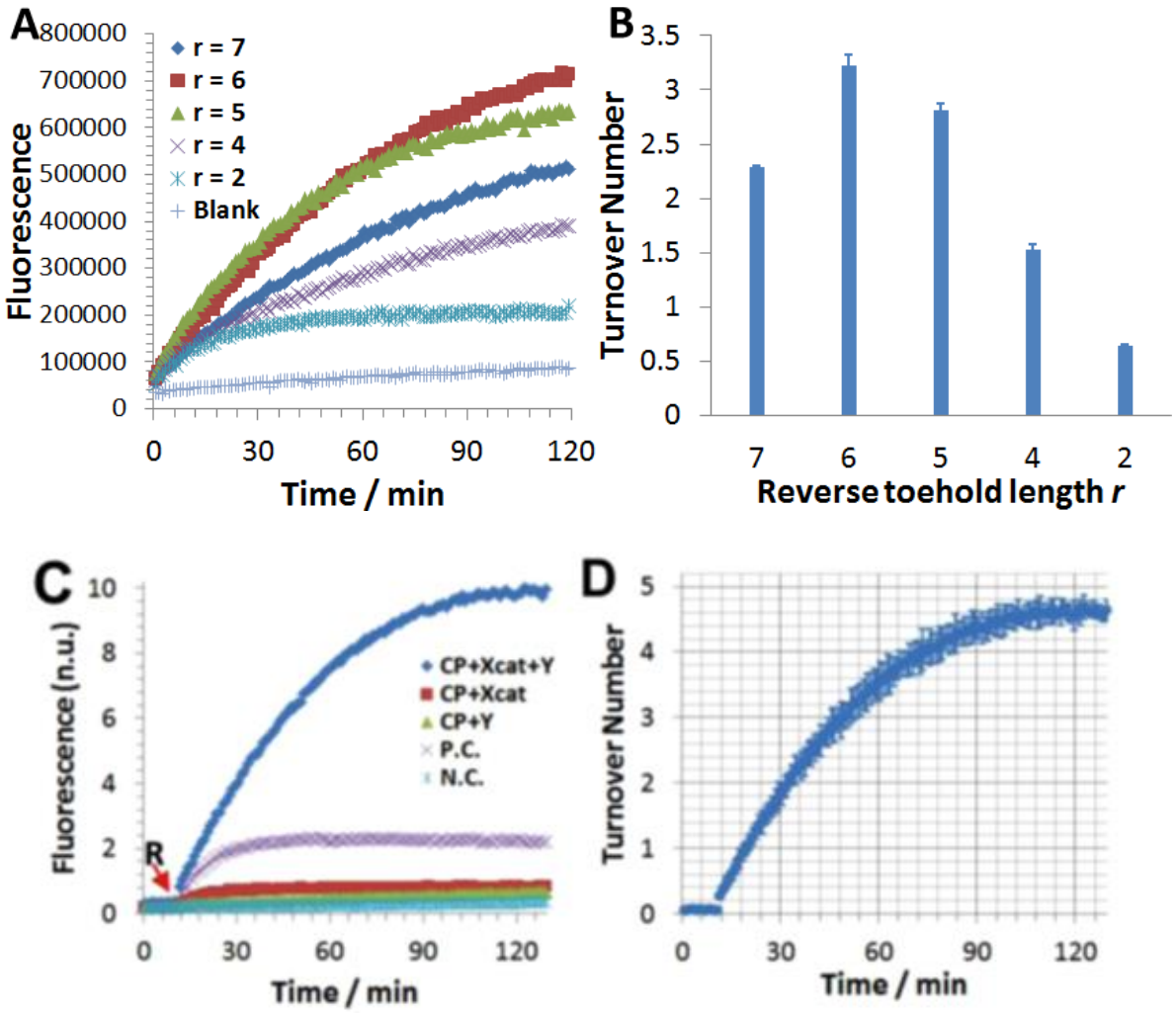

Figure 4-15. Effect of catalyst X_{cat} designs on the performance of the A-teohold-mediated DNA catalysis. Each reaction mixture contained 2 nM catalyst X_{cat} of varying reverse toehold length r (domain 3b*) from 2 to 7 (X-2 to X-7), 20 nM CP, 20 nM Y, and 100 nM R-8-7. The blank contained identical reagent in the reaction mixture, except that there was no catalyst X_{cat} added. The turnover number (*TON*) was calculated by first normalizing fluorescence into normalized units by using the X (r = 0) as a positive control. Equation 2 was then used to determine the *TON*. The optimal *TON* was achieved (at 120 min) when reverse toehold length r equal to 6 (X-6). (C) Real-time monitoring of DNA catalysis activation and progression. For DNA catalysis: [X-6] = 2 nM; [Y] = 20 nM; [CP] = 20 nM; [R-8-7] = 150 nM. For controls: [X] = 2 nM; [CP] = 20 nM;

[R1] = 250 nM. (D) *TON* as a function of reaction time. *TON* at each time point was determined using eq 2. Error bars represent one standard deviation from triplicate analyses.

4.6 Conclusion

Here the allosteric DNA toehold (A-toehold) strategy is a new addition to the current toolbox of DNA strand displacement techniques. It has the potential to simplify DNA sequence designs to achieve dynamic and selective control of DNA strand displacement. It is also adaptable to other toehold activation mechanisms and thus could be used in combination with other strand displacement strategies to build complexed DNA devices. For example, we have demonstrated an allosteric DNA catalysis system which was achieved by combining A-toehold with toehold-exchange mechanisms.

4.7 Future Work

Constructing a 3-D DNA nanosensor for DNA detection using the A-toehold strand displacement reaction:

The conventional toehold strand displacement reaction is used for design of 3-D DNA nanosensor for target DNA detection. To that end, we want to develop new 3-D DNA nanosensor that is based on the A-toehold strand displacement reaction to detect target DNA. The new 3-D DNA nanosensor design for DNA detection can be addressed in future work.

Chapter 5

Experimental

Constructing a Three-Dimensional DNA Nanomachine to Achieve Rapid Isothermal Signal Amplification for Nucleic Acids Detection

5.1 Materials and Reagents

Solution of gold nanoparticles (AuNPs) (20 nm in diameter), magnesium chloride hexahydrate ($MgCl_2 \cdot 6H_2O$), Tween 20, Dithiothreitol (DTT), salmon sperm DNA fragments, 10 × phosphate buffered saline (PBS) solution, and human serum (Product Number, H6914) were purchased from Sigma (Oakville, ON, Canada). Ammonium persulfate (APS), N,N,N',N'-tetramethylethylene-diamine (TEMED), 40% Acrylamide/Bis solution, DNA loading buffer, and 20 bp Molecular Ruler were purchased from Bio-Rad Laboratories, Inc. (ON, Canada). Nicking endonuclease (Nb.BbvCI) and cut smart buffer (NEBuffer) were purchased from New England Biolabs (Canada). Proteinase K and Plasma/Serum Circulating DNA Purification Kit were purchased from Norgen Biotek Corp. (Thorold, ON, Canada). NANOpure H_2O (> 18.0 MΩ), purified using an Ultrapure Milli-Q water system, was used for all experiments. All DNA samples were purchased from Integrated DNA Technologies (Coralville, IA) and purified by high performance liquid chromatography (HPLC).

5.2 DNA Sequences and Modifications

DNA name		Sequences
DNA probes for 3-D DNA nanomachine	**DW-57**	5'-SH-T-50-T-CCTCAGC-3'
	DW-42	5'- SH-T-35-T-CCTCAGC-3'
	SR	5'-SH- T-10-T- GC*TGA GGAT-FAM-3'(*cleavage site)
	Poly dT	5'-SH-T-19-T-3'
DNA probes for MTB DNA nanosensor	**DW**	5'-SH-T-40-T-ATTC ATG GGC CAG AACA CCTCAGC-3'
	Target DNA	5'- AGC TGA GCCA ATTC ATG GGC CAG AACA-3'
	Scrambled DNA	5'- CGC AGT CCC CAA CCT CC A ATC ACT CAC-3'
	P-5	5'- TG AGG TGTT CTG GCC CAT GAAT TGG CT-3'
	P-6	5'- TG AGG TGTT CTG GCC CAT GAAT TGG CTC-3'
	P-7	5'- TG AGG TGTT CTG GCC CAT GAAT TGG CTC A-3'
	P-8	5'- TG AGG TGTT CTG GCC CAT GAAT TG GCT CAG-3'
	P-9	5'- TG AGG TGTT CTG GCC CAT GAAT TGG CTC AGC-3'
	P-10	5'- TG AGG TGTT CTG GCC CAT GAAT TGGC TCA GCT-3'
DNA targets and controls for differentiating single point mutation (T = target C = control; numbers represent corresponding reverse toehold length)	**T-6**	5'- GCTG AGC CA ATTC ATG GGC CAG AAC-3'
	C-6	5'- GCTG AGC CA ATTC ATG G**A**C CAG AAC-3'
	T-7	5'- GCTG AGC CA ATTC ATG G**G**C CAG AA-3'
	C-7	5'- GCTG AGC CA ATTC ATG G**A**C CAG AA-3'
	T-8	5'- GCTG AGC CA ATTC ATG G**G**C CAG A-3'
	C-8	5'- GCTG AGC CA ATTC ATG G**A**C CAG A-3'
	T-9	5'- GCTG AGC CA ATTC ATG G**G**C CAG-3'
	C-9	5'- GCTG AGC CA ATTC ATG G**A**C CAG -3'
	T-10	5'- GCTG AGC CA ATTC ATG G**G**C CA-3'
	C-10	5'- GCTG AGC CA ATTC ATG G**A**C CA-3'

5.3 Construction of 3-D DNA Nanomachine

Preparation of DW-SR-AuNP

The thiolated DNA Walker (DW) and Signal Reporter (SR) oligonucleotides were mixed at a ratio of 1 to 20. A 105 μL solution of this mixture containing 5 μL of 5 μM DW oligonucleotides and 100 μL of 5 μM SR oligonucleotides were mixed with 500 μL 1 nM AuNPs. This mixture was placed at room temperature for 12 hrs, and then was slowly mixed with 165 μL of 3 M NaCl, followed by 10 secs of sonication. This process of addition of NaCl and sonication was repeated for 5 times at 1 hr intervals, to maximize the oligonucleotide loading amounts. The solution was then incubated at room temperature for 24 hrs. After incubation, the solution was centrifuged at 13,500 rpm for 30 min to separate the DNA functionalized AuNPs (DNA-AuNPs) from the unreacted reagents. The DNA-AuNPs were washed 3 times with 0.5 × PBS buffer (pH 7.4) containing 0.005% Tween20, and finally redispersed in 0.5 × PBS buffer.

Preparation of SR-AuNP Control

A 100 μL solution of 5 μM SR oligonucleotides was mixed with 500 μL 1 nM AuNPs. This mixture was incubated at room temperature for 12 hrs, and then was slowly mixed with 165 μL of 3 M NaCl, followed by 10 secs of sonication. This process of addition of NaCl and sonication was repeated for 5 times at 1 hr intervals, to maximize the oligonucleotide loading amounts. The solution was then incubated at room temperature for 24 hrs. After incubation, the solution was centrifuged at 13,500 rpm for 30 min to separate the DNA functionalized AuNPs (DNA-AuNPs) from the unreacted reagents. The DNA-AuNPs were washed 3 times with 0.5 × PBS buffer (pH 7.4) containing 0.005% Tween20, and finally redispersed in 0.5 × PBS buffer.

Preparation of DW-PolyT-AuNP Cross Reaction Control

The thiolated DNA Walker (DW) and polyT oligonucleotides were mixed in a ratio of 1 to 20. A 105 μL volume of this mixture containing 5 μL of 5 μM DW oligonucleotides and 100 μL of 5 μM polyT oligonucleotides was mixed with 500 μL 1 nM AuNPs. This mixture was incubated at

room temperature for 12 hrs, and then was slowly mixed with 165 µL of 3 M NaCl, followed by 10 secs of sonication. This process of addition of NaCl and sonication was repeated for 5 times at 1 hr intervals, to maximize the oligonucleotide loading amounts. The solution was then incubated at room temperature for 24 hrs. After incubation, the solution was centrifuged at 13,500 rpm for 30 min to separate the DNA functionalized AuNPs (DNA-AuNPs) from the unreacted reagents. The DNA-AuNPs were washed 3 times with 0.5 × PBS buffer (pH 7.4) containing 0.005% Tween20, and finally redispersed in 0.5 × PBS buffer.

Principle of Nicking cleavage on the 3-D DNA nanomachine

A reaction mixture containing 12.5 nM DW-SR-AuNP and 20 U/100 µL nicking endonuclease and a mixture of control containing 12.5 nM DW-SR-AuNP were incubated at 37 ºC for an hour. Each mixture was incubated with 50 mM DTT for another hour. The reaction mixtures as well as a blank control of the SR mixture, was then loaded onto a 12% PAGE gel and a voltage of 110 V was applied. After electrophoresis, the gel was stained with SYBR Green and imaged using Gel Doc XR+ Imager System (BioRad).

Performance Testing of the 3-D DNA Nanomachine

For each nanomachine operation experiment (except for the enzyme concentration experiment and 3-D DNA nanomachine concentration experiment), a reaction mixture containing 100 pM DNA nanomachines, 20 U nicking endonucleases, and 1 × NEB cut smart buffer was incubated at 37 °C in a 96-well microplate. Fluorescence signals were measured immediately after adding the enzyme. This measurement was carried out every 1 min for 120 minutes from the microplate using a multi-mode microplate reader with excitation/emission wavelength of 485/535 nm to monitor the released FAM-labeled SR.

Preparation of different densities of DW 3-D DNA Nanomachine

The thiolated DNA Walker (DW) and Signal Reporter (SR) oligonucleotide solutions were mixed at a ratio of 1 to 5, 1 to 10, and 1 to 20. A series of 105 µL volumes of this mixture containing

5 μL of 20 μM DW, 5 μL of 10 μM DW, and 5 μL of 5 μM DW oligonucleotides and 100 μL of 5 μM SR oligonucleotides were mixed with 500 μL 1 nM AuNPs. These mixtures were incubated at room temperature for 12 hrs, and then each of them was slowly mixed with 165 μL of 3 M NaCl, followed by 10 secs of sonication. This process of addition of NaCl and sonication was repeated for 5 times at 1 hr intervals, to maximize the oligonucleotide loading amounts. The solution was then incubated at room temperature for 24 hrs. After incubation, each solution was centrifuged at 13,500 rpm for 30 min to separate the DNA functionalized AuNPs (DNA-AuNPs) from the unreacted reagents. The DNA-AuNPs were washed 3 times with 0.5 × PBS buffer (pH 7.4) containing 0.005% Tween20, and finally redispersed in 0.5 × PBS buffer.

Density testing

The density of SR oligonucleotides on each AuNP was determined by releasing SR from AuNP using 20 mM DTT and measuring fluorescence of the FAM dye that was labelled on SR. Fluorescence was measured using a multi-mode microplate reader (SpectraMax i3, Molecular Devices) and SR density was quantified by using FAM-labeled SR oligos as external standards. The density of DW on each AuNP was then estimated according to the SR density and the initial ratio between DW and SR.

Preparation of different densities of SR 3-D DNA Nanomachine

A series of mixtures of the thiolated DNA Walker (DW), Signal Reporter (SR) and polyT oligonucleotides were produced at a ratio of 1: 20: 0, 1: 16: 4, 1: 12: 8, 1: 8: 12, 1: 4: 16, and 1: 0: 20. A series of 105 μL volumes of mixture were made containing 5 μL of 5 μM DW oligonucleotides and 100 μL of 5 μM SR oligonucleotides, 80 μL of 5 μM SR oligonucleotides and 20 μL of 5 μM polyT, 60 μL of 5 μM SR oligonucleotides and 40 μL of 5 μM polyT, 40 μL of 5 μM SR oligonucleotides and 60 μL of 5 μM polyT, 20 μL of 5 μM SR oligonucleotides and 80 μL of 5 μM polyT, 100 μL of 5 μM polyT; each mixture was combined with 500 μL 1 nM AuNPs. These mixtures were incubated at room temperature for 12 hrs, and then each of them was slowly

mixed with 165 μL of 3 M NaCl, followed by 10 secs of sonication. This process of addition of NaCl and sonication was repeated for 5 times at 1 hr intervals, to maximize the oligonucleotide loading amounts. The solution was then incubated at room temperature for 24 hrs. After incubation, each solution was centrifuged at 13,500 rpm for 30 min to separate the DNA functionalized AuNPs (DNA-AuNPs) from the unreacted reagents. The DNA-AuNPs were washed 3 times with 0.5 × PBS buffer (pH 7.4) containing 0.005% Tween20, and finally redispersed in 0.5 × PBS buffer.

Preparation of different DW Length 3-D DNA Nanomachine

A mixture of the thiolated DNA Walker 42 nt (DW-42) or 57 nt (DW-57) and Signal Reporter (SR) oligonucleotides were mixed at a ratio of 1 to 20. A series of 105 μL volumes of this mixture containing 5 μL of 50 μM DW-42 or DW-57 and 100 μL of 5 μM SR oligonucleotides were mixed with 500 μL 1 nM AuNPs. These mixtures were incubated at room temperature for 12 hrs, and then each of them was slowly mixed with 165 μL of 3 M NaCl, followed by 10 secs of sonication. This process of addition of NaCl and sonication was repeated for 5 times at 1 hr intervals, to maximize the oligonucleotide loading amounts. The solution was then incubated at room temperature for 24 hrs. After incubation, each solution was centrifuged at 13,500 rpm for 30 min to separate the DNA functionalized AuNPs (DNA-AuNPs) from the unreacted reagents. The DNA-AuNPs were washed 3 times with 0.5 × PBS buffer (pH 7.4) containing 0.005% Tween20, and finally redispersed in 0.5 × PBS buffer.

Study of Concentration of 3-D DNA Nanomachine (AuNP)

A series of reaction mixtures containing 6.25 pM, 12.5 pM, 25 pM, 50 pM, 100 pM, 200 pM DNA nanomachines, 20 U nicking endonucleases, and 1 × NEB cut smart buffer was incubated at 37 °C in a 96-well microplate. Fluorescence signals were measured immediately after adding the enzyme. This measurement was carried out every 1 min for 120 minutes from the microplate using a multi-mode microplate reader with excitation/emission wavelength of 485/535 nm to monitor the released FAM-labeled SR.

Study of Concentration of Nicking Endonuclease

A series of reaction mixtures each containing 100 pM DNA nanomachines, 0.3 U, 0.6 U, 1.3 U, 2.5 U, 5 U, 10 U, 20 U nicking endonuclease, and 1 × NEB cut smart buffer was incubated at 37 °C in a 96-well microplate. Fluorescence signals were measured immediately after adding the enzyme. This measurement was carried out every 1 min for 120 minutes from the microplate using a multi-mode microplate reader with excitation/emission wavelength of 485/535 nm to monitor the released FAM-labeled SR.

5.4 Engineering the 3-D DNA Nanomachine into 3-D DNA Nanosensor

5 μM DW was first hybridized with an equal amount of the protecting DNA P through an annealing process. The annealed DW/P and Signal Reporter (SR) oligonucleotides were mixed at a ratio of 1 to 20. A 105 μL volume of this mixture containing 5 μL of 5 μM DW/P oligonucleotides and 100 μL of 5 μM SR oligonucleotides was mixed with 500 μL 1 nM AuNPs. This mixture was incubated at room temperature for 12 hrs, and then was slowly mixed with 165 μL of 3 M NaCl, followed by 10 secs of sonication. This process of addition of NaCl and sonication was repeated for 5 times at 1 hr intervals, to maximize the oligonucleotide loading amounts. The solution was then incubated at room temperature for 24 hrs. After incubation, the solution was centrifuged at 13,500 rpm for 30 min to separate the DNA functionalized AuNPs (DNA-AuNPs) from the unreacted reagents. The DNA-AuNPs were washed 3 times with 0.5 × PBS buffer (pH 7.4) containing 0.005% Tween20, and finally redispersed in 0.5 × PBS buffer.

Gel Electrophoresis of Target-Probe Interaction

A reaction mixture containing 1 μM annealed DW/P duplex of varying toehold lengths, 1 μM free DW, and 1 μM target MTB DNA was incubated at 37 °C for 30 min. Reaction mixtures were then loaded into 12% PAGE gel and a voltage of 110 V was applied. After electrophoresis, the gel was stained with Ethidium Bromide and imaged using Gel Doc XR+ Imager System (BioRad).

Study of Probe Length of Toehold on 3-D DNA Nanosensor

5 μM DW was first hybridized with equal amounts of the protecting DNA P with varying toehold lengths through an annealing process. Each annealed DW/P was mixted with Signal Reporter (SR) oligonucleotide at a ratio of 1 to 20. A 105 μL solution of this mixture containing 5 μL of 5 μM DW/P oligonucleotides and 100 μL of 5 μM SR oligonucleotides were mixed with 500 μL 1 nM AuNPs. This mixture was incubated at room temperature for 12 hrs, and then was slowly mixed with 165 μL of 3 M NaCl, followed by 10 secs of sonication. This process of addition of NaCl and sonication was repeated for 5 times at 1 hr intervals, to maximize the oligonucleotide loading amounts. The solution was then incubated at room temperature for 24 hrs. After incubation, the solution was centrifuged at 13,500 rpm for 30 min to separate the DNA functionalized AuNPs (DNA-AuNPs) from the unreacted reagents. The DNA-AuNPs were washed 3 times with 0.5 × PBS buffer (pH 7.4) containing 0.005% Tween20, and finally redispersed in 0.5 × PBS buffer.

For a typical reaction, reaction mixtures containing 100 pM DNA nanosensors and 20 nM of target DNA were incubated at 37 °C for 10 min. To this mixture, 20 U nicking endonucleases was then added. Immediately after adding the enzyme, fluorescence signals were measured every 1 min from the microplate containing the reaction mixture using a multi-mode microplate reader with excitation/emission wavelength of 485/535 nm.

Detection of Target DNA in PBST buffer Using 3-D DNA nanosensor

For a typical reaction, mixtures containing 100 pM DNA nanosensors and varying concentrations of target DNA were incubated at 37 °C for 10 min. To each mixture, 20 U nicking endonuclease was then added. Immediately after adding the enzyme, fluorescence signals were measured every 1 min for 120 min from the microplate containing the reaction mixture using a multi-mode microplate reader with excitation/emission wavelength of 485/535 nm.

Effect of Incubation Time for 3-D DNA nanomachine in DNA Detection

The reaction mixtures containing 100 pM DNA nanosensors and 20 nM target DNA were incubated at 37 °C for 0 min, 5 min, 10 min, 20 min, 30 min, 45 min, 60 min. To each mixture, 20

U nicking endonuclease was then added. Immediately after adding the enzyme, fluorescence signals were measured every 1 min for 120 min from the microplate containing the reaction mixture using a multi-mode microplate reader with excitation/emission wavelength of 485/535 nm.

Detection of Target DNA Using Initial Rate Method

The reaction mixtures containing 100 pM DNA nanosensors and varying concentrations of target DNA were incubated at 37 °C for 30 min. To each mixture, 20 U nicking endonuclease was then added. Immediately after adding the enzyme, fluorescence signals were measured every 1 min for 5 min from the microplate containing the reaction mixture using a multi-mode microplate reader with excitation/emission wavelength of 485/535 nm.

Detection of Target DNA Using End-Point Method

The reaction mixtures containing 100 pM DNA nanosensors and varying concentrations of target DNA were incubated at 37 °C for 30 min. To each mixture, 20 U nicking endonuclease was then added. Immediately after adding the enzyme, fluorescence signals were measured at 1 hr end-point method from the microplate containing the reaction mixture using a multi-mode microplate reader with excitation/emission wavelength of 485/535 nm.

Specificity Testing

The reaction mixtures containing 100 pM DNA nanosensors, 20 nM of target DNA and salmon sperm genome were incubated at 37 °C for 30 min. 20 U nicking endonucleases was then added. Immediately after adding the enzyme, fluorescence signals were measured every 1 min for 120 min from the microplate containing the reaction mixture using a multi-mode microplate reader with excitation/emission wavelength of 485/535 nm.

Single Point Mutation Detection

The reaction mixtures containing 100 pM DNA nanosensors, 20 nM of target DNA or single point mutated target DNA were incubated at 37 °C for 30 min. To each reaction mixture, 20 U nicking endonucleases was then added. Immediately after adding the enzyme, fluorescence signals

were measured every 1 min for 120 min from the microplate containing the reaction mixture using a multi-mode microplate reader with excitation/emission wavelength of 485/535 nm.

Detection of Target DNA in a Complicated Mixture

Target DNA in 10 times Diluted Human Serum Sample

The reaction mixtures containing 100 pM DNA nanosensors and various concentrations of target DNA spiked in 10 times diluted human serum sample were incubated at 37 °C for 30 min. To each reaction mixture, 20 U nicking endonuclease was then added. Immediately after adding the enzyme, fluorescence signals were measured every 1 min for 120 min from the microplate containing the reaction mixture using a multi-mode microplate reader with excitation/emission wavelength of 485/535 nm.

To each reaction mixture, 20 U nicking endonucleases was then added. Immediately after adding the enzyme, fluorescence signals were measured at 1 hr end-point method from the microplate containing the reaction mixture using a multi-mode microplate reader with excitation/emission wavelength of 485/535 nm.

Target DNA in Undiluted Human Serum Sample

Various concentrations of target DNA were spiked into undiluted human serum sample first. Target DNA was isolated and preconcentrated by using the serum circulating DNA isolation kit. The reaction mixtures containing 100 pM DNA nanosensors and various concentrations of isolated target DNA were incubated at 37 °C for 30 min. To each reaction mixture, 20 U nicking endonuclease was then added. Immediately after adding the enzyme, fluorescence signals were measured every 1 min for 120 min from the microplate containing the reaction mixture using a multi-mode microplate reader with excitation/emission wavelength of 485/535 nm.

To each reaction mixture, 20 U nicking endonuclease was then added. Immediately after adding the enzyme, fluorescence signals were measured at 1 hr end-point method from the

microplate containing the reaction mixture using a multi-mode microplate reader with excitation/emission wavelength of 485/535 nm.

Method for converting fluorescence of SR to concentration of SR

We define the following relation between concentration of SR and fluorescence

$$870000\ F = C_{SR}$$

$$C_{SR} = D_{SR} \times [AuNP]$$

F: fluorescence;

C_{SR} : concentration of SR;

D_{SR} : density of SR on each gold nanoparticle;

[AuNP]: concentration of gold nanoparticle.

Regulation of DNA Strand Displacement using an Allosteric DNA Toehold

5.5 Materials and Reagents

Magnesium chloride hexahydrate ($MgCl_2 \cdot 6H_2O$), sodium chloride (NaCl), 100 × Tris-EDTA (100 × TE) buffer, and TWEEN 20 solution were purchased from Sigma (Oakville, ON, Canada). Ammonium persulfate (APS), N,N,N',N'-tetramethylethylenediamine (TEMED), 40% acrylamide/bis-acrylamide solution, and DNA loading buffer were purchased from Bio-Rad Laboratories, Inc. (ON, Canada). NANOpure H_2O (>18.0 MΩ), purified using an Ultrapure Milli-Q water system, was used for all experiments. All DNA samples were purchased from Integrated

DNA Technologies (Coralville, IA) and purified by high-performance liquid chromatography (HPLC).

5.6 DNA Sequences and Design

DNA name		Sequences
A-toehold-mediated strand displacement	C	5'-T GAC ACA TGG GAT ACA CGC TT-3'
	P	5'- GTC TCT C AA GCG TGT ATC CCA TGT GTC A-3'
	X	5'-AA GCG TGT ATC CCA TGT GTC A-3'
	Xg	5'-T-30-T-AA GCG TGT ATC CCA TGT GTC A-3'
	R1	5'- CA CGC TT GAG AGA C-3'
Toehold-mediated strand displacement (X'-toehold length)	X'-7	5'- T GAC ACA TGG GAT ACA CGC TT GAG AGA C -3'
	X'-6	5'- T GAC ACA TGG GAT ACA CGC TT GAG AGA-3'
	X'-5	5'- T GAC ACA TGG GAT ACA CGC TT GAG AG-3'
	X'-4	5'- T GAC ACA TGG GAT ACA CGC TT GAG A-3'
	X'-3	5'- T GAC ACA TGG GAT ACA CGC TT GAG-3'

	X'-0	5'- T GAC ACA TGG GAT ACA CGC TT-3'
Displacement beacon	C1	5'-6-FAM-T GAC ACA TGG GAT ACA CGC TT-3'
	P1	5'-GTC TCT C AA GCG TGT ATC CCA TGT GTCA-Iowa Black FQ-3'
	C2	5'-TAMRA-T GAC ACA TGG GAT ACA CGC TT-3'
	P2	5'-CTG GTG A AA GCG TGT ATC CCA TGT GTCA-Iowa Black FQ-3'
Allosteric regulator R (R-n-m)	R-7-3	5'- CA CGC TT GAG-3'
	R-7-4	5'- CA CGC TT GAG A-3'
	R-7-5	5'- CA CGC TT GAG AG-3'
	R-7-6	5'- CA CGC TT GAG AGA-3'
	R-7-7 (R1)	5'-CA CGC TT GAG AGA C-3'
	R-3-7	5'- C TT GAG AGA C-3'
	R-4-7	5'- GC TT GAG AGA C-3'
	R-5-7	5'- CGC TT GAG AGA C-3'
	R-6-7	5'- A CGC TT GAG AGA C-3'
	R-7-7	5'- CA CGC TT GAG AGA C-3'
	R-8-7	5'- ACA CGC TT GAG AGA C-3'
	R-9-7	5'- TACA CGC TT GAG AGA C-3'
	R-10-7	5'- ATACA CGC TT GAG AGA C-3'
	R2	5'- CA CGC TT TCA CCAG -3'
Inhibitor	I	5'- GTCT CTC AA GCG TG-3'
Input X (X-r) in toehold-exchange reactions	X-7	5'-AA GCG TGT ATC CCA-3'
	X-6	5'-AA GCG TGT ATC CCA T-3'
	X-5	5'-AA GCG TGT ATC CCA TG-3'
	X-4	5'-AA GCG TGT ATC CCA TGT-3'
	X-2	5'-AA GCG TGT ATC CCA TGT GT-3'
	X-0	5'-AA GCG TGT ATC CCA TGT GTC A-3'
Allosteric regulation of non-covalent DNA catalysis	C	5'-FAM-T GAC ACA TGG GAT ACA CGC TT-3'
	P	5'- GTC TCT C AA GCG TGT ATC CCA TGT GTC A-Quencher-3'
	X (X-6)	5'-AA GCG TGT ATC CCA T-3'
	R	5'- CA CGC TT GAG AGA C-3'
	Y	5'-TAT CCC ATG TGT CA-3'

5.7 Annealing

All annealing processes were performed using a BioRad T100 thermocycler. The samples (typically at a final duplex concentration of 5 μM) were heated to 95 °C for 5 min and then gradually cooled to room temperature at a constant rate over a period of 2 h.

5.8 Characterization of A-Toehold-Mediated Strand Displacement Using Spectrofluorimetry

All spectrofluorometric measurements were performed at 25 °C with a SpectraMax i3 multimode microplate reader (Molecular Devices). DNA probes C and P were labelled with a fluorophore and a quencher, respectively. CP was then annealed to make the displacement beacon at a stock concentration of 5 μM. When in use, CP was diluted using TE-Mg buffer to a final concentration of 20 nM. For a typical A-toehold-mediated strand displacement reaction, the reaction mixture contained 20 nM CP, varying concentrations of R, and varying concentrations of X in TE-Mg buffer. All reaction mixtures were prepared at a final volume of 100 μL in a 96-well microplate. Fluorescence was monitored in real-time with excitation/emission wavelength at 485 nm/515 nm at a frequency of 1 data point per minute.

5.9 Dynamic Regulation of Strand Displacement Using A-Toehold

The reaction mixture contained 20 nM CP displacement beacon and 10 nM input X in TE-Mg buffer and was transferred into a 96-well microplate. The fluorescence was then recorded every 1 min for 10 min. Regulator R was then quickly added into the reaction mixture at a final concentration of 20 nM. The fluorescence was then measured every 1 min for another 5 min. After 5 min, inhibitor I was then added at a final concentration of 40 nM and the fluorescence was recorded for another 10 min. The cycles for adding R and I were then repeated, and the effective concentration of R ($[R]_{eff}$) was maintained at 20 nM and the effective concentration of I ($[I]_{eff}$) was also maintained at 20 nM.

5.10 Selective Activation of Multiple Strand Displacement Reactions Using A-Toeholds

The reaction mixture contained 20 nM 6-FAM-labelled C1P1 displacement beacon, 20 nM TAMRA (5-Carboxytetramethylrhodamine) -labelled C2P2 displacement beacon, and 10 nM input X in TE-Mg buffer and was transferred into a 96-well microplate. R1 or R2 was then added to the reaction mixture at a final concentration of 100 nM. The fluorescence was then monitored using

the multimode microplate reader at both “FAM channel” (485 nm/515 nm) and “TAMRA channel” (535 nm/585 nm) every 1 min for 1 h.

5.11 Allosteric Regulation of Noncovalent DNA Catalysis

The reaction mixture contained 20 nM CP, 20 nM Y, and 2 nM catalyst Xcat in TE-Mg buffer and was transferred into a 96-well microplate. The fluorescence was then monitored using the multimode microplate reader every 1 min for 10 min. The allosteric regulator R1 was then quickly added into the reaction mixture at a final concentration of 150 nM. The fluorescence was then monitored for another 2 h.

Reference

1. Alberts, B., Bray, D., Hopkin, K., Johnson, A., Lewis, J., Raff, M., ... & Walter, P. (2013). *Essential cell biology*. Garland Science.
2. Bartels, C. L., & Tsongalis, G. J. (2009). MicroRNAs: novel biomarkers for human cancer. *Clinical Chemistry*, *55*(4), 623-631.
3. Galeazzi, M., Morozzi, G., Piccini, M., Chen, J., Bellisai, F., Fineschi, S., & Marcolongo, R. (2003). Dosage and characterization of circulating DNA: present usage and possible applications in systemic autoimmune disorders. *Autoimmunity Reviews*, *2*(1), 50-55.

4. Mullis, K. B. (1990). The unusual origin of the polymerase chain reaction. *Scientific American*, *262*(4), 56-61.

5. Lawyer, F. C., Stoffel, S., Saiki, R. K., Chang, S. Y., Landre, P. A., Abramson, R. D., & Gelfand, D. H. (1993). High-level expression, purification, and enzymatic characterization of full-length Thermus aquaticus DNA polymerase and a truncated form deficient in 5'to 3'exonuclease activity. *Genome Research*, *2*(4), 275-287.

6. Barany, F. (1991). Genetic disease detection and DNA amplification using cloned thermostable ligase. *Proceedings of the National Academy of Sciences*, *88*(1), 189-193.

7. Wiedmann, M., Wilson, W. J., Czajka, J., Luo, J., Barany, F., & Batt, C. A. (1994). Ligase chain reaction (LCR)-overview and applications. *PCR Methods Appl*, *3*(4), S51-64.

8. Salas, M. (2012). My Life with Bacteriophage φ29. *Journal of Biological Chemistry*, *287*(53), 44568-44579.

9. Zhao, W., Ali, M. M., Brook, M. A., & Li, Y. (2008). Rolling circle amplification: applications in nanotechnology and biodetection with functional nucleic acids. *Angewandte Chemie International Edition*, *47*(34), 6330-6337.

10. Kuhn, H., Demidov, V. V., & Frank-Kamenetskii, M. D. (2002). Rolling-circle amplification under topological constraints. *Nucleic Acids Research*, *30*(2), 574-580.

11. Johne, R., Müller, H., Rector, A., Van Ranst, M., & Stevens, H. (2009). Rolling-circle amplification of viral DNA genomes using phi29 polymerase. *Trends in Microbiology*, *17*(5), 205-211.

12. Murakami, T., Sumaoka, J., & Komiyama, M. (2009). Sensitive isothermal detection of nucleic-acid sequence by primer generation–rolling circle amplification. *Nucleic Acids Research*, *37*(3), e19-e19.

13. Lee, J. B., Hong, J., Bonner, D. K., Poon, Z., & Hammond, P. T. (2012). Self-assembled RNA interference microsponges for efficient siRNA delivery. *Nature Materials*, *11*(4), 316-322.

14. Nilsson, M., Malmgren, H., Samiotaki, M., Kwiatkowski, M., Chowdhary, B. P., & Landegren, U. (1994). Padlock probes: circularizing oligonucleotides for localized DNA detection. *Science*, *265*(5181), 2085-2088.

15. Banér, J., Nilsson, M., Mendel-Hartvig, M., & Landegren, U. (1998). Signal amplification of padlock probes by rolling circle replication. *Nucleic Acids Research*, *26*(22), 5073-5078.

16. Van Ness, J., Van Ness, L. K., & Galas, D. J. (2003). Isothermal reactions for the amplification of oligonucleotides. *Proceedings of the National Academy of Sciences*, *100*(8), 4504-4509.

17. Tan, E., Erwin, B., Dames, S., Ferguson, T., Buechel, M., Irvine, B., ... & Niemz, A. (2008). Specific versus nonspecific isothermal DNA amplification through thermophilic polymerase and nicking enzyme activities. *Biochemistry*, *47*(38), 9987-9999.

18. Terpe, K. (2013). Overview of thermostable DNA polymerases for classical PCR applications: from molecular and biochemical fundamentals to commercial systems. *Applied Microbiology and Biotechnology*, *97*(24), 10243-10254.

19. Yan, L., Zhou, J., Zheng, Y., Gamson, A. S., Roembke, B. T., Nakayama, S., & Sintim, H. O. (2014). Isothermal amplified detection of DNA and RNA. *Molecular BioSystems*, *10*(5), 970-1003.

20. Zhao, Y., Chen, F., Li, Q., Wang, L., & Fan, C. (2015). Isothermal amplification of nucleic acids. *Chemical Reviews*, *115*(22), 12491-12545.

21. Ali, M. M., Li, F., Zhang, Z., Zhang, K., Kang, D. K., Ankrum, J. A., ... & Zhao, W. (2014). Rolling circle amplification: a versatile tool for chemical biology, materials science and medicine. *Chemical Society Reviews*, *43*(10), 3324-3341.

22. Hurst, S. J., Lytton-Jean, A. K., & Mirkin, C. A. (2006). Maximizing DNA loading on a range of gold nanoparticle sizes. *Analytical Chemistry*, *78*(24), 8313-8318.

23. Zhang, D. Y., & Winfree, E. (2009). Control of DNA strand displacement kinetics using toehold exchange. *Journal of the American Chemical Society*, *131*(47), 17303-17314.

24. Seeman, N. C. (2010). Nanomaterials based on DNA. *Annual Review of Biochemistry*, *79*, 65-87.

25. Long, E. C. (1996). Fundamentals of nucleic acids. *Bioorganic Chemistry: Nucleic Acids, ed. SM Hecht, Oxford University Press, New York*, 3-35.

26. Seeman, N. C. (2004). Nanotechnology and the double helix. *Scientific American*, *290*(6), 64-75.

27. Aldaye, F. A., Palmer, A. L., & Sleiman, H. F. (2008). Assembling materials with DNA as the guide. *Science*, *321*(5897), 1795-1799.

28. Shih, W. M., & Lin, C. (2010). Knitting complex weaves with DNA origami. *Current Opinion in Structural Biology*, *20*(3), 276-282.

29. Yurke, B., Turberfield, A. J., Mills, A. P., Simmel, F. C., & Neumann, J. L. (2000). A DNA-fuelled molecular machine made of DNA. *Nature*, *406*(6796), 605-608.

30. Chen, X. (2012). Expanding the rule set of DNA circuitry with associative toehold activation. *Journal of the American Chemical Society*, *134*(1), 263-271.

31. Genot, A. J., Zhang, D. Y., Bath, J., & Turberfield, A. J. (2011). Remote toehold: a mechanism for flexible control of DNA hybridization kinetics. *Journal of the American Chemical Society*, *133*(7), 2177-2182.

32. Yang, X., Tang, Y., Traynor, S. M., & Li, F. (2016). Regulation of DNA Strand Displacement Using an Allosteric DNA Toehold. *Journal of the American Chemical Society*, *138*(42), 14076-14082.

33. Radding, C. M., Beattie, K. L., Holloman, W. K., & Wiegand, R. C. (1977). Uptake of homologous single-stranded fragments by superhelical dna: Iv. branch migration. *Journal of Molecular Biology*, *116*(4), 825-839.

34. Zhang, D. Y., & Seelig, G. (2011). Dynamic DNA nanotechnology using strand-displacement reactions. *Nature Chemistry*, *3*(2), 103-113.

35. Yurke, B., Turberfield, A. J., Mills, A. P., Simmel, F. C., & Neumann, J. L. (2000). A DNA-fuelled molecular machine made of DNA. *Nature*, *406*(6796), 605-608.

36. Zhang, D. Y., & Winfree, E. (2009). Control of DNA strand displacement kinetics using toehold exchange. *Journal of the American Chemical Society*, *131*(47), 17303-17314.

37. Yurke, B., & Mills, A. P. (2003). Using DNA to power nanostructures. *Genetic Programming and Evolvable Machines*, *4*(2), 111-122.

38. Yin, P., Choi, H. M., Calvert, C. R., & Pierce, N. A. (2008). Programming biomolecular self-assembly pathways. *Nature*, *451*(7176), 318-322.

39. Yurke, B., Turberfield, A. J., Mills, A. P., Simmel, F. C., & Neumann, J. L. (2000). A DNA-fuelled molecular machine made of DNA. *Nature*, *406*(6796), 605-608.

40. Seelig, G., Soloveichik, D., Zhang, D. Y., & Winfree, E. (2006). Enzyme-free nucleic acid logic circuits. *Science*, *314*(5805), 1585-1588.

41. Zhang, D. Y., Turberfield, A. J., Yurke, B., & Winfree, E. (2007). Engineering entropy-driven reactions and networks catalyzed by DNA. *Science*, *318*(5853), 1121-1125.

42. Zhang, D. Y., & Winfree, E. (2008). Dynamic allosteric control of noncovalent DNA catalysis reactions. *Journal of the American Chemical Society*, *130*(42), 13921-13926.

43. Genot, A. J., Fujii, T., & Rondelez, Y. (2013). Scaling down DNA circuits with competitive neural networks. *Journal of The Royal Society Interface*, *10*(85), 20130212.

44. Zhang, D. Y. (2010). Cooperative hybridization of oligonucleotides. *Journal of the American Chemical Society*, *133*(4), 1077-1086.

45. Chen, S. X., Zhang, D. Y., & Seelig, G. (2013). Conditionally fluorescent molecular probes for detecting single base changes in double-stranded DNA. *Nature Chemistry*, *5*(9), 782-789.

46. Wang, J. S., & Zhang, D. Y. (2015). Simulation-guided DNA probe design for consistently ultraspecific hybridization. *Nature Chemistry*, *7*(7), 545-553.

47. Wu, L. R., Wang, J. S., Fang, J. Z., Evans, E. R., Pinto, A., Pekker, I., ... & Zhang, D. Y. (2015). Continuously tunable nucleic acid hybridization probes. *Nature Methods*, *12*(12), 1191-1196.

48. Wang, C., Bae, J. H., & Zhang, D. Y. (2016). Native characterization of nucleic acid motif thermodynamics via non-covalent catalysis. *Nature Communications*, *7*, 10139.

49. Xiaolong Yang, Yanan Tang, Sean D. Mason, Junbo Chen, Feng Li (2016). Enzyme-powered threedimensional DNA nanomachine for DNA walking, payload release, and biosensing. *ACS Nano*, 10, 2324-2330.

50. Lilley, D. M., & Clegg, R. M. (1993). The structure of the four-way junction in DNA. *Annual Review of Biophysics and Biomolecular Structure*, *22*(1), 299-328.

51. Zadeh, J. N., Steenberg, C. D., Bois, J. S., Wolfe, B. R., Pierce, M. B., Khan, A. R., ... & Pierce, N. A. (2011). NUPACK: analysis and design of nucleic acid systems. *Journal of Computational Chemistry*, *32*(1), 170-173.

52. Ambros, V. (2004). The functions of animal microRNAs. *Nature*, *431*(7006), 350-355.

53. Bartel, D. P. (2004). MicroRNAs: genomics, biogenesis, mechanism, and function. *Cell*, *116*(2), 281-297.

54. Lapitan Jr, L. D., Guo, Y., & Zhou, D. (2015). Nano-enabled bioanalytical approaches to ultrasensitive detection of low abundance single nucleotide polymorphisms. *Analyst*, *140*(12), 3872-3887.